An Investigation of a Vertical Test Method for Large Deformation Bending of High Strain Composite Laminates

Kelsey M. Herrmann

A thesis
submitted in partial fulfillment of the
requirements for the degree of

Master of Science of Aeronautical and Astronautical Engineering

University of Washington
2017

Committee:
Dr. Anthony Waas, UW
Dr. Juan 'Johnny' Fernandez, NASA LaRC

Program Authorized to Offer Degree:
Aeronautical and Astronautical Engineering

University of Washington

Abstract

An Investigation of a Vertical Test Method for Large Deformation Bending of High Strain Composite Laminates

Kelsey M. Herrmann

Chair of the Supervisory Committee:
Boeing-Egtvedt Chair Dr. Anthony Waas
William E. Boeing Department of Aeronautics and Astronautics

Research to date indicates that traditional composite material failure analysis methods are not appropriate for thin laminates in flexure. Thin composite structures subjected to large bending deformations often attain significantly higher strain-to-failure than previously anticipated tensile and compression coupon test data and linear material model assumption predict. At NASA Langley Research Center, a new bend test method is being developed for High Strain Composite (HSC) structures. This method provides an adequate approximation of a pure moment, large deformation bend test for thin-ply, high strain composites to analyze the large strain flexure response of the laminates. The objective of this research was to further develop this new test method to measure the true bending stiffness and strain-to-failure of high strain composite materials. Of primary importance is the ability to characterize composite laminates that are of interest for current NASA deployable structures in both materials and layups.

Two separate testing campaigns were performed for the development of the testing procedure. Initially six laminates were bend tested in three different fiber orientations. These laminates were some combination of unidirectional intermediate modulus (IM) carbon, high tenacity (HT) carbon plain weave, and astroquartz plain weave composite materials. The second test campaign was performed as a more detailed look into the simplest composite laminates at thicknesses that better represented deployable boom structures. The second campaign tested three basic, thinner laminates, again in three different fiber orientations. All testing was monotonic loading to failure. The thickness of the laminates tested ranged from 0.166mm (campaign 2) to 0.45mm (campaign 1).

The measured strains at failure for the unidirectional material were approximately 2.1% and 1.4% at the compression and tension sides, respectively, failing as fiber tensile fracture. Both of these values differ from what would be expected from considering much thicker coupons tested under pure compression and tension, that show a strain-to-failure of 1.0-1.1% and 1.6-1.7%, respectively. The significant differences in strain values obtained at the outer surfaces of the coupon is thought to be related to the shift in neutral axis that the specimen experiences during the large deformation bending test as a result of fiber material nonlinearities at higher strains. The vertical test nature of the CBT when compared to other test methods proves to be helpful for visually capturing with Digital Image Correlation the distinct behavior of the flexure on both the compressive and tensile sides.

It was found that the thinner the laminate tested, the more confirmation of a nonlinear response of this classification of composites. The moment versus curvature curves were predominantly nonlinear resulting in a near linear bending stiffness versus curvature response. At these large strains, carbon fibers are highly nonlinear resulting in the laminate flexure modulus increasing by up to 5x. The theoretical bending stiffness values calculated using Classical Lamination Theory analysis are within small differences with respect to the experimentally measured values: errors of approximately 5-10% for both D_{11} and D_{22}. The error between the finite element model computed strain response and the experimental values was on average around 22%, with 35% of the laminates and orientation having errors less than 7%. Comparison between CLT, FEA, and experimentation show that the Column Bend Test appears to be a promising candidate for characterization of large deformation bending behavior of thin-ply high strain composite laminates.

Dedication

To my amazing family for all of their support and encouragement.

Acknowledgements

I would like to thank my thesis advisor, Dr. Anthony Waas, for all of his guidance, encouragement, and support. I am privileged to have been able to learn from Dr. Waas's immense expertise.

I also would like to thank my mentor at NASA Langley Research Center, Dr. Juan 'Johnny' Fernandez, for giving me the opportunity to pursue cutting edge research with such a gifted team. It was an honor to work at NASA and with Dr. Fernandez. A special thank you to everyone at the Structural Dynamics Branch at NASA Langley Research Center for welcoming me into the fold and always being available to help, especially Gregory Dean for his support with fixture fabrication and 3D printing and Gabrielle Snyder for her amazing technical support.

The Composite Layup Laboratory at LaRC was an immense help. A huge thank you to Kevin McLain and Arthur White for working tirelessly with me getting the composite panels fabricated. A particular thank you to Kevin McLain for his patience in instructing in all aspects of composite manufacturing. Thank you to Janet Dail and Steve Whitt for cutting the extremely thin composite panels into the dozens of coupons required, no small feat.

And lastly, a special thank you to Sarvi Ghaffari for all of her help.

An Investigation of a Vertical Test Method for Large Deformation Bending of High Strain Composite Laminates

by

Kelsey M. Herrmann

B.S. Mechanical Engineering, Bucknell University, 2009

M.S. Aeronautical and Astronautical Engineering, University of Washington, 2017

Contents

List of Figures

List of Tables

Chapter 1: Introduction

At NASA Langley Research Center, a new high strain bending test method is being developed with Opertus Research and Development Inc. for High Strain Composite (HSC) structures. This method is a large deformation bending test for thin-ply, high strain composites to analyze the large strain flexure response of the laminates. The bending stiffness for the materials often used for deployable space structures can be tested, measured, and compared to analytical predictions and computational models. The objective of this research was to further develop a new test method to measure the true bending stiffness and strain-to-failure of high strain composite materials, found to be significantly higher than the ASTM standard tension and compression test predictions.

A large flexure test was developed to measure the bending stiffness and strain response of thin-ply, HSC materials using a pure moment design under large flexural strains. Two separate testing campaigns were performed for the development of the testing procedure. The first test campaign was to assess the validity of the test and the performance of the laminates and to see which laminates should be explored further. Initially six laminates were bend tested in three different fiber orientations, ultimately about 70 coupons. These laminates were some combination of unidirectional carbon composite, carbon plain weave composite, and astroquartz plain weave composite. The second test campaign was to determine the material properties for a proper material characterization of specific composite materials and to validate the test design and procedure and accompanying analytical model. The second campaign tested three basic laminates, again in three different fiber orientations, approximately 65 coupons. All testing was monotonic loading to failure.

In addition to experimental data, this study also used a new design tool plug-in for Abaqus called Autodesk Helius Composite to model the composite laminates being tested. Test data using the analysis tool developed at NASA Langley was compared to micromechanics and Classical Lamination Theory (CLT) predictions and to a simple, pure bending FEA model. Comparing nonlinear test data to linear models, while not ideal, emphasizes the nonlinearity evident in the experiments and showcases the need for better nonlinear computational models in future work.

1.1 Motivation and Background

The development of thin-ply composite laminates for deployable space structures has been a major motivation for NASA and the space exploration community as a whole. Deployable structures made of thin composites are ideal for space missions because of their high strength-to-weight ratio and for their lack of reliance on mechanical mechanisms for structure packaging and on orbit unfolding.[1,2] These deployable structures are used for high power solar arrays, parabolic reflectors, phased array antennas, linear antennas, gravity gradient booms, solar sails, and instrument booms, to name a few.[3] In application, the laminates are elastically folded to allow a structure to be compactly stowed during launch and subsequently deployed to a much larger operational configuration once in orbit. This basic technology enables the operational configuration to be efficiently packaged and launched within the payload envelope of conventional launch vehicle fairings.[4]

While the use of composite laminates in deployable structures is widely accepted, in operation they are subjected to strain levels and deformations outside of traditional composite structural applications. As such, their behavior is poorly understood, making deployable structure design and analysis extremely difficult and reliant on extensive material testing which drives up costs. Research to date indicates that traditional composite material failure analysis methods are not appropriate for thin laminates in flexure as carbon fibers are highly nonlinear at high strains. Currently, standardized ASTM test methods are used to determine composite material strengths and linear-elastic stiffnesses under traditional loading applications such as axial and transverse tension, compression, and shear. Data from these tests yield accurate, basic properties that are useful for laminate design, but they fail to characterize the nonlinear constitutive behavior over the full strain range common to deployable structures.[4] Therefore, the characterization of High Strain Composites (HSC) for new deployable composite structures is in high demand. High Strain Composite structures often use thin carbon fiber reinforced laminates undergoing large flexural deformations. While the deformations are elastic, they can involve extreme fiber axial compressive strains of up to 2.5%, much larger than the 1% compressive strain limit typically observed in thicker structures.[5] At these large strains, carbon fibers are highly nonlinear with modulus increasing by two-fold in tension and softening to near zero in compression.[5] Reli-

able design of High Strain Composite structures that exhibit this form of nonlinearity requires accurate predictions of laminate strength and stiffness that fully account for fiber nonlinear behaviors.[5] The challenge lies in understanding the increased strain capacity observed in these thin composite flexures during bending. Of primary importance is the ability to test composite laminates that are directly applicable to deployable structures in both materials and geometry. By doing so, the need to extrapolate from the extremes of thick, ASTM standard coupon or single fiber test results is eliminated. In addition, it is imperative to acquire direct load and deflection measurements throughout the test profile, not just failure, to fully characterize the behavior, including the aforementioned nonlinearities.[4]

With the analysis of the flexural response of the High Strain Composite structures, a detailed picture of the properties and performance expectations can be drawn. The understanding of the High Strain Composite structures' capacity and capability help validate the design of the new deployable composite structures for space missions and potential future terrestrial applications.

1.2 Thesis Outline

This thesis comprises seven chapters. After the present introductory chapter, Chapter 2 begins with a literature review conveying a brief overview of the development of high strain composites and their use in deployable structures. The review starts with the development of the deviation of high strain composite classification from more traditional composites detailing testing methodologies and analytical modeling to characterize the materials. The application of these high strain composites, often noted as HSCs, as thin composite flexural elements for stored strain energy deployable structures is then explored.

Chapter 3 details the Column Bend Test (CBT) method, explaining the testing set up, the analytical model derived from the new test method, and data processing procedures.

Chapter 4 is the discussion of the first test campaign. The materials and laminates used are detailed followed by the initial data analysis from test campaign 1, exploring the laminates' failure behavior and strain response to bending. The data from all six laminates is analyzed and discussed. The aforementioned first test campaign's purpose was to assess validity of the test and the performance of the laminates and to evaluate which ones should be explored further.

Chapter 5 expands on the previous data with a second testing campaign of thinner laminates to validate the test procedure and analytical model for deployable booms and determine the material properties for a proper material characterization of the common materials. This chapter goes into detail about the manufacturing of the specimens for testing and the challenges faced there. The addition of a new testing fixture is detailed in full. Adjustments to the testing procedure and data processing are also reviewed as the new thicknesses of the laminates provided new challenges to the test procedure.

Chapter 6 is the data analysis and analytical model discussion for the second test campaign. Further analysis is performed comparing the experimental data to classical lamination theory theoretical predictions. A simple finite element model created with Abaqus is also compared to experimental data and the analytical model.

Finally, Chapter 7 provides a summary of the research findings regarding the use of the new testing campaign and its use to induce a pure moment to thin laminates in large flexural strains. Also discussed is the suggested incorporation of creep testing, the reliability of the analytical model, and the future work required for more robust testing and to better understand the behavior of high strain composites.

Chapter 2: Literature Review

2.1 High Strain Composites

Composite materials and composite structures are well defined and explored avenues in both academia and industry concerned with aeronautical and astronautical paradigms. However, characterization and understanding of so called "high strain" composites is a rather fledgling but rapidly growing field of interest especially for space structures. In 2014, the AIAA Spacecraft Structures Technical Committee recognized that the level of active research and development in high strain composites warranted a focused group to distinguish high strain composites as a technical area with uniquely identifiable challenges, technologies, mechanics, test methods, and applications.[6] The High Strain Composites Technical Subcommittee was formed to champion this area and a review paper was written by the subcommittee. The authors represent an open international collaboration of government, academic, and private industry experts that have made significant contributions to the field.[7] In this comprehensive paper, published in 2015, high strain composites was categorized as a field of research that encompasses structures that undergo large deformations through composite materials capable of large strains.[7] The composites are typically high performance continuous carbon or glass fibers reinforcing a polymer matrix. Considering bulk properties, HSC materials have a combination of high stiffness and large strains to allow HSC structures to carry loads, yet reconfigure through deformation.[7] A unique feature of high strain composites is that their material properties are often dependent on the structural configurations materials are used in; they inherently couple structural and material mechanics.[7] High Strain Composite materials can do substantial work through the release of stored strain energy. HSC materials span traditional stiff matrix composites, elastomeric matrix composites, and rigidizable/softenable matrix composites.[7]

As mentions above, in 2015, Murphey et al. as the High Strain Composites Technical Subcommittee composed a comprehensive paper documenting the development of high strain composites as a competitive material for deployable structures, with the history, motivation, and research up to that point. This paper provides a survey and references for materials, testing, mechanics, and examples of past structures. While there are broader applications, the paper

focuses on high strain composites used in deployable space structures. A summary of the history is found below:

The use of high strain elements in spacecraft deployable structures has been prolific since the early days of the space industry.[7] In the 1960s, various deployable concepts were first developed with considerable success. These technologies formed the foundation for the development and creation of deployment structures and technologies that continue to be widely used today. Some of the first examples include the deployment of 18m gravity gradient booms on the 1961 TRAAC mission24 as well as the 1962 Alouette I mission, Canada's first spacecraft.[7] Perhaps the most notable deployable concept was the incorporation of slit-tubes to deploy and retract flexible solar array blankets in the 1990 Hubble Space Telescope mission.[7] Today resilient metal structures continue to be used in the majority of high strain deployable spacecraft architectures and excel where the greatest compaction ratios and electrical conductivity are required.[7] However, metals, when compared to composites, are intrinsically limited to having high densities, large coefficients of thermal expansion, and lower strain capacities.[7] These properties limit their use in spaceflight where missions often impose the most extreme precision and weight requirements. The limited strain capacity of metals also restricts the geometries and structural architectures that can be achieved.

The incorporation of non-metallic materials into high strain deployable structures emerged concurrently with the 1960s metallic-based systems, although in a more limited fashion.[7] One of the first widely used HSC systems for spaceflight was the helically coiled continuous longeron masts (CLMs) which first flew in 1974.[7] This technology has since flown on dozens spaceflight missions and includes several high profile campaigns such as Voyager (1977), Galileo (1989), Mars Observer (1992), and the GOES constellation (1994-present).[7] Over the last decade, new carbon fiber based high strain composites have been developed that significantly surpass the performance of metals and glass fiber composites in terms of density, dimensional stability, and the balancing of stiffness and strain.[7] These new structures and materials enable architectures that are more competitive, and perhaps superior to the current performance of rigid element mechanical deployable structures.[7]

Table 1: Important developmental and flight examples of deformable structures in the history of high strain composites[7]

Structure Common Name	Material	Invention	Development History	Flight History
Tape-spring Hinge	Spring steel sheet	Unknown	Unknown	Unknown
Storable Tubular Extendible Member (STEM)	Metal sheet	George J. Klein	Developed by de Havilland Canada and Spar Aerospace Ltd.	1961-AH2 Transit Research and Attitude Control (TRAAC), launched in 1961; Alouette 1, launched in 1962
Wrap Rib Antenna, C-Shaped Ribs	Aluminum sheet	Jack V. Miller, filed 1963	Developed by Lockheed Missiles & Space Company starting in 1962	ATS-6, launched in 1974
Lenticular Tube	Stainless steel sheet	Unknown	Developed by NASA Lewis Research Center in 1965.	Unknown
Continuous Longeron Mast	S2 fiberglass rods	Hagen R. Mauch, filed 1967	Developed by Astro Aerospace.	USAF S-3 Magnetometer Boom, launched in 1974
Geo-Truss	Titanium sheet	Unknown	Developed by General Dynamics, Convair Division in 1968.	Unknown
Lattice Lenticular Tube	Steel music wire	Unknown	Developed by Astro Research Corporation in 1969.	Unknown
Wrap Rib Antenna, Lenticular Ribs	CFRP laminate (Fiberite HMS/33)	Unknown	Developed by Lockheed Missiles & Space Company. Prototypes in late 1970s; integrated ground demonstration in 1982.	Unknown
Spring-back Antenna Parabolic Reflector	CFRP laminate	Stephen A. Robinson, filed 1995	Developed by Hughes Space and Communications Group	Mobile Sat-1, launched in 1996
Foldable Flattenable Tubes	Fiberglass and Kevlar laminate	Goeff Marks, filed 1999	Developed by TRW Astro Aerospace. Conceived for Sounder Antenna of NASA EUROPA Orbiter Spacecraft.	Mars Express MARSIS antennas, launched in 2003.
Conical Tube	Kevlar fabric with rigidizable matrix	Unknown	Developed by L'Garde	Cibola Flight Experiment, launched 2007.

2.1.1 Thin-Ply Composite Testing

At the Air Force Research Laboratory (AFRL), in 2010, a simple test method of flattening a flexure coupon between two parallel platens was used to investigate the large strain flexure of 0.135 mm, 0.259 mm, and 0.383 mm thick unidirectional carbon fiber reinforced epoxy plates.[8] Coupons were folded in a U-shape and compressed between parallel platens while platen separation and load were measured up to failure allowing an estimate of the flexure bending moment and curvature from the platen load and separation.[8] With such thin materials being tested, the data offered a few unexpected results. Test results show a nonlinear material response resulting in bending stiffness softening as curvature increases.[8] Bending failure strains were larger than expected and increased as coupon thickness decreased, ranging from 2.15% to 2.75%.[8] Also unex-

pected, the failure occurred in a tensile mode on the outside coupon surface, not in a compressive mode.[8] These results indicated to the community that thin flexures could be used at strains and curvatures larger than previously thought. The authors surmised that regardless of whether or not one believes the extreme nonlinearities and large compressive strains indicated by their paper, the curvatures achieved in thin flexures are approximately two times greater than one would expect, so understanding the conditions under which such large strains can be exploited is critical to achieving more compactable and higher performance deployable structures.[8]

In 2011, Sanford et al. developed a new test method to quantify the bending moment vs curvature behavior of thin composite laminates to further explore the unexpected response of thin composites.[4]

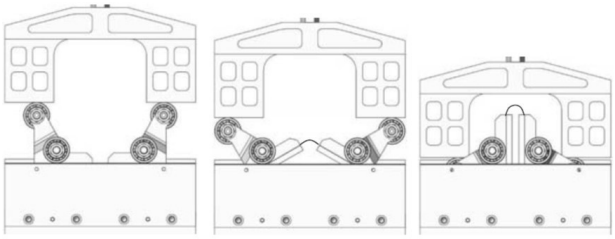

Figure 1: Progressive views of the pure moment test fixture.[4]

The fixture was designed to impart a pure moment into the coupon, a necessary improvement to prior test methods where results are obtained by fitting material properties in a nonlinear structural analysis of the test.[4] The fixture mechanics allowed for direct calculation of the coupon flexural modulus and allowable flexural strain based on two key measurements: fixture displacement and applied load. In this paper the fixture and method was proposed but no composites were actually tested.

In parallel with the new pure moment test method for determining flexure properties of thin composite laminates, Murphey et al. were also exploring a nonlinear elastic constitutive model for large strains in carbon fiber composite flexures. In a paper published in 2011, first and second order empirical strain and stress based models with different parameters in tension and compression were investigated to model the compressive strains that were approximately two times larger than those observed in similar axially loaded, thick composites of the same materials.[3] The large compressive strains of 2.2% and tensile strains of 1.8% observed in thin

unidirectional intermediate modulus carbon fiber reinforced epoxy flexure present a unique opportunity to investigate the large strain nonlinear elastic constitutive behavior of carbon fibers.[3] In this paper, a bimodal constitutive model with different quadratic parameters in tension and compression was shown to accurately represent flexure behavior for moderate strains, but not large strains.[3] The model was subsequently modified to reduce the fiber modulus to zero at a critical compressive strain to more accurately represent the behavior of thin flexures subjected to large strain deformations.[3]

In this paper, the model assumes stress is a quadratic function of strain in tension and compression with the same slope at zero strain, however, the parameters that determine nonlinear behavior (γ_{T} and γ_{C}) are allowed to be different in tension and compression.[3] The model is given by,

$$E(\epsilon) = E_0(1 + \gamma_{\mathrm{C}}\epsilon\langle\epsilon < 0\rangle + \gamma_{\mathrm{T}}\epsilon\langle\epsilon > 0\rangle) \tag{1}$$

where E_0 is the modulus at zero strain and the notation $\langle\epsilon\rangle$ is used to indicate a step function that is 1 if the enclosed condition is true and 0 if the condition is false. The sigmoid or logistics function is used here,

$$\langle\epsilon < 0\rangle = \frac{1}{1 + e^{\tau\epsilon}} \tag{2}$$

$$\langle\epsilon > 0\rangle = \frac{1}{1 + e^{-\tau\epsilon}} \tag{3}$$

where τ is a parameter that determines the sharpness of the transition between 0 and 1. Equation 1 accurately represents flexure behavior up to moderate strains when parameters are derived from standardized thick composite tensile and compressive tests. At larger strains, it was required to modify the model to allow modulus to drop to near zero at a critical value of compressive strain,

$$E(\epsilon) = E_{\mathrm{b}}\langle\epsilon < \epsilon_{\mathrm{cr}}\rangle + E_0(1 + \gamma_{\mathrm{C}}\epsilon)\langle\epsilon_{\mathrm{cr}} < \epsilon < 0\rangle + E_0(1 + \gamma_{\mathrm{T}}\epsilon)\langle 0 < \epsilon\rangle. \tag{4}$$

The new test method designed in 2011 was further explored and a paper published in 2013 investigated the method further with actual testing of intermediate modulus (IM7 and IM10) and high modulus (M55J) carbon fibers and structural fiberglass (S2).[9] The large deformation four point bending fixture was used to test thin unidirectional composite plates under large

flexural strains. The tests allowed investigation of the large strain elastic constitutive behavior. Thermoset plastic coupons reinforced with these fibers and ranging in thicknesses from 0.1 mm to 0.5 mm were tested.[9] Intermediate modulus carbon fibers were found to be significantly nonlinear while glass fibers were essentially linear.[9] High modulus carbon fibers exhibited a more complex flexural response with stiffness initially slightly increasing followed by a moderate reduction in stiffness and finally, a sharp reduction in stiffness and failure.[9] A nonlinear empirical constitutive model was used to represent fiber axial tensile and compressive behavior and through a structural model, predict coupon nonlinear flexural response and estimate constitutive model parameters.[9] In an accompanying paper in the same year, Peterson and Murphey took the bending stiffness of a thin carbon and glass fiber composite tape spring measured with the large deformation four point bending test fixture and compared them to analytical predictions.[1] Coupons failed in a fiber tensile mode at a surface bending strain of 2.2%.[1] Modified micromechanics and classical lamination theory analysis were used to predict laminate stiffness properties but test results were 10% less than the predicted values.[1]

This new test fixture and method for measuring the nonlinear axial properties of composites used in deployable space structures continued to be explored. In a paper published in 2015, Murphey et al. used this test method to investigate the large strain elastic constitutive behavior of two more aerospace-grade intermediate modulus carbon fibers, a high modulus carbon fiber and a structural glass fiber, reinforced with thermoset plastic.[10] The test coupons had thicknesses again ranged from 0.1 to 0.5 mm.[10] When compared to the testing from 2013, the results were repeatable; intermediate modulus carbon fibers were found to be significantly nonlinear with modulus linearly increasing with strain while the modulus of the glass fibers was essentially constant.[10] Although the data was useful for understanding the nonlinear stiffness response of thin laminates, the unidirectional laminas tested here were sensitive to failure at the test fixture clamps and the results did not provide a good measure of flexure strength.[10]

For complete composite material characterization, Murphey et al. proposed a three-step flexible composite material characterization process that was described and partially carried out in their 2015 paper. First, a tensile test is performed to determine fiber initial modulus and tensile nonlinear parameter. Second, a large deformation bending test is performed to determine

the compressive nonlinear parameter. Finally, a platen test is performed to determine tensile and compressive stresses and strains at failure by simply bending a coupon into a U shape between two flat and parallel platens. This test sequence isolates fiber properties (initial modulus and nonlinear parameters) from composite material behavior. The first two tests determine fiber properties.[10] As there are many different resin systems and fiber volume fraction combinations, the relatively simple platen test needs to be performed to determine failure stresses and strains.[10]

In 2016, Peterson and Murphey further expounded their nonlinear elastic constitutive model for large strains in carbon fiber composite flexures used along with high strain lamina flexural mechanics in attempts to describe the strain response in high strain composite laminates.[11] Furthermore Peterson and Murphey laid out a workflow, detailing the various test approaches employed to determine the essential material constants (composite constituent moduli, tensile/compressive nonlinear parameters, etc.) required to identify the failure modes at play in these materials.[11] Their proposition is as follows:

1. ASTM D638 Tensile Test[12] to determine matrix modulus (E_{m}) from neat resin tensile specimens provided by composite manufacturer.
2. ASTM D3039 Tensile Test[13] to determine initial fiber modulus (E_0) and tensile nonlinear parameter (γ_{T}) from unidirectional composite data fit.
3. Optical Micrographing for true thickness measurements.
4. Large Deformation Four Point Bending (LD-FPB) Test for isolation and determination of the compressive nonlinear parameter (γ_{C}).
5. Platen Flexure Test for realistic composite failure observation at the materials true capacity.

These high strain composite (HSC) laminates possess unique characteristics desirable to the aerospace deployables community as they have been found to exhibit elevated strength and deformation capacities prior to failure in comparison to those observed in thicker traditional composite structures.[11] For this reason, HSCs are regarded as a prime candidate for strain energy driven deployable space structures for their ability to endure high levels of stress and strain enforced during the stowage process.[11] Means of quantifying this phenomenon have been met with difficulty due to current limitations in testing methodologies, typically resulting in

lower material capacities non-representative of those observed in thin HSCs in bending.[11] The community is continuing to explore new test methodologies and constitutive models to evaluate HSC laminates and predict performance.

2.2 Deployable Structures: Booms and Tape Springs

The vast interest in high strain composites is predominantly for the purpose of deployable space structures. In application, these laminates are elastically folded to allow a structure to be compactly stowed during launch and subsequently deployed to an operational state once in orbit. This basic technology enables operational systems containing structures such as solar arrays, reflectors, antennas, and booms to be efficiently packaged and launched within the payload envelope of conventional launch vehicle fairings.[4] There is significant interest in the use of high stiffness, yet flexible, composites to replace traditional mechanisms. Spacecraft require structures that can be compactly packaged during launch and subsequently deployed to a much larger operational configuration. Most commonly, these deployable structures are used for high power solar arrays and parabolic reflectors but can also be used for phased array antennas, linear antennas, gravity gradient booms, solar sails, and instrument booms.[3]

As mentioned above, deployable structures have been growing with the space program since its inception. In the last decade, the newly explored high strain composites have surpassed the performance of metals and glass fiber composites in terms of density, dimensional stability, and the balancing of stiffness and strain.[7] These new structures and materials enable architectures that are more competitive and elaborate for space structures.

In 2002, the Mars Express Spacecraft was equipped with a lightweight deployable antenna for the Mars Advanced Radar for Subsurface and Ionosphere Sounding (MARSIS) Experiment.[14] The antenna structure consisted of lightweight S-Glass/Kevlar composite tubes that were folded at points along the length where cutouts in the side of the tube prevent a singularity in the material and then compressed for stowage.[14] Unfortunately it did not deploy as desired, experiencing a deployment anomaly attributed to creep in its composite laminate. A reduction in deployment moment was observed in the folded composite booms forming the antenna after a long period of stowage and has been attributed to energy dissipation in the viscoelastic matrix.[15] The re-

alization was discovered at post launch, in 2009, that the stowed booms retained a high level of stored energy that resulted in an uncontrolled boom deployment rather than a predictable boom deployment.[16] Since deployable structures are often stowed for a long time and subject to varying temperature environments, a reliable analysis needs to take into account the viscoelastic behavior of the material.[15]

Exploration into tape springs has been an industry interest since the concept of deployable structures was introduced. A tape spring is a thin-walled, straight strip of material with curved cylindrical cross-section. Metallic tape springs have been used for many years, but the current trend is towards tape springs made of carbon fiber reinforced plastic (CFRP), for their tailorable properties, low mass, and low coefficient of thermal expansion.[17] The moment-rotation behaviour of a tape spring can be described as linear-elastic for small rotations and constant-moment for large rotations.[17] Tape springs play a huge role in the determination of high strain composite deployable structures.

At the DLR Institute for Composite Structures and Adaptive Systems and the company Kayser-Threde extremely lightweight and stiff deployable carbon fiber reinforced plastics (CFRP) booms and deployment mechanisms have been developed since the early 2000's, their main target application being to develop an ultra-light-weight solar sail for deep space satellite propulsion.[18]

Given the response of flown composite boom structures and research into tape springs, awareness of visoelastic relaxation and creep in the structures has grown. In 2010, Kwok et al. published a paper investigating the shape recovery behavior of a simple beam and a tape spring made of LDPE under prescribed deformation history at room temperature.[2] A LDPE tape spring was fabricated and tested to provide an example of a simple deployable structure that recovers its deployed shape through a viscoelastic process for both equal sense and opposite sense folding.[2] This observation opened avenues for further research for the HSC community.

Due to the historical practice of abandoning in orbit decommissioned spacecraft, payload fairings, and launch vehicle upper stages, there is currently a shell of synthetic debris around the Earth.[19] As of October 2013, the U.S. Space Surveillance Network is tracking over 13,000 Earth-orbiting space debris objects larger than 10 cm.[19] The threat this poses to active and future spacecraft is an ever growing problem, in particular for LEO altitude regions where the

accumulation of debris is more severe.[19] In 2014, Surrey Space Center and ESA explored a low-cost solution to the space debris problem with a composite solar sail deorbiter.[19] The Gossamer Deorbiter proposed was designed as a scalable stand-alone system that can be attached to a low-to-medium mass host satellite for end-of-life disposal from low Earth orbit.[19]

Recent advances in ultrathin composite materials (HSCs) have made it possible to build low-cost and ultra-lightweight thin-walled structures that can be folded elastically and are able to self-deploy. In late 2014, Mallikarachi and Pellegrino presented a study that developed a manageable approach for developing optimized designs, shown through analysis and experimental demonstration, that are a significant improvement on those obtained from a more direct approach based on physical intuition.[20] A simple boom construction based on a thin-walled tube made of two plies of plain-weave carbon fiber (T300-1k) in an epoxy matrix (Hexply 913) was considered.[20] Given that the current approach at the time was strongly based on experimental verification, which severely limits the range of potential designs, this approach was designed to mitigate some of the limitations and costs of deployable structure design.

The long list of advantages that small satellites can offer in terms of fast development time, low cost, possibility of large swarm missions, scientific and/or educational return on investment are, in general, in conflict with the challenging mass and volume constraints imposed on the spacecraft subsystems.[21] Many systems such as solar panels, antennas, sensors, telescopes, solar sails, drag sails, sun shades, radiators, and payloads are in need of reliable deployment of structural booms and arrays for power generation, communications, propulsion, deorbiting, thermal control, and scientific instruments.[21] In early 2017, J.M. Fernandez presented a purposely designed boom structural characterization test method with gravity off-loading to compare the structural performance of the booms under expected operational and general load cases.[21]

Several low-cost solar sail technology demonstrator missions are under development in the United States.[22] However, the mass saving derived benefits that composites can offer to such a mass critical spacecraft architecture have not been realized yet.[22] This is due to the lack of suitable composite booms that can fit inside CubeSat platforms and ultimately be readily scalable to much larger sizes, where they can fully optimize their use.[22] With this aim, a new effort focused at developing scalable rollable composite booms for solar sails and other deployable

structures has begun.[22] Seven-meter booms used to deploy a $90m^2$ class solar sail that can fit inside a 6U CubeSat have already been developed.[22] The NASA road map to low-cost solar sail capability demonstration consists of increasing the size of these composite booms to enable sailcrafts with a reflective area of up to $2000m^2$ housed aboard small satellite platforms.[22]

Deployable boom structures built with high strain composite materials is still a rich field of research. The understanding of these materials and structures is still very preliminary. These nascent understandings require further test method development and modeling modifications to reach industry desired levels. Based on the growth of the deployable space structures world and the expansion of uses for high strain composites, new discoveries will continue to teach and inspire the community for years to come.

Chapter 3: Column Bend Test Method

As discussed, thin composite structures subjected to large bending deformations often attain significantly higher strain-to-failure than previously anticipated tensile and compression coupon test data and linear material model assumption predict. It can be observed during bending that these composite materials exhibit fiber tensile stiffening and compression softening subsequently leading to the net effect of a gradual increase in bending stiffness as strain increases.[7] The nonlinear behavior and stabilization of the compressive side of the material through microbuckling has a beneficial effect on the strain-to-failure properties of these HSC materials.[7]

The Structural Dynamics Branch at NASA Langley Research Center in conjunction with Opertus Research and Development Inc. have developed a new Column Bend Test (CBT) to measure plate bending properties primarily for large deformation bending in thin flexures through a pure moment model. The CBT was initially developed by Dr. Thomas Murphey at Opterus Research and Development Inc., NASA Langley Research Center (LaRC) is further refining and evaluating the test process, as well as using it to assess properties of current laminates of interest. The objective of this test is to measure bending moment versus curvature up to failure of various composite materials and laminate layups. The slope of said curve provides the measure of the plate bending stiffness terms and the material nonlinearities can be accurately measured. The knowledge of the curvature of the material at failure provides the laminate maximum curvature in addition to allowing for analysis to back out the stress-strain state of the laminate at failure. For the kinematic representation of this test campaign, constant curvature is assumed.

3.1 Test Set Up and Procedure

The test set up is rather simple in design. To achieve a pure moment condition on the coupon being tested, a load is applied, in compression, to a pivot point connected to a rigid arm. Another pivot point is fixed and connected to an identical rigid arm with the test specimen secured between the two arms. As the loaded pivot displaces, moving toward the fixed pivot, the rigid arms sweep out, bending the laminate coupon fixed between them into a U-shape. As the test frame compresses the fixture, a load is applied and the coupon flexes until fiber failure

occurs. Figure 2 gives a general view of the typical test frame set up.

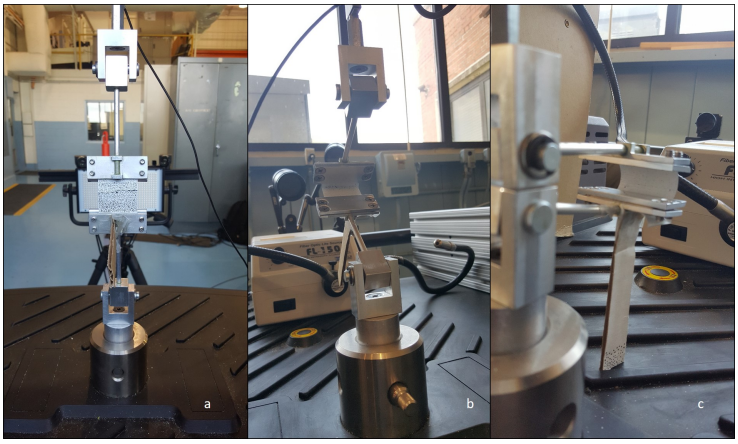

Figure 2: Progressive views of the pure moment Column Bend Test (CBT), a) initially, b) approximately midway through, c) bent to 90°

Setting up the sample and aligning it in the fixture is critical. The alignment method is rather uninspired but provides dependable results. Initially the desired grip separation, i.e. gauge length, is measured with calipers and marked on the coupon. The coupon is then placed into the fixture at the approximate desired separation length. The grips are ensured to be at the correct distance apart and the coupon forced square to the grips with the placement of precision blocks. Once the coupon is confirmed to be placed perpendicular to the grips and with the appropriate length, the fixture itself is aligned to a rigid, precision straight edge to constrain the rigid arms and pivot points to be parallel to the straight edge and the coupon and perpendicular to the grips. The coupon must be perfectly aligned in the fixture, and thus with the load frame, for the test results to be valid.

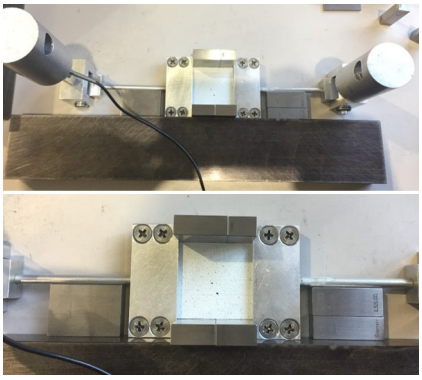

Figure 3: Alignment of coupons in fixture using precision blocks

All testing was done as displacement driven loading. The test fixture and coupon were installed into a tabletop, MTS Criterion Model 43 C43.504 Load Frame. Using MTS TestSuite Essential[43] the load frame was programmed to compress the fixture by displacing at a rate of 25.4mm/min until failure. A Futek load cell sensor is attached, in line, at the top of the fixture to measure the applied load. The MTS C43.504 has a built-in load cell but the applied loads in this test procedure are so small, based on the size and thickness of the test specimen, the MTS load cell is not sensitive enough to give reliable readings. The Futek load cells ranging from 10 to 50 lbs accurately track the applied load as the MTS load frame displaces at the programmed rate. The load cell captures data at a rate of 2000 Hz. During the test, crosshead displacement, via the MTS C43.504 load frame, and applied load, via a Futek load cell, are measured. Two Digital Image Correlation (DIC) systems with high-resolution stereo cameras (5 MP), VIC3D and Aramis, are set up to track and measure the strain state on both the tension and compression sides of the test coupon. Both DIC systems take images at a rate of ½ Hz throughout the test. To ensure appropriate resolution for DIC data capture, a speckled pattern of black and white regions on the coupon is required. The coupons were spray painted white and airbrushed with black "spots" to create a randomized black/white pattern on the coupons. A fine-point black Sharpie was then used on many samples to enhance the black spots on the painted white coupon for image tracking on both the tension and compression sides, ensuring the best data from the VIC3D and Aramis DIC systems. The lighting on the DIC systems is adjusted for each coupon to ensure accurate speckle tracking and strain measurements.

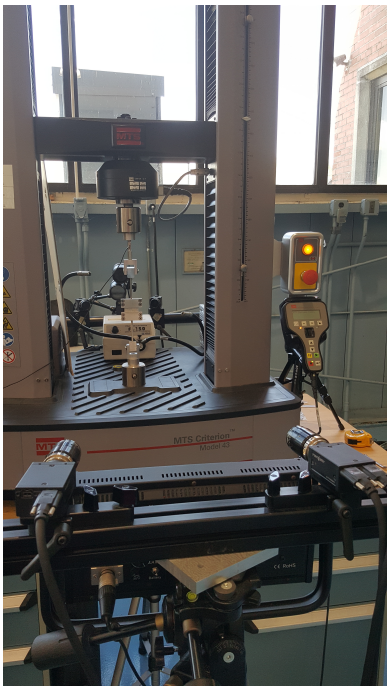

Figure 4: Complete test frame set-up

The test campaign for each coupon is run from a slightly prebuckled state, to ensure the coupon bends in the appropriate direction for the DIC capturing software, to a maximum 90° bend or until the specimen fails. Failure is desired so grip separation is adjusted to endeavor to achieve failure at or near 90°. All testing is monotonic loading to failure. For these purposes failure is defined as fiber fracture. The initial angle of prebuckling is measured, as well as the angle of progress of the coupon throughout the test, i.e. the rotation angle of the fixture arm. An angle tracking arm is attached to the face of the fixture on the lower half, tension side. A camera films the profile of the test following the angle arm, imaging at rate of ½ Hz as well. The still images are then fed to VIC2D DIC software that ultimately outputs the deflection angle of the fixture throughout the test.

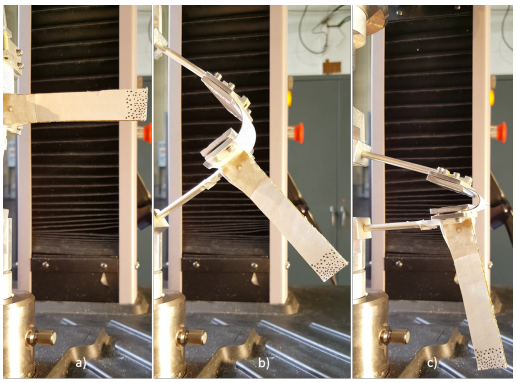

Figure 5: Angle arm tracking at the a) initial, b) midway through test, and c) final stages

3.1.1 Load Cell Calibration

It is noted that, the calibration of the Futek load cells slipped during testing, all of the Futek load cells, 10lb, 25lb, and 50lb, were offset by a constant factor during initial testing. With significant testing of the load cells by adding known weights in 200 gram increments and measuring the outputs, that factor for each load cell was found. All load cell data was adjusted by these factors, 11.160 for the 10lb, 4.745 for the 25lb, and 2.25 for the 50lb, to give the correct force reading for data processing and analysis. A sample of the load cell correction assessment for the 25lb cell can be found in Figure 6.

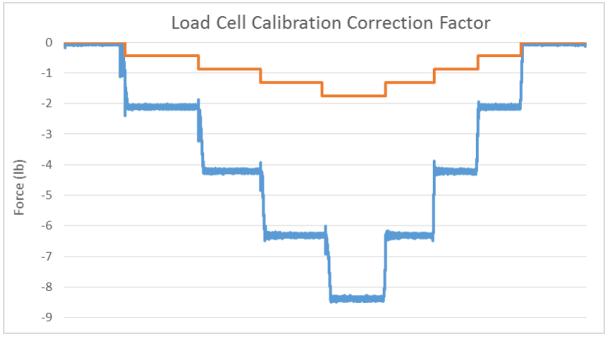

Figure 6: Load cell correction factor test for the 25lb load cell

The Futek load cells were then re-calibrated with the data sheet provided by the manufacturer (see Appendix A for a sample) and retested to verify the correct outputs were being recorded. The Futek calibration parameters for voltage output based on force input are provided in the data sheet. The load cell was then verified by checking the outputs with known loads. The load

cell was manually loaded with 200 gram weight increments and the outputs measured before and after calibration, verifying the calibration with the correct load outputs and capturing the correction factor to adjust the test data from the load cell outputs prior to calibration.

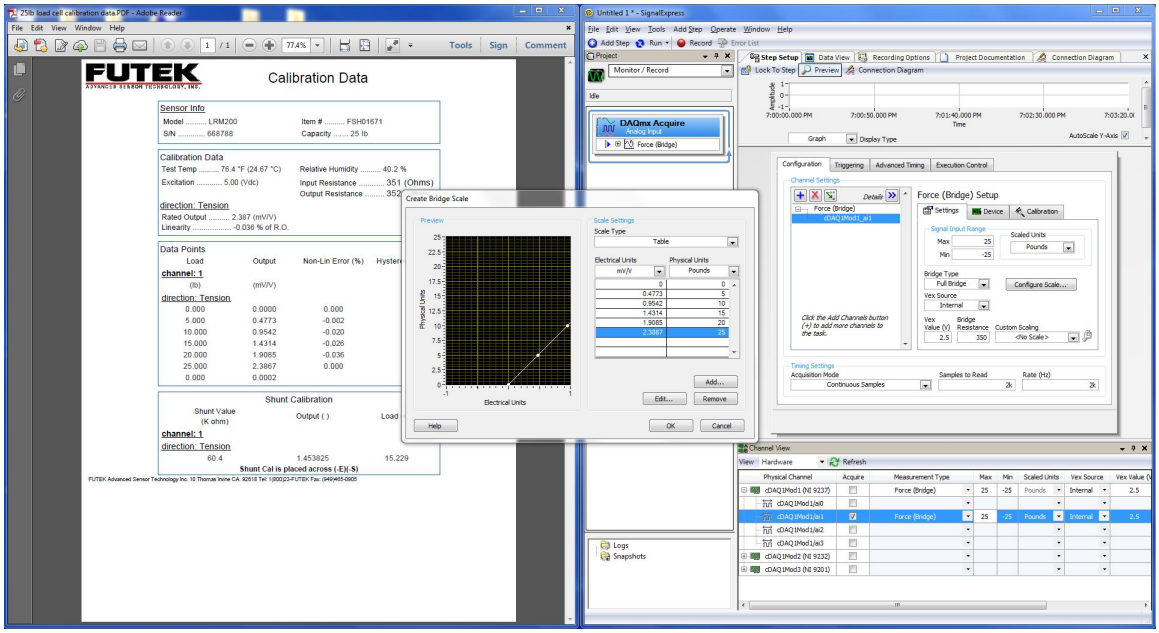

Figure 7: Calibration of 25lb load cell with Futek calibration data

The data processing is performed off of an analytical model created, previously at LaRC and developed at Opertus R&D, for this pure moment bend test. This model takes the load, angle, and moment arm inputs and calculates performance properties such as bending stiffness, curvature, moment, deflection angle, etc.

3.2 Analytical Model Derivation

A simplified version of the kinematics of the Column Bend Test (CBT) can be readily represented with the assumption of constant curvature of the specimen throughout the test. In reality the moment varies in the coupon from minimum to maximum, with a variation of less than 15%, typically less than 6%. This moment variation then leads to curvature variations. Inaccuracies from this assumption are still being explored.

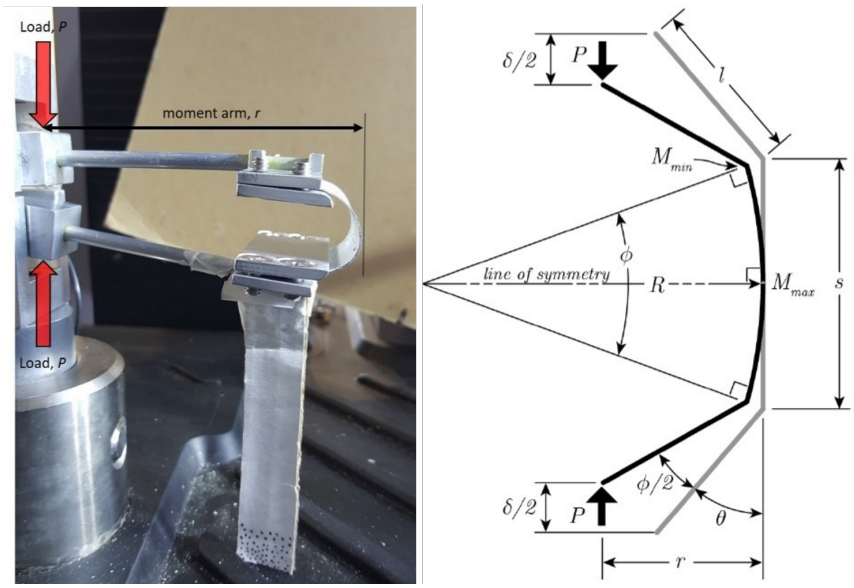

Figure 8: Bending moment schematic

In Figure 9, s is defined as the free length of the coupon in between the clamps, l is the effective distance of the rigid arm, θ is the initial angle of the rigid arm, ϕ is the change in rigid arm angle due to deflection, δ is the linear displacement of the fixture, P is the load applied to the fixture, r is the effective moment arm length, and R is the radius of curvature of the displaced sample. Since the maximum curvature occurs near the middle of the sample and since the variation between the minimum and maximum moments is relatively small, a constant curvature of the sample is assumed. With this assumption, the kinematic equations of motion are simple and the relationship between the displacement of the fixture ends, δ, to the change in the rigid arm angle, ϕ, is:

$$\frac{\delta}{s} = 1 - \frac{2}{\phi}\sin\frac{\phi}{2} + 2\frac{l}{2}(\cos\theta - \cos(\theta + \frac{\phi}{2})). \tag{5}$$

It is worth noting that Equation 5 is transcendental and thus ϕ cannot be solved for directly. In order to determine ϕ, numerical methods are needed. This is implemented in MATLAB[44]. Using the arc length formula, the curvature of the sample, $\kappa = 1/\mathrm{R}$, can then be determined by:

$$\kappa = \frac{\phi}{s}. \tag{6}$$

The rigid arm angle, ϕ, and the moment arm, r, are calculated using trigonometry based on the geometry of the fixture and the applied load, P. The moment arm, r is determined by:

$$\frac{r}{s} = \frac{1}{\phi}(1 - \cos(\theta + \frac{\phi}{2}) + \frac{l}{s}\sin(\theta + \frac{\phi}{2})) \tag{7}$$

where s is the coupon length, θ is the measured angle of rotation, and l is effective length of the rigid arm. Using the moment arm length, r, and the load sensor data to determine the load, P, the maximum moment acting on the sample can be determined by:

$$M_{\max} = Pr. \tag{8}$$

Using the effective length, l, the sensor load, P, the rigid arm angle, ϕ, and the initial measured angle of rotation, θ, the minimum moment acting on the sample can be determined by:

$$M_{\min} = Pl\sin(\theta + \frac{\phi}{2}). \tag{9}$$

With the moment and curvature data it is possible to obtain a plot of moment vs curvature throughout the deflection of each coupon. With this plot the material bending stiffness, D, can be determined through the following relation:

$$D = \frac{\partial M_{\max}}{\partial \kappa}. \tag{10}$$

With the curvature of the sample, it is then possible to find the surface strain of the laminate, ϵ, using the thickness of the coupon, t, by:

$$\epsilon = \frac{\kappa t}{2}. \tag{11}$$

With these equations, it can be seen that the only independent variables that require measurement are the linear displacement of the fixture arms, δ, and the load acting on the fixture from bending of each coupon, P. The former is controlled by the MTS load frame, while the latter is measured by a Futek load cell in line with the CBT fixture.

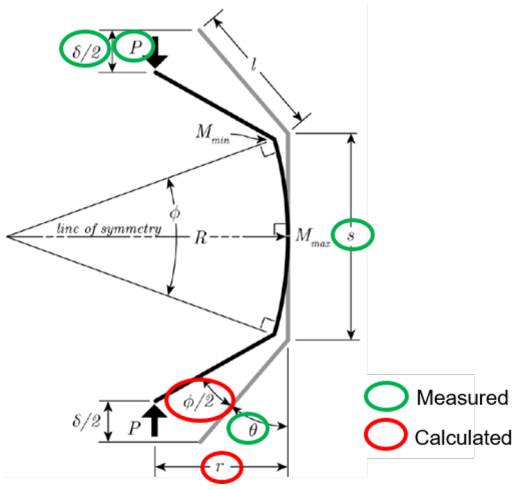

Figure 9: Moment arm and deflection angle derivation

Though constant curvature is assumed, in reality the moment varies in the coupon from a minimum to maximum state leading to curvature variation in the sample. Therefore the constant curvature assumption leads to inaccuracies in the analysis. Moment variation does have advantages in that the maximum moment is highest away from the grips which prevents grip-induced failures and allows for realistic failures, at least on samples that have a significant grip separation/gauge length.

3.3 Data Processing

As with all experimental testing, the raw data output must be processed with various software packages for analysis. The MTS C43.504 load frame outputs the displacement, load, and time. The load cell outputs the precise applied load. DIC cameras snap photos every two seconds during the entire run of the test, on both the tension and compression sides of the coupon when applicable. The two different DIC analysis software packages, VIC3D[45] and Aramis[46], analyze the DIC images and output a vast number of conditions; the interest here is in the strain observed on the sample to track the performance of the coupon. A camera is set to video the edge profile of the sample and track the angle arm. That video is converted to photos and fed to the VIC2D analysis system[47] to calculate and track the angle of displacement of the fixture and coupon. The initial angle of prebuckling is measured from these images with the software Gimp[48].

Uploaded to a MATLAB script is an Excel file containing the measured grip separation, i.e.

specimen or gauge length, and the initial angle of prebuckling, as well as the output files from the MTS Criterion 43.504 load frame, crosshead displacement, load, and time, and the load from the Futek load cell output data. For the kinematic representation of this test campaign, constant curvature is assumed. The MATLAB script based analysis method assumes the coupon bends in a perfect circle of constant curvature which is known to not be reality but is a valid assumption for simplification of the calculations. The MATLAB script then outputs the coupon's performance and properties, including data as well as plots and relationships for curvature, moment, bending stiffness, radius, and angle.

Table 2: MATLAB Column Bending Analysis script output

Moment, Curvature, and Bending Stiffness	
Phi [rad]	Deflection angle in radians
R [in]	Coupon radius of curvature in inches
Curvature [in^{-1}]	Coupon curvature
Max Moment [lb-in]	Maximum moment applied to coupon
Min Moment [lb-in]	Minimum moment applied to coupon
Bending Stiffness [lb-in]	Coupon bending stiffness
Bending Stiffness 5pt Avg. [lb-in]	Coupon bending stiffness averaged over 5 points to reduce the noise in the data
Analytical Displacement Angle	
Time [s]	Time of test in seconds
Phi/2 [rads]	Analytical deflection angle in radians
Phi/2 [degs]	Analytical deflection angle in degrees

The measured angle data taken from profile video tracking the angle arm is processed by turning the video into images and processing those in VIC2D to track the angle of the specimen in real time. The measured angle data is then compared to calculated data from the MATLAB script analysis and plotted.

Table 3: Angle arm experimental deflection angle tracking output

Experimental Displacement Angle	
File Number	Index
Approx time	Time of test in seconds
Phi/2 (rad)	VIC2D output of deflection angle in radians
Phi/2 (deg)	Deflection angle in degrees

Being categorized as "high strain composites," the strain progress and strain-to-failure properties are of the most interest. The Digital Image Correlation software uses two high resolution stereo cameras each to create a three-dimensional video of the coupon from images taken during testing. The DIC analyzes the images to track and map the strain response of the specimen in real time. Each software package, VIC3D and Aramis, tracks a side of the specimen to see the response and crack initiation on the compression and tension sides. The strain of interest is in the axial direction, ϵ_{11}. The Aramis software categorizes the strain in stage points along the specimen by tracking the speckle pattern painted on the coupon. Four-to-five stage points are selected along the midplane of the specimen to track the maximum strain throughout the test (see Figure 10a). The four-to-five strain points exported from Aramis as Epsilon Y are averaged for a comprehensive strain reading through the test. Most of the Aramis data was taken from the tension side of the specimen. The VIC3D also tracks the specimen through the speckle pattern on the specimen but the output strain is selected in a rectangular region of interest at the midplane of the specimen (see Figure 10b). VIC3D exports the desired strain as eyy[1]-engr which is then converted to a strain percentage.

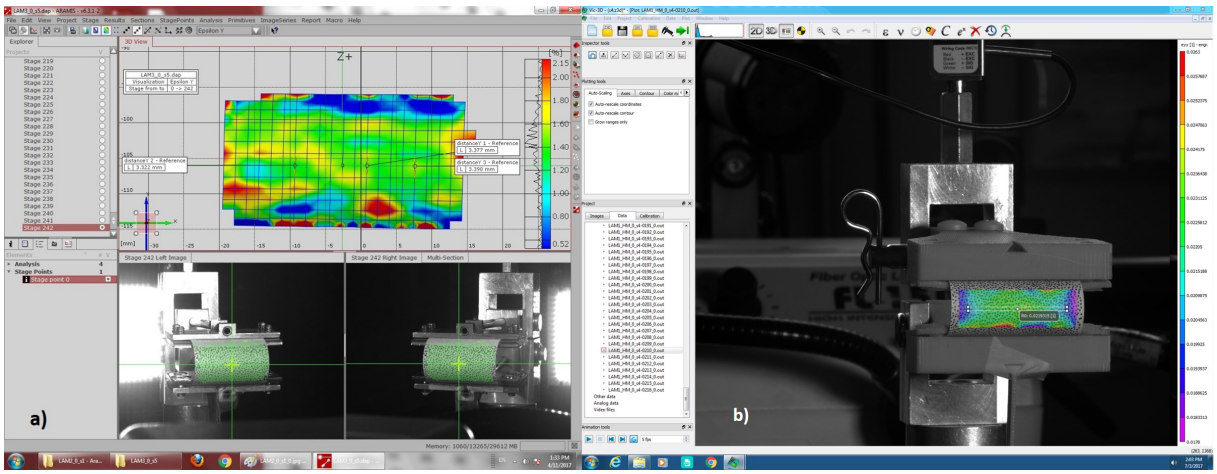

Figure 10: DIC software strain selection a) Aramis (LAM3_0_s5) and b) VIC3D (LAM1_0_s4)

The strain data captured by the DIC systems is then compared for all samples and orientations for trends and to build a comprehensive strain response for each laminate and material. It should be noted that both DIC systems were not used for all samples tested.

From test observations, DIC data, and the processed raw data through the MATLAB script

analysis, a rough picture of the laminate's material properties can be drawn. The material properties of all samples are compared to build a characterization profile for each laminate. The maximum moment, maximum curvature, and bending stiffness trends and nonlinearities are statistically correlated to draw conclusions about the material for subsequent use in deployable booms and structures.

Table 4: List of test observations and raw material properties from processed data

- Failure Location
- Failure Description
- Smooth side in tension or compression and material of smooth side (i.e. PW or UD)
- Grip Separation
- Compressive Side Initial Failure
  - Frame #
  - Strain %
- Tensile Side Initial Failure
  - Frame #
  - Strain %
- Minimum Diameter
- Maximum Failure Moment
- Initial Bending Stiffness
- Final Bending Stiffness

The full MATLAB script for data processing and subsequent analysis can be found in Appendix B.

Chapter 4: Column Bend Test Campaign 1 Data Analysis and Results

4.1 Materials and Laminates

4.1.1 Fiber and Matrix Materials

High strain composites are composed of thin-ply materials. Thin-ply composites are categorized by the cure ply thickness (CPT). Thin-ply CPTs are below 0.065mm for unidirectional materials, noted as UD going forward, and around twice that for plain weave fabrics, noted as PW. Traditional composites possess UD material with a standard ply thickness and a CPT of approximately 0.125mm, so thin-ply materials live up to their name, significantly. With a growing interest in thin-ply composites and HSC materials, commercially available prepregs and dry fabrics are now available with ply thicknesses as thin as 0.015mm for UD materials and 0.050mm for weaved fabrics.[23] Thin-ply composites hold potential for reducing structural mass and increasing performance when compared to standard-ply-thickness laminates in terms of: resistance to micro cracking, resistance to delamination, improved damage tolerance, improved aging and fatigue resistance, reduced minimum-gauge thickness, and increased scalability.[23]

The common materials used in boom and composite structures at NASA Langley were explored. To understand the building blocks for future composite work, a high tenacity plain weave fabric and an intermediate modulus unidirectional fiber pre-impregnated with the same epoxy resin matrix were used for all composite panels tested in campaign 2. The dry plain weave material, HTA40, provided by The Composites Store is a spread tow fabric making it ideal for HSC purposes. Spread tow fabric is a type of lightweight fabric whose production involves spreading a tow into thin and flat unidirectional tape and weaving the tapes to a woven fabric. The technique for manufacturing spread tow fabric increases the mechanical properties of the material and reduces the weight of future composites. As tenacity is the resistance to breaking and analogous to specific strength, the high tenacity fabric is optimal for the high strength yet low weight requirement for space structures. The unidirectional material, MR60H, provided by Oxeon is pre-impregnated (prepregged) with PMT-F7 epoxy resin by the manufacturer. The intermediate modulus composites were originally developed for the aerospace industry to provide

high tensile strength yet meet rigid weight requirements. The MR60H fiber is utilized heavily in deployable boom research and production at NASA Langley Research Center. The MR60H UD fiber is prepregged by the manufacturer however, the HTA40 PW fabric is prepregged at NASA Langley Research Center. The epoxy resin matrix infused into the HTA40 PW is the same as the MR60H UD, PMT-F7 provided by Patz Materials & Technologies. Resin film PMT-F7 is a latent 350°F curing epoxy resin matrix featuring a very high resin modulus. All material data sheets can be found in Appendix C.

Table 5: Thin-ply composite material and properties used for testing in campaigns 1 and 2

Material (fiber/resin)	**Fabric Form**	**Roll Width (mm)**	**FAW (g/m^2)**
MR60H / PMT-F7	Unidirectional Spread Tow	50	38
HTA40 / PMT-F7	Plain Weave Spread Tow	1000	61

Material (fiber/resin)	**Ply AW (g/m^2)**	**Cured Ply Thickness (mm)**	**E_{11} (GPa)**
MR60H / PMT-F7	56	0.040±0.005	174.3
HTA40 / PMT-F7	90	0.067±0.005	75.9

Material (fiber/resin)	Compression ϵ_{11u} (%)	**Vendor (fiber/resin)**	**Prepregged by**
MR60H / PMT-F7	1.1	Oxeon / Patz	Patz
HTA40 / PMT-F7	1.03	The Composites Store / Patz	NASA

4.1.2 Laminates

Large panels of each layup and laminate were fabricated and cut into flexure coupons of desired dimensions and orientations. For test campaign 1, six different layups and three different materials were tested in two-to-three different orientations. Unidirectional carbon fiber laminate (CUNI), 9 plies, was bent in the 0° direction and the +45° direction.. Carbon fiber plain weave laminate (CPW), 8 plies, was tested in the 0° direction (i.e. 0-90 weave) and the +45° direction (i.e. ±45 weave). Four different laminates were fabricated with the unidirectional and plain weave lamina. The carbon fiber plain weave will be noted with angle and PW going forward, i.e. 45PW is one ply of ±45° weave and 0PW is a 0°-90° weave. The unidirectional lamina will be simply noted with the fiber orientation angle. Laminate 1, noted as LAM1, is the only sym-

metrical laminate, [45PW$_2$/0$_2$/45PW$_2$]. Laminate 2, noted as LAM2, is [45PW$_3$/0$_3$]. The third laminate, LAM3, is comprised of plain weave exclusively as [45PW$_3$/0PW$_3$]. The fourth, LAM4, is [45PWaq$_3$/0PWc$_3$] with the difference between LAM3 and LAM4 being that the $\pm$45^{o}PW plies in LAM4 are astroquartz, not carbon fiber. To gather the complete material property profile of each material, all laminates were tested in the 0^o and 45^o orientations with LAM1 also being tested in the 90^o orientation. The 0^o direction provided axial bending stiffness, D$_{11}$, and the 90^o provided the transverse, D$_{22}$. Each laminate was also tested varying which side was in compression and which in tension as that has significant affect on the material's performance.

4.2 Test Campaign 1 Data Analysis

Campaign 1 provided a robust data set with plenty of properties to explore and validate. It was discovered after processing the data that at some unknown point throughout testing the load cell in use was damaged and the data corrupted. The data that were most affected were the LAM1 and CUNI samples. As discussed above, it was also discovered that the load cells were not calibrated properly for testing. All data was adjusted with the appropriate factor as per the procedure explained in section 3.1.1. After all data was processed it was categorized, evaluated, and interpreted to determine the material properties of each laminate. Tables 5 and 6 show the average values of all evaluated properties for the data from campaign 1. The complete compilation of all of the data analysis for campaign 1 can be found in Appendix D.

Table 6: Average of experimental data for all of campaign 1 (T: Tension; C: Compression)

Laminate	**Orientation**	**Max Moment [N-m]**	**Min Diameter [mm]**	**Initial Bending Stiffness [N-m]**	**Final Bending Stiffness [N-m]**	**Change in Bending Stiffness [%]**
CPW	0	0.5781	51.7	0.5659	0.5433	-3.994
CPW	45	0.411	32.0	0.2068	0.3141	51.886
CUNI	0	1.6169	25.1	0.7203	0.7739	7.441
CUNI	45	0.0696	51.9	0.0557	0.1548	177.917
CUNI	90	0.2784	47.8	0.2373	0.2486	4.762
LAM1	0	0.0724	15.6	0.0254	0.0078	-69.291
LAM1	45	0.168	25.4	0.0565	0.1186	109.912
LAM1	90	0.1534	23.8	0.072	0.0932	29.444
LAM2	0	0.913	12.9	0.226	0.2147	-5.000
LAM2	45	0.1139	11.7	0.0287	0.0373	29.965
LAM3	0	0.1685	30	0.0621	0.1149	85.024
LAM3	45	0.1131	28.6	0.0467	0.1007	115.632
LAM4	0	0.1319	22.3	0.0497	0.0563	13.280
LAM4	45	0.153	18.6	0.0446	0.0482	8.072
Laminate	**Orientation**	**Max Moment [lb-in]**	**Min Diameter [in]**	**Initial Bending Stiffness [lb-in]**	**Final Bending Stiffness [lb-in]**	**Change in Bending Stiffness [%]**
CPW	0	5.1163	2.0352	5.0083	4.8083	-3.993
CPW	45	3.638	1.2606	1.83	2.78	51.913
CUNI	0	14.3105	0.9898	6.375	6.85	7.451
CUNI	45	0.6157	2.0433	0.4933	1.37	177.721
CUNI	90	2.464	1.8805	2.1	2.2	4.762
LAM1	0	0.6405	0.6125	0.225	0.069	-69.333
LAM1	45	1.4866	0.9994	0.5	1.05	110.000
LAM1	90	1.3578	0.9355	0.6375	0.825	29.412
LAM2	0	8.0805	0.5075	2	1.9	-5.000
LAM2	45	1.0078	0.4622	0.254	0.33	29.921
LAM3	0	1.4917	1.1797	0.55	1.0167	84.855
LAM3	45	1.0008	1.1252	0.4133	0.8917	115.751
LAM4	0	1.167	0.8762	0.44	0.498	13.182
LAM4	45	1.3545	0.734	0.395	0.4267	8.025
Laminate	**Orientation**	**Grip Separation [in]**	**Grip Separation [mm]**	**Compressive Failure Strain [%]**	**Tensile Failure Strain [%]**	**Approximate Slope of Bending Stiffness vs Curvature Response [N-m^2]**
CPW	0	1.7	43.18	0.857	0.898	0
CPW	45	1.5	38.1	1.838	1.272	0.0015
CUNI	0	1.35	34.29	2.057	1.62	0
CUNI	45	1.95	49.53	1.077	0.68	0.0024
CUNI	90	0.95	24.13	1.271	1.114	0
LAM1	0	0.7	17.78	1.4	1.89	-0.00009
LAM1	45	1.1	27.94	1.845	1.247	0.0007
LAM1	90	0.9	22.86	1.825	1.42	-0.0001
LAM2	0	0.55	13.97	3.8	2.95	0 if UD in C/ -0.0006 if UD in T
LAM2	45	0.55	13.97	N/A	1.614	0.0002 if UD in C/ -0.0002 if UD in T
LAM3	0	1.3	33.02	1.528	N/A	0.0006 if 0PW in C/ 0.0009 if 0PW in T
LAM3	45	1.2	30.48	1.546	0.962	0.0009 if 45PW in C/ 0.0006 if 45PW in T
LAM4	0	0.7	17.78	1.616	1.012	-0.0005 if 45PWaq in C/ 0.0001 if 45PWaq in T
LAM4	45	0.55	13.97	2.336	1.254	2nd order polynomial

Table 7: Average observed failure for all of campaign 1 testing (C: Compression; T: Tension)

Laminate	**Orientation**	**Failure**
CPW	0	Crack in 90° direction, C side
CPW	45	±45° zigzag crack, C side
CUNI	0	Broke close to the center, sheared off at one grip
CUNI	45	2 piece failure in ±45° direction
CUNI	90	Snapped into multiple pieces; 90° crack near grips
LAM1	0	±45° zigzag crack, C side
LAM1	45	Crack in 90°, C side, central region, through width
LAM1	90	Crack ±45° zigzag, C side
LAM2	0	Crack ±45° zigzag, C side, some delamination on edges
LAM2	45	Crack in ±45°, C side
LAM3	0	Crack in ±45° zigzag, C side if 0-90PW in T/crack in 90°, C side if 0-90 in C
LAM3	45	Crack in ±45° zigzag, C side if 0-90PW in T/crack in 90°, C side if 0-90 in C
LAM4	0	Crack in 90°, C side
LAM4	45	±45 zigzag crack , C side if ±45PWc in C/crack in 90°, C side if ±45PWc in T; Mid Bending Stiffness higher than initial and final BS for all

For campaign 1, the coupon grip separations were varied numerous times to find close to the 90° bend failure point for each laminate and in search of the ideal and optimized gauge length. These variations, though usually small, affect the data and make true one-to-one comparison difficult. It can be seen from that data that there is clear correlation between material and whether it is in tension or compression, coupon thickness, grip separation, and the material properties gleaned from the test. Figures 13, 14, 16 are samples of successful failures for each laminate tested in campaign 1.

4.2.1 Bending Stiffness

The CPW coupons, in the 0° direction, or 0-90PW, show a fairly linear M-κ curve that results in an almost constant bending stiffness throughout the tests (see Figure 11), while the ±45PW CPW coupons, or those in the 45° direction, seem to have a near linear, with a shallow slope (approximately 0.0015 N-m^2), increase in bending stiffness as curvature increases, indicative of a nonlinear response in the M-κ curve (see Figure 12b). Fracture patterns are as expected, failing on the compression side of each specimen with a zigzag or jogging pattern depending on fiber direction. For the ±45PW CPW coupons, fiber fracture is in a ±45 zigzag pattern and the 0-90PW coupons fail along the midplane in the 90° with interruptions in the crack at the 0° fibers of the weave (see Figure 13a).

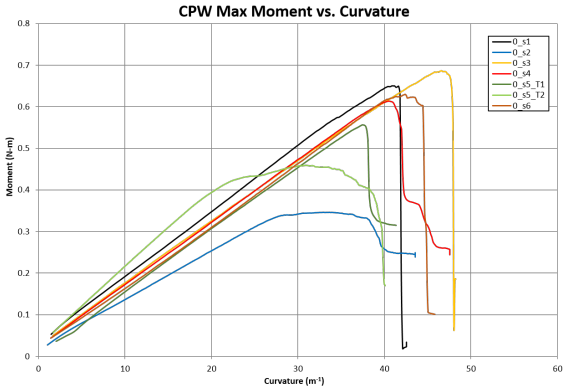

(a) Maximum moment vs curvature, κ for CPW at 0° fiber orientation

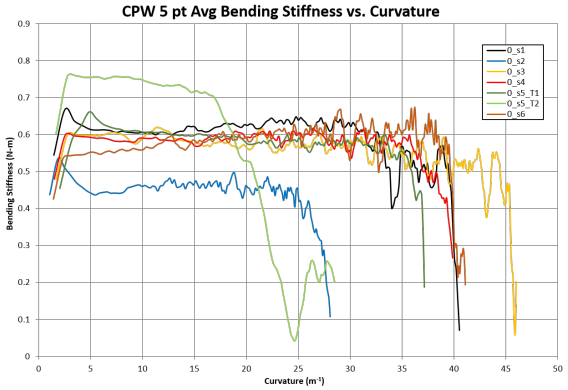

(b) 5pt Avg bending stiffness, D_{11}, vs curvature, κ

Figure 11: Maximum moment, M_{max}, and bending stiffness, D_{11} vs curvature, κ for CPW at 0° fiber orientation

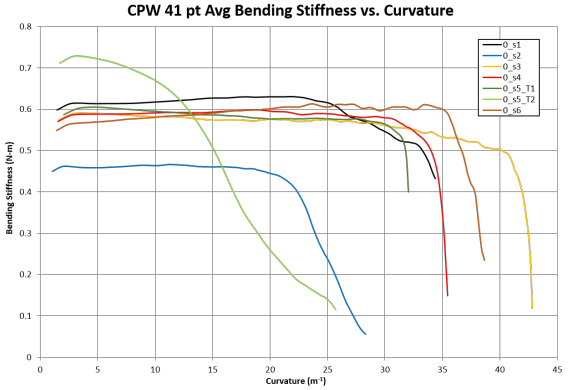

(a) Bending stiffness, D_{11}, vs curvature, κ for 0°

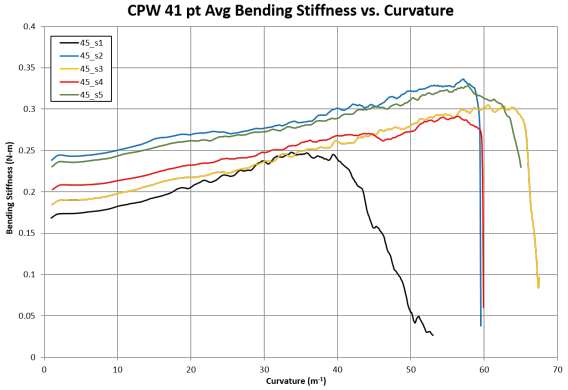

(b) Bending stiffness, D_{11}, vs curvature, κ for 45°

Figure 12: 41pt Average bending stiffness, D_{11} vs curvature, κ for CPW at a) 0° and b) 45° PW fiber orientation

Much like the CPW coupons, the CUNI, 0° direction samples have a fairly linear M-κ curve and an almost constant bending stiffness while those in the 45° direction have an approximately linearly increasing bending stiffness as the test progresses, at a slope of 0.0024 N-m^2. The CUNI, 90° samples behave similarly to the 0° with a nearly constant bending stiffness. Fracture of the CUNI coupons is generally abrupt and in the fiber direction: the CUNI split along the fiber direction often causing two piece, or more, failure. The 45° and 90° coupons snap along the 45° and 90° directions respectively. The 0° coupons split in the 0° direction but as the coupon is clamped at the end of the coupon, the cracks are arrested or the fibers fail at the grips.

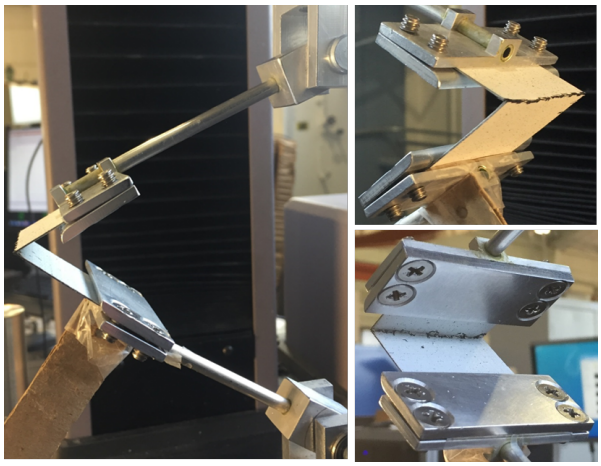

(a) Broken coupon CPW $[0PW]_8$, sample 3, orientation 0^o

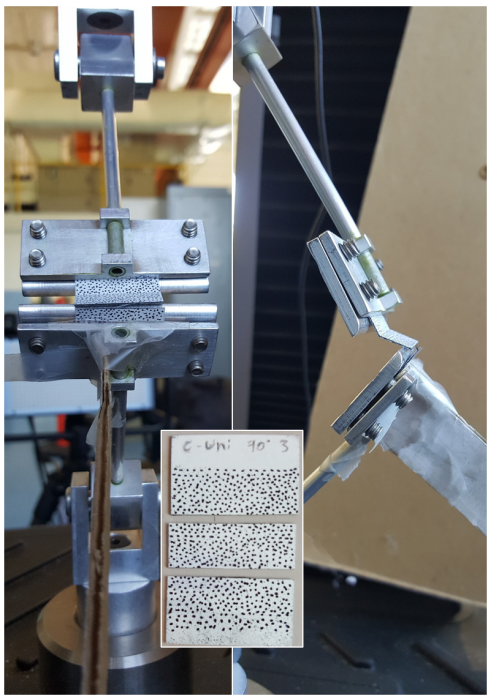

(b) Broken coupon CUNI $[0]_9$, sample 3, orientation 90^o

Figure 13: Test campaign 1 broken coupons a) CPW and b) CUNI

The LAM1, $[45PW_2/0_2/45PW_2]$, data is questionable as the load cell was damaged but the trends are similar to that of the CPW and CUNI which makes sense as it is a symmetrical laminate composed of the CPW and CUNI lamina. The numbers may be off but the observations are sound. With the CPW lamina on the outside surfaces of the laminate, failure looks similar to the CPW coupons. LAM1, 90^o and 0^o both have ± 45PW as the outside four lamina, so the fiber failure is visible as a $\pm 45^o$ zigzag crack on the compression side. LAM1, 45^o, has 0-90PW as the top and bottom surfaces so visible cracking is along the 90^o direction on the compression side (see Figure 14a). All three directions tested have a seemingly linear bending stiffness response though some increasing and some decreasing. While this requires more testing, it is apparent that there is a nonlinear response in the moment vs curvature relation.

LAM2 is not symmetric as it is comprised of PW and UD lamina laid abreast, $[45PW_3/0_3]$. With this in mind, the bend orientation, which side PW or UD is in compression, has a drastic effect on the laminate performance. For LAM2 with the UD in both the 0^o and 45^o directions, the bending stiffness is stiffer when the MR60H UD is in compression and the HTA40 PW in

tension. For LAM2, 0°, the bending stiffness is near constant for the UD in compression, with a slope 0f -0.00008 N-m^2, but has a slight linear decrease, slope of -0.0002 N-m^2, when the UD is in tension. In the LAM2, 45° with the 0-90PW in tension (UD compression), the coupons have a minor linear increase in bending stiffness as curvature increase, with a slope of 0.0002 N-m^2. With the 0-90PW in compression, the bending stiffness has a slight linear decrease as curvature increases, slope of -0.0002 N-m^2. The moment vs curvature response of LAM2 is clearly nonlinear for both orientations and bend directions.

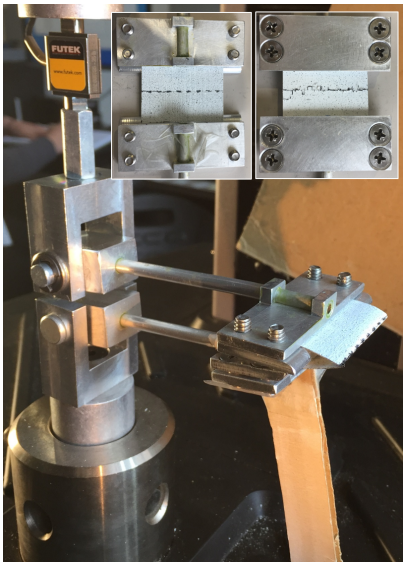

(a) Broken coupon LAM1 [45PW$_2$/0$_2$/45PW$_2$], sample 5, orientation 45°, smooth side in tension/rough side in compression

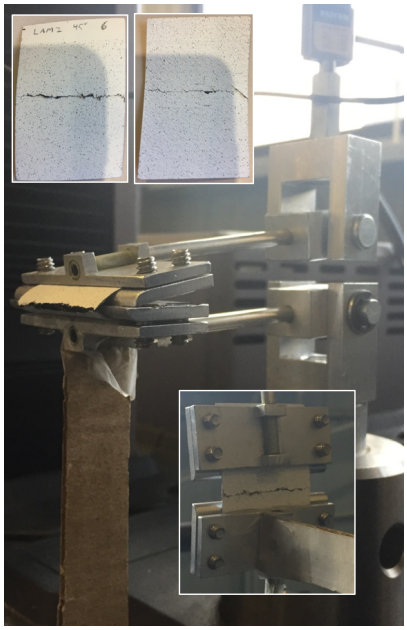

(b) Broken coupon LAM2 [45PW$_3$/0$_3$], sample 6, orientation 45°, ±45 PW (smooth) in tension/0° UD (rough) in compression

Figure 14: Test campaign 1 broken coupons a) LAM1 and b) LAM2

LAM3 and LAM4, [45PW$_3$/0PW$_3$], are the same composite layup but with different materials. Both are comprised of entirely spread tow plain weave material with LAM3 being all carbon fiber and LAM4 being a combination of carbon fiber and astroquartz. For both materials the bend direction dictates fracture patterns and crack propagation, though much more severely in the LAM4 laminate. Both fiber orientations tested 0° and 45° for LAM3 are redundant. The driving factor for this laminate is which PW orientation is in compression and which in tension.

When the 0-90PW side is in tension, ±45PW in compression, the bending stiffness has a steeper linear trend, with a slope of 0.0009 N-m^2, as when the 0-90PW is in compression, with a slope of 0.0006N-m^2, though both result in similar stiffnesses at the end of the test. As expected, the material is stiffer when 0-90PW is in compression, as the HTA40PW fabric is stiffer in the 0^o direction than in the 45^o due to the fibers being in the loading direction when in the 0^o orientation. Failure, again, was due to fiber fracture along the compression side of the coupons. The direction of the crack was dependent on which PW was in compression: if 0-90PW in compression then a 90^o crack propagated; if the ±45PW in compression then a ±45^o zigzag crack was the failure mechanism. An example of LAM3 coupon failure can be found in Figure 16a.

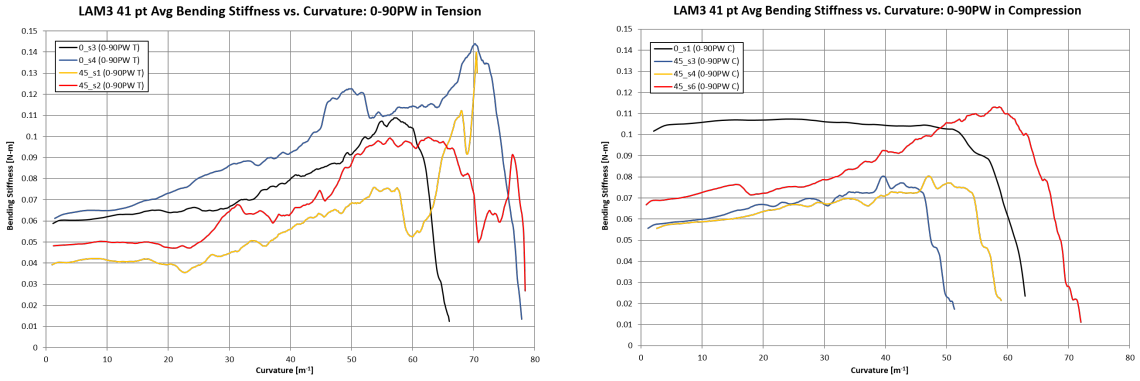

Figure 15: 41pt Average bending stiffness, D_{11} vs curvature, κ for LAM3 with the 0-90PW plies in tension or compression

For LAM4, the astroquartz, ±45PWaq for the 0^o direction and 0-90PWaq for the 45^o direction was the driving factor in laminate performance. Due to the vastly different properties between the astroquartz and carbon fiber materials, delamination was a big contributor to laminate failure. When the astroquartz fabric was in a 0-90PW weave (LAM4 in the 45^o direction), the bending stiffness was drastically nonlinear, sloping upward to a peak value and then decreasing back to almost the initial value at the end of the test. It is suspected that the decrease prior to visible failure is cracks forming or delamination starting, so actually the true material failure. Visible failure was all on the compression side while distorting the tension side. The fiber failure was driven by the weave in compression 0-90PW resulting in 90^o cracking or ±45PW resulting in ±45^o zigzag cracking. With the ±45PWaq, the bending stiffness had an approximately linear trend as curvature increased, with a minor increase, slope of 0.0001 N-m^2, as the ±45PWaq was

in tension and decreasing when in compression, slope of -0.0005 N-m^2. An example of LAM4 coupon failure can be found in Figure 16b.

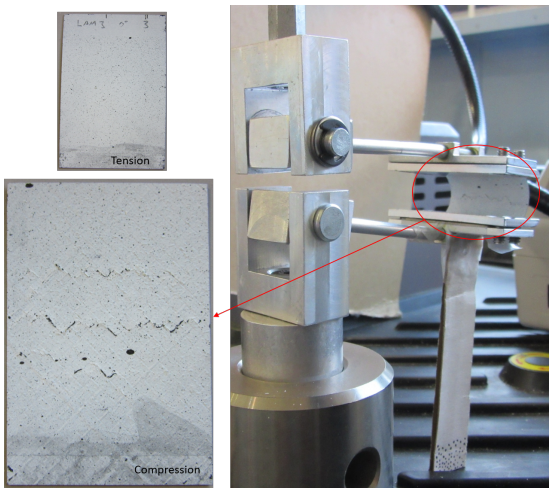

(a) Broken coupon LAM3 [0PWc$_3$/45PWc$_3$], sample 3, orientation 0°

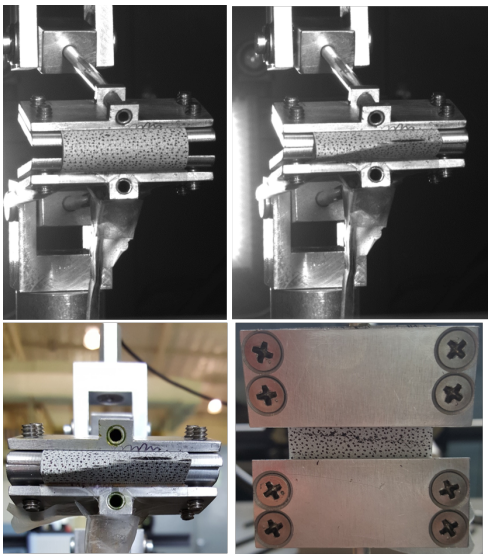

(b) Broken coupon LAM4 [0PWc$_3$/45PWaq$_3$], sample 3, orientation 45°

Figure 16: Test campaign 1 broken coupons a) LAM3 and b) LAM4

4.2.2 Strain

As previously mentioned, DIC optical methods and equipment were used to measure the full-field strain at both sides of the thin flexures. For most of campaign 1, Aramis was used for tracking the tension side and VIC3D, the compression.

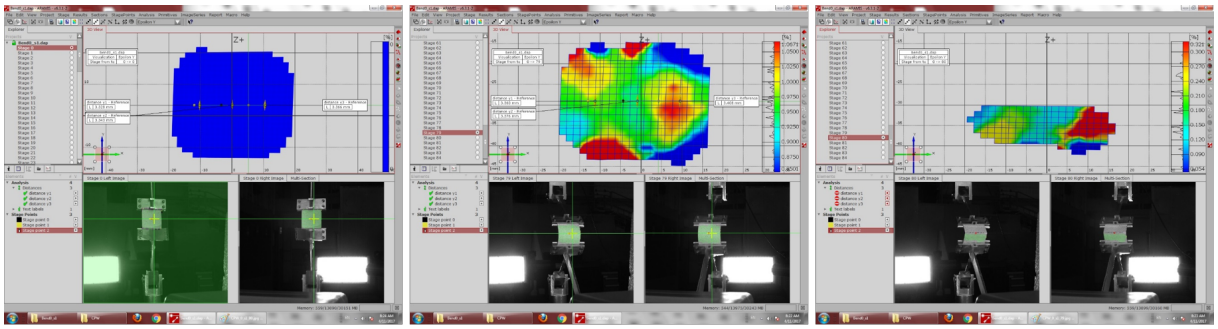

a) b) c)

Figure 17: Aramis calculated strain on the tension side of CPW coupon 1, orientation 0° at a) start of test, b) the frame immediately before failure, and c) at failure

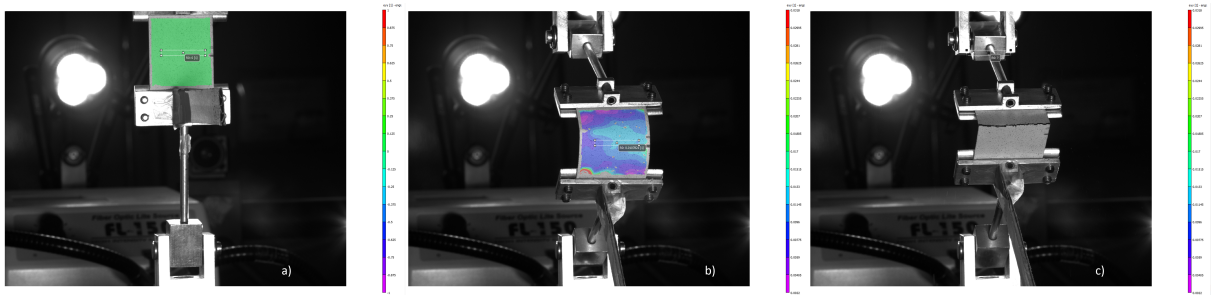

Figure 18: VIC3D calculated strain on the tension side of CPW coupon 3, orientation 0° at a) start of test, b) the frame immediately before failure, and c) at failure

Figure 19 shows the strain values throughout the test for one of the CUNI coupons, sample 3, 0° orientation. Given the rotational kinematics of the CBT, the strain vs time curve is not linear as shown in Figure 19a. However, as expected for this material and direction tested, the strain vs curvature curves are fairly linear over the test, particularly for the compressive side (see Figure 19b). The measured strains at failure were 2.1% and 1.4% for the compression and tension sides, respectively, with the coupons suffering from fiber tensile fracture. Both of these values differ from what would be expected from considering the fiber manufacturer's data sheet for much thicker coupons tested under pure compression and tension, which have a strain-to-failure of 1.0-1.1% and 1.6-1.7%, respectively. The significant differences in strain values obtained at both surfaces of the coupon is thought to be related to the shift in neutral axis that the specimen experiences during the large deformation bending test, as a result of fiber material nonlinearities at higher strains. As the tensile side stiffens and the compressive side softens at high strains, the neutral axis moves towards the tension side, and thus the distance to the surface under tension

diminishes, resulting in smaller strains when compared to the surface under compression. Thus, being able to distinguish these strains is critical in accurate performance predictions of the material. The vertical test nature of the CBT when compared to other test methods proves to be helpful for capturing the distinct behavior of the flexure at both of its sides.

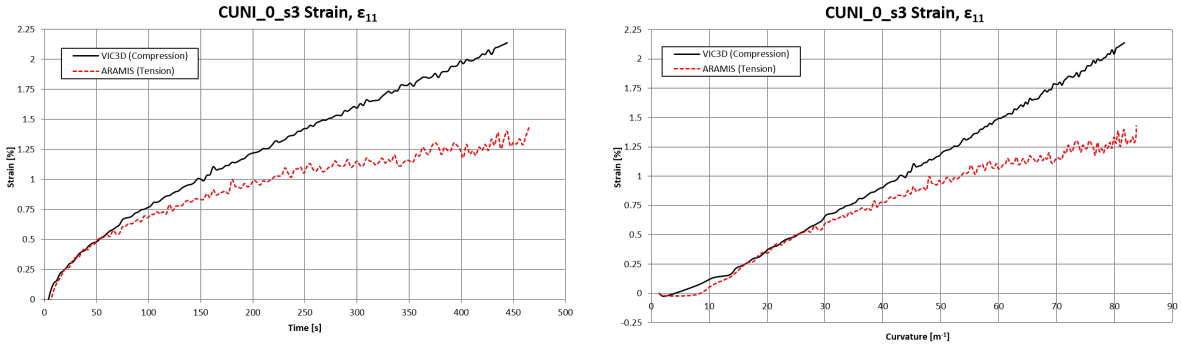

(a) Axial strain, ϵ_{11} [%] vs. time [sec]

(b) Axial strain, ϵ_{11} [%] vs. curvature, κ [m^{-1}]

Figure 19: Surface axial strain, ϵ_{11}, at both sides of a CUNI, $[0]_9$, coupon vs (a) test time, and (b) curvature, κ.

The strains observed for each laminate can be found in Table 7 below.

Table 8: Average surface axial strain at failure, ϵ_{11}, observed for all laminates tested in campaign 1 in both tension and compression where applicable

Laminate	**Orientation**	**Compressive Failure Strain [%]**	**Tensile Failure Strain [%]**
CPW	0	0.857	0.898
CPW	45	1.838	1.272
CUNI	0	2.057	1.620
CUNI	45	1.077	0.680
CUNI	90	1.271	1.114
LAM1	0	1.400	1.890
LAM1	45	1.845	1.247
LAM1	90	1.825	1.420
LAM2	0	3.800	2.950
LAM2	45	–	1.614
LAM3	0	1.528	–
LAM3	45	1.546	0.962
LAM4	0	1.616	1.012
LAM4	45	2.336	1.254

Chapter 5: Coupon Fabrication and Test Fixture Modification

The second test campaign was performed as a more detailed look into the simplest composite laminates at thicknesses that better represented deployable boom structures. The materials used are the same as those in campaign 1: intermediate modulus unidirectional carbon fiber, MR60H, high tenacity plain weave fabric, HTA40, and high modulus epoxy resin, PMT-F7. Large sheets of each layup and laminate were fabricated and cut into flexure coupons of desired dimensions and orientations. For test campaign 2, three different layups and two different materials were tested in three-to-four different orientations. Unidirectional carbon fiber laminate, CUNI, 4 plies, was bent in the 0^o direction, the 90^o direction, the $+45^o$ direction, and the -45^o direction. Carbon fiber plain weave laminate, CPW, 3 plies, was tested in the 0^o direction (i.e. 0-90 weave), the 90^o direction (though the same as the 0^o direction), and the 45^o direction (i.e. ± 45 weave). Laminate 1 (LAM1), $[45PW_2/0_2/45PW_2]$, was retested at 6 plies as the original data from campaign 1 was affected by a damaged load cell. Once again, to gather the complete material property profile of the material, LAM1 was tested in the 0^o, 90^o, $+45^o$, and -45^o orientations. All laminates tested in campaign 2 are symmetrical so varying the sides in compression or tension was not necessary. In campaign 1, each laminate had a rough side (vacuum bag) and a smooth side (caul plate) due to the curing process. For the fabrication of campaign 2, top and bottom caul plates were used so each side of each laminate has a smooth surface finish further eliminating the need for observation of which side experienced which form of loading.

5.1 Panel Fabrication and Coupon Preparation

The raw materials listed above had to be prepared, the composite panels fabricated, cured, and cut for testing to proceed. The spools of dry fabric, HTA40 PW, were cut to ply panels of appropriate size using an Eastman M9000 Static Table Cutting System (see Figure 20). For the CPW, 3 ply panel, 3 14"x14" square panels at 0-90^o were cut. For the LAM1, 6 ply panel, 4 12"x24" rectangular panels at $\pm 45^o$ were cut.

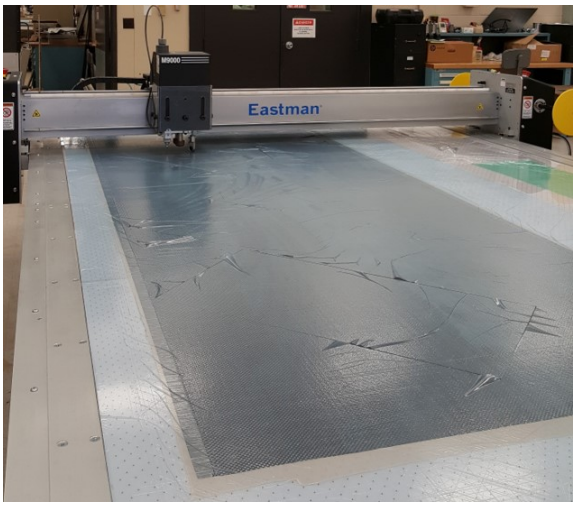

Figure 20: Eastman ply cutter cutting dry plain weave fabric into correct ply panel size and fiber orientation

The next step is to pre-impregnate, colloquially referred to as 'prepregging', the dry HTA40 PW panels with PMT-F7 epoxy resin. This process is rather tedious but entirely necessary for composite manufacturing. With the pre-cut HTA40 PW panels, a strip of the resin film material is cut to the same length. Unfortunately the width of the resin film roll was not the same as the width of the HTA40 PW panels so multiple strips of the resin film were needed to fill the width of the dry fabric panel. The dry fabric panels were placed onto resin film strips and a hot iron was briefly swept over the panel to activate the resin flow and create tackiness to allow the dry fibers and resin to adhere together. The pair was then placed in a Digital Knight DK20S 16x20 swing-away heat transfer press and pneumatically pressed for 2.5 minutes at 210°F. The manufacturer prepregged MR60H UD strips were simply cut to panel length for future panel layup.

Figure 21: Cutting resin film to panel length for prepregging dry fiber plain weave panels with epoxy resin

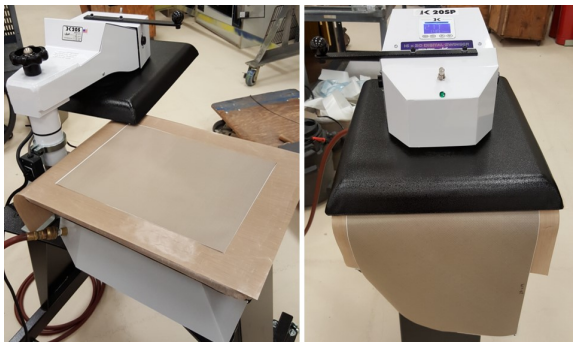

Figure 22: DK20S Press pre-impregnating dry fiber plain weave panels with epoxy resin

Once all dry fibers are prepregged and UD material cut to size, the panels are ready for manual layup. Each composite panel was hand laid up to the specific laminate layup. As mentioned above, the HTA40 PW plies were cut to rectangles to fit under the necessary caul plates and the MR60H UD material was cut to length with the tape width being prescribed by the manufacturing of the fibers. The prepregged UD strips were laid coincident across the width to fill out the plate width. The panels were laid up on the autoclave tool, covered with a caul plate to the specified dimensions, bagged and placed under vacuum at 29inHg. The vacuum pressure was held overnight to pull out all air and continually compress the hand layup, at about 14.7 psi, to draw out any errors from the manual layup process. The panels were then cured in the autoclave under 29inHg (14.7 psi) vacuum and at a constant pressure of 3 psi with temperature ramping to 350^{o}F to cure the composite. The panels were cured at 3 psi, as opposed to a higher pressure, to replicate the curing process of the deployable boom structures. The autoclave cure cycle can be seen in Figure 26.

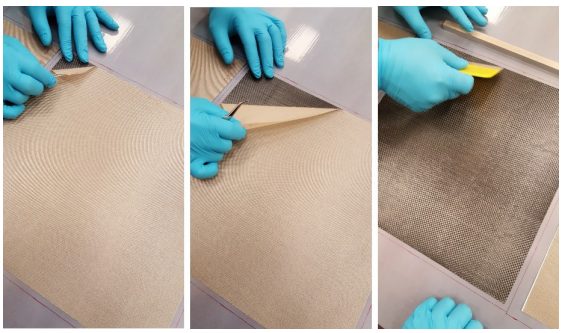

Figure 23: Manual laying up prepregged HTA40 PW for CPW panel

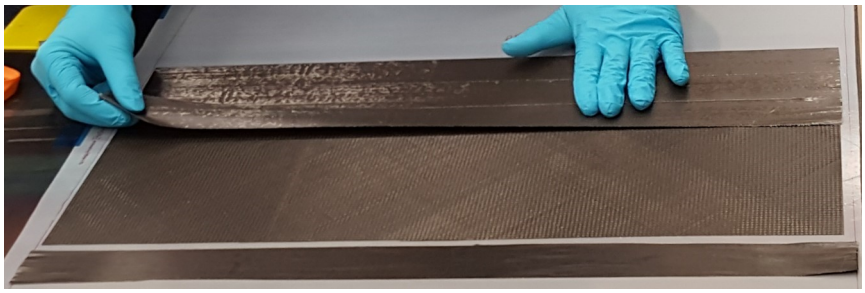

Figure 24: Manual laying up prepregged MR60H UD strips to create LAM1 composite panel

Figure 25: Panels held under vacuum prior to curing in the autoclave

(a) Pressure, vacuum, and temperature profiles

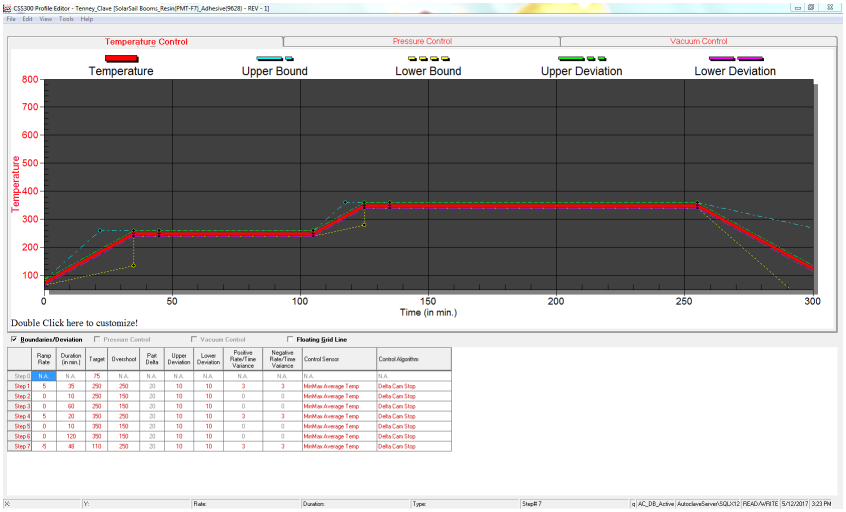

(b) Temperature ramp rates and bounds

Figure 26: Autoclave cure cycle for composite panels

After cure, the panels were removed from the autoclave and the extra resin was sanded off the end and the panels were cleaned and prepared for cutting. It was noticed after cure that the CUNI, 4 ply MR60H UD panel did not have great cohesion; the laminate seemed to be trying to be in UD strips rather than a solid panel. The resin did not flow enough during cure to join the UD strips together. Working with such thin panels was a challenge: even after cure the panels felt rather flimsy. A new half-bond staggering process will be used when fabricating other panels to avoid seams or weakness points between the manually placed tape in the final product.

The extreme thinness of the composite panels also proved to be quite a challenge for cutting into the necessary coupon dimensions for the Column Bend Test (CBT). The requirements for the CBT coupons at such minimal thickness are 2" long by 1.5" wide (0.0508 x 0.0381 m) with a tolerance of 0.005"(about 0.1mm). The most important constraint is parallelism of all sides. As this is a bend test, the coupon edges must be perfectly square to one another to provide valid results. CNC cutting was not possible as the panels were far to thin, so manually run machines by skilled operators, NASA LaRC personnel, were necessary. Due to the minuscule thickness, the composite panels were sandwiched between two panels of G10 and cut. The G10 protected the composite panel from damage due to the saw blade or water lubrication during cutting as well as providing rigidity to prevent splitting or cracking or other damage of the composite panel during cutting. Due to the manual nature of the cutting, the panel drawings needed slight adjustments to fit machine and operator capabilities and for efficiency.

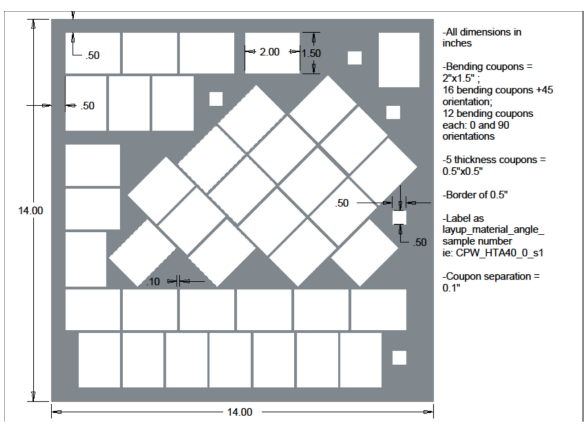

(a) Coupon cutting for CPW 14"x14" panel of 3 ply HTA40 PW

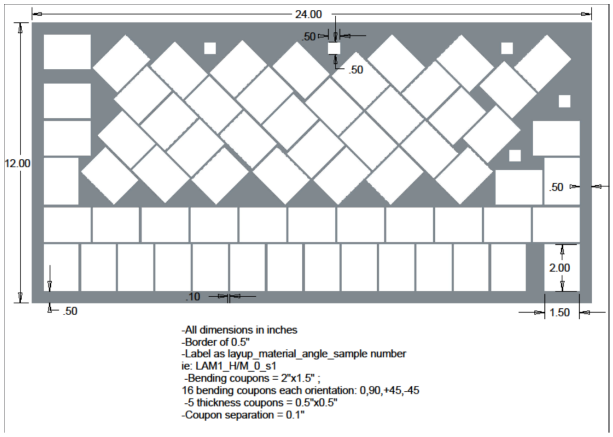

(b) Coupon cutting for CUNI and LAM1 12"x24" panels

Figure 27: Template drawings for coupon cutting from composite panels

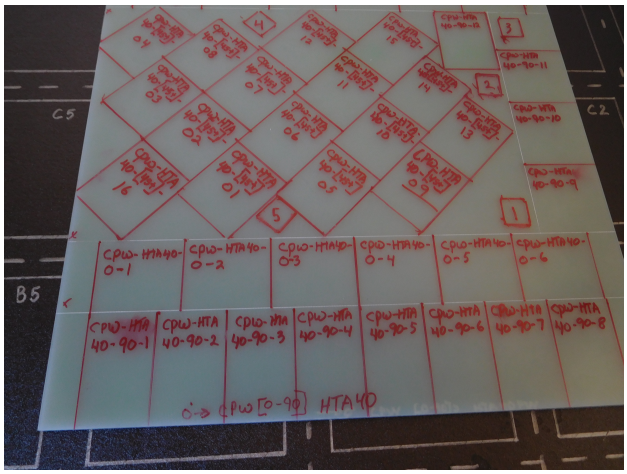

Figure 28: Coupon cutting plan operator adjustments

The G10 sandwich requirement caused a significant obstacle as the panel had to be re-taped and secured in the G10 after every subsequent cut. This intricate process, while slow, provided the tight tolerances and rigid constraints necessary for accurate bend testing with the CBT. A border of approximately 0.25" to 0.5" (approximately 6-13mm) was cut from the panels to avoid issues evident and more commonplace at the edges of the panels due to the manual layup. Space on each panel was optimized to get maximum and equal numbers of each fiber orientation (0,90,-45,+45) where possible. Five 0.5"x0.5" (12.7 x 12.7mm) squares were cut for micrographing and accurate thickness measurements from various locations on each panel. Each panel was photographed through cutting to allow for individual coupons to be traced back to a location on the panel if questions should arise.

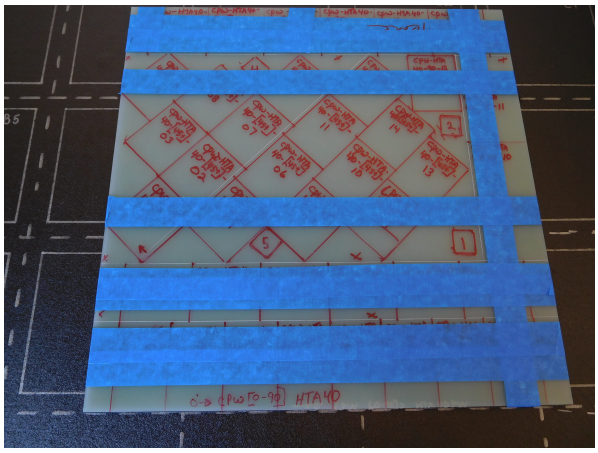

(a) Taping the G10 panels to maintain integrity of composite panel cutting

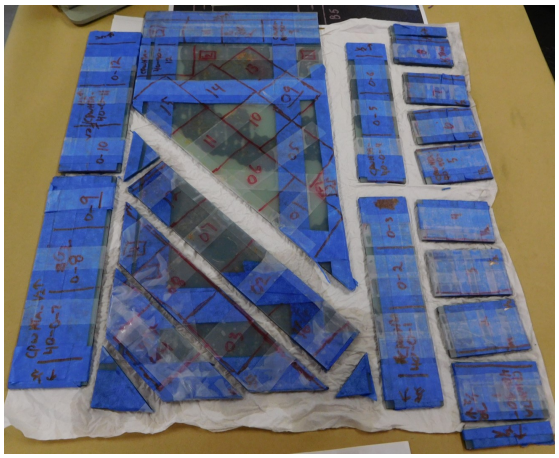

(b) Partially cut CPW panel

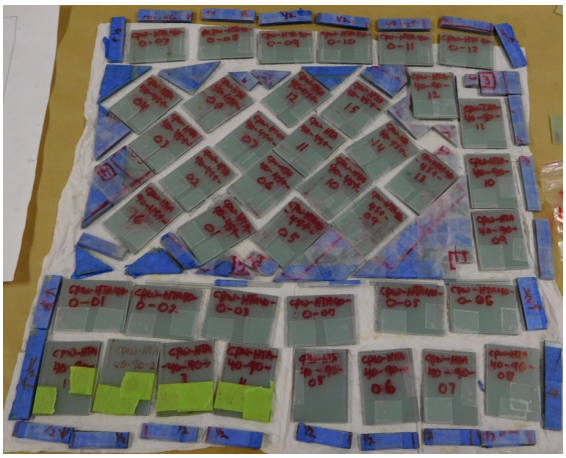

(c) Complete cut of CPW panel

Figure 29: Coupon cutting from composite panels

Once cut and cleaned, the individual CBT coupons were painted to allow for DIC imaging during testing. Both sides of each coupon were spray painted white with a flat white enamel and then subsequently speckled with a thin black Sharpie prior to testing for proper image capture and tracking. The Sharpie, as opposed to further painting or airbrushing, provided small enough black dots in a tighter pattern for optimal DIC capture.

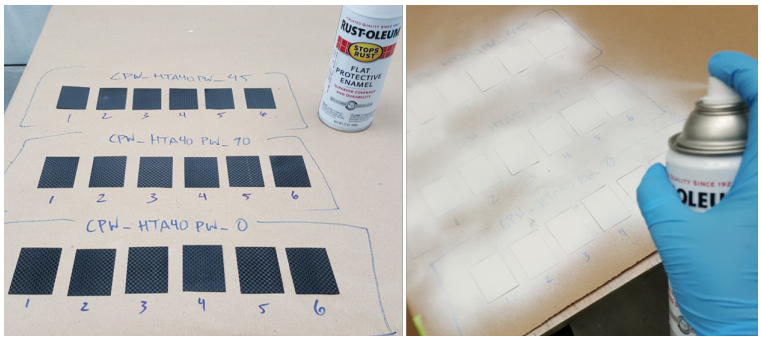

Figure 30: Coupon painting for DIC imaging

5.2 New Light Weight Fixture

The testing fixture has gone through a few iterations both in aluminum and various additive manufacturing polymers. The first fixture was made of aluminum and was too heavy. Due to the vertical orientation of the test, the fixture was prone to gravity loading, the arms produced their own moment obscuring the data for the composite coupons. The second iteration was still aluminum, with the same fasteners though significantly lighter. This fixture was used for the majority of the testing, all of campaign 1 and much of campaign 2, but it was limited in versatility. Since the initial procedure of the pure moment bending test method has been confirmed, adding a component to measure and track creep in the sample coupons is desired for future work. A new fixture was designed using Creo Parametric[49] to enable the sample to be removed from the load frame in the bent position, placed in a thermal chamber for viscoelastic relaxation testing using the Time-Temperature Superposition Principles[24], and then placed back in the load frame and unloaded to "flat." As these HSCs are vulnerable to creep, the creep response of the laminates is a very important property. While the removable feature of the new fixture was not explored in this thesis, the lighter weight of the fixture and the versatility it provided was utilized greatly for campaign 2.

As mentioned, the aluminum fixture is prone to gravity loading so a new fixture was explored, improving the test rig to make it lighter and make the compression side of the coupon more visible for the DIC software are higher flexure angles. Secondarily, the bent removal feature for the subsequent creep testing is not possible with the metal parts. With these requirements in mind, a new fixture was designed and printed with additive manufacturing for optimal design

and real-time updates and modifications. The new fixture has gone through seven iterations to date, though most were minor adjustments to update the original polymer fixture design. The seventh iteration was used for the plastic fixture testing for campaign 2 which was a large portion of the testing regime.

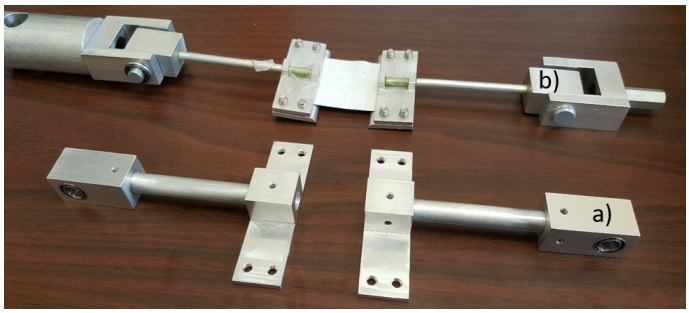

Figure 31: Aluminum CBT fixture a) initial "heavy" fixture and b) modified "light" fixture used in most of the testing

The first attempt at the new plastic fixture design was one continuous piece (actually two with the base plate) as opposed to the three pieces (four with base plate) fasted together to form the metal fixture. The design was based off of the dimensions of the larger "heavy" aluminum fixture with the most important consideration being weight savings. The fixture, v1, was printed in PLA (polylactic acid) plastic from an Ultimaker 3D printer with 40% infill for the body of the fixture and the angle tracking arm and 75% infill for the base plate that is fastened to the body and holds the composite coupon. The goal of significant weight savings from the "heavy" aluminum fixture was achieved. The new PLA fixture weight was calculated to be approximately 43.4g (not including the screws, fasteners, and bearings) versus the original fixture weighting 141.75g. The fixture was designed to use the same U-shaped head as the metal fixtures allowing for no disruption to the fixture connection to the MTS C43.504 test frame. The fixture is equipped with a clevis pin with clotter pin release to remove the fixture from the U-shaped head and the test frame easily. For future creep testing options slots for zip (cable) ties were designed into the body of the fixture to allow ties to be inserted to fasten the two pieces of the fixture together to keep the flexed shape after removing from the testing frame. Tracking of the deflection angle was not easily incorporated into the metal fixtures so an angle arm was taped to the fixture every time a new coupon was installed. This was not ideal, so for the new fixture a

removable angle arm feature was incorporated to track the angle during testing, but be removed from the fixture to install and align the samples.

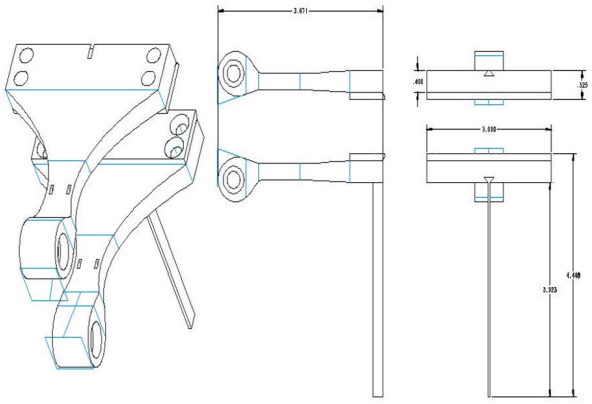

(a) Rough Creo drawing of v1 fixture design

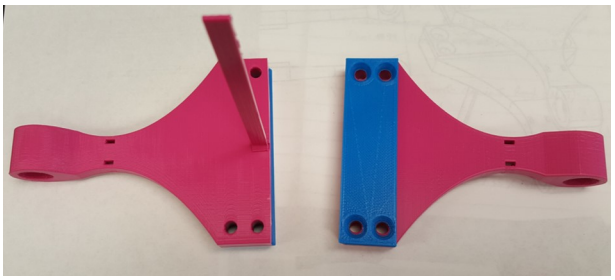

(b) Printed fixture v1

Figure 32: New fixture v1

After researching fasteners and bearings and lead time on printing multiple fixtures, it was decided to split the fixture at the neck to remove the sample and base plate portion but keep the pivot attached so only four clevis pins and bearings are needed as opposed to four each per fixture. This provided a significant cost reduction. Another modification was the implementation of nylon screws as opposed to the metal in use at the time. This afforded improved weight savings as the four screws, each side, eight total, connecting the base plate to the fixture body are located at the end of the rigid arm and could contribute to gravity loading. To allow for the split, two screws were incorporated at the joint to fasten the pivot to the plate; the zip holes were also moved to keep with the removable plate.

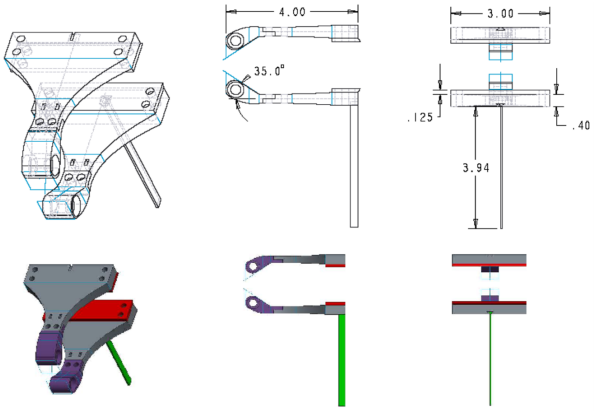

(a) Creo model of v3 fixture design

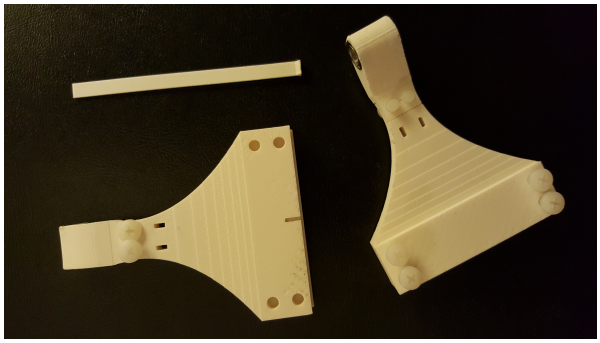

(b) Printed fixture v3

Figure 33: New fixture v3

The third iteration came swiftly after the second. The third iteration, and all subsequent versions, were printed on a Stratasys Dimension Elite FDM printer, using ABS-P430. The Stratasys does not have as much control over infill as the Ultimaker. The infill options are "high density," "solid," or "low density" printing with no manual infill adjustments. The approximation of the density classification is solid =100%, high = 67%, low = 33%. Fixture v3 was printed with "high density" infill. With a desire to get better visualization (and DIC images) of the compression side of the fixture during testing, a kink/bend was introduced to the fixture designed to be 35°. The bend in the fixture allows for complete 90° flexure without the fixture obscuring the view of the sample. With this bend however, the equations of motion needed to be modified to include this new fixed angle. This was a simple modification as the fixture bend only affected the moment arm. With the new fixture design, the effective distance of the rigid arm, l, is different, though only marginally, from the straight armed metal fixture. The fixture itself was measured with calipers for length and angle of bend to calculate a value for l. That value was compared to the Creo CAD model (and STL file for 3D printing) length measurement to confirm an appropriate value for l. With trigonometric relations, a new l can be established for the ABS (Acrylonitrile butadiene styrene) fixture. Based on the geometry of the fixture, the new l was found to be:

$$l = w + h\sin(\alpha) \tag{12}$$

where w is the length of the top plate of the fixture from end to bend point, measured to be

77.5mm and Creo CAD measured to be 77.5mm, and h is the distance from the bend of the fixture to the radius of the bearing hole, measured to be 19.5mm and Creo measured to be 19.6mm, and α is the bend angle, measured to be 30°. The bend angle did not achieve the 35° as designed due to tolerance limits of the Stratasys Dimension Elite FDM printer. This simple relation results in a calculated value of 94.67mm and a Creo value of 94.44mm for the new rigid arm length. This new l value was incorporated into the data processing for when the plastic fixture was used during testing.

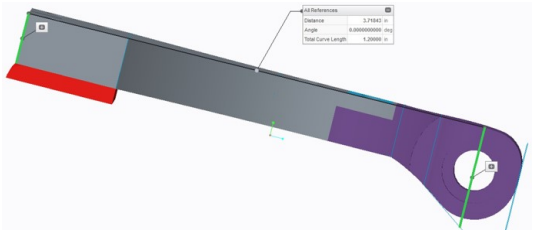

(a) Creo rigid arm, l, measurement

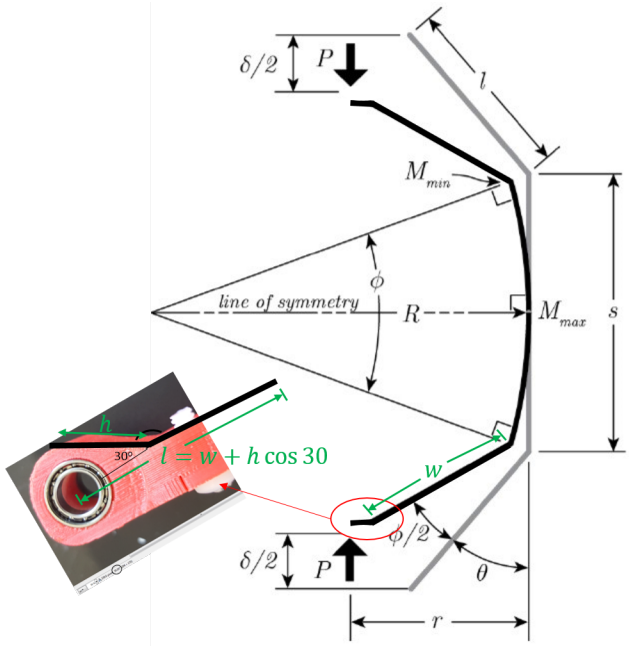

(b) Rigid arm, l, calculation from actual fixture measurement

Figure 34: New fixture rigid arm, l, determination

The measured weight of v3 with screws and bearings was 71g, half of the weight of the original metal fixture.

Due to the tolerances of the 3D printing, there was not enough space for the nylon screws at

the pivot-plate joint to fasten them properly. The joint was widened for version 4 of the fixture. Another adjustment was adding material to the pivot section (bottom) of the joint, moving the cut at the split joint off of the mid-plane, so more material was at the pivot to allow for more teeth to grip the screw at that point. The area around the bearing was thickened to ensure strength during testing and so the bearing could not break out. Minor adjustment were made to the screw holes to allow for easier tapping of the hole for the nylon screws (lessened to 0.15" instead of 0.19") and the hole for the clevis pin was increased a tiny bit to avoid friction with the rough surface finish and the pin. New fixture mass was calculated to be approximately 63.46g (not including the screws and bearings) and measured to be 76.52g (with screws and bearings), which is not enough weight reduction from the light metal fixture (v2) weight of 87.91g, (with screws and bearings).

Furthermore, upon installation of the fixture into the test frame at the U-head, it was discovered that again the tolerance of the Stratasys caused another fit issue. By adding the tapered edge to widen the pivot-plate connection to fit the screws, the pivot head was now slightly too wide to swivel freely when attached to the U-head. A 25.4mm diameter circle was cut out of the pivot around the bearing to give the appropriate clearance without affecting any other part of the fixture. The head opening is 20.32mm wide and the width of the pivot after the cut hole is 19.76. That clearance should allow for free movement without too much "wiggle" between the fixture and the head, considering the tolerance of the machining of the metal head and the resolution abilities of the Stratasys Dimension Elite. The metal v2 fixture width is 19.3mm and has too much freedom of lateral movement inside the head.

Version 5 of the plastic fixture also included a large modification. The entire assembly was narrowed to match the lighter, v2, aluminum fixture. Both the top and bottom plates were narrowed from 76.2mm to 55.88mm wide. The radius on the edge of the slip joint (pivot to plate) was increased from 50.8mm to 63.5mm to further narrow the width by keep the smooth edges. Not enough weight was saved between Metal_v2 and Printed_v4 so more material was being removed. Also for printing, a 33% "low density" infill was used instead of the 66% "high density" previously used since the fixture is quite hearty at the 66%. To expedite the process two different pivots were printed to see which should be employed moving forward. A 19.3mm

wide pivot and a 19.8mm wide pivot were printed and fit checked to see how much the plastic expands during cooling and what design tolerances are the limit. As tight a fit without friction as possible is the desired outcome. The 19.3mm pivot head was selected.

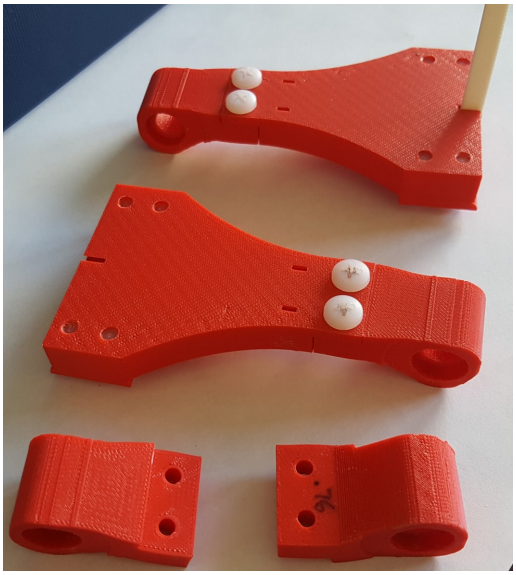

Figure 35: New fixture v5 with 19.3mm (0.76") and 19.8mm (0.78") wide pivot options

The sixth iteration of the fixture included very minor modifications. The angle arm needed adjustment to be shortened so as to not hit the bottom of the MTS C43.504 test frame when a 90^{o} bend angle was achieved; the current arm was grazing the bottom at a length of 101.6mm inches. The new angle arm length was reduced 50.8mm to about 88.9mm long. The end of the angle arm was also widened to a "flag" to provide a large surface for speckling for DIC tracking of the angle in real time. The mate surface was also updated from 3.8mm to 4.6mm at the base of the triangle to try to lessen the "wiggle" in the arm and get more repeatable and accurate angle tracking. The triangle being more important than the flag, the build direction was adjusted to allow for tighter tolerances on that piece of the arm. New fixture mass was calculated to be approximately 25.95g (not including the screws and bearings) and measured to be 42.52g (with screws and bearings), which is a substantial weight reduction from the Metal_v2 fixture at 87.88g.

```
% Fixture Iteration 6
% Used pivot_76

T1=1.60564; % volume of fixture_plate_v5 [in^3]
T2=0.482173; % volume of fixture_pivot_v5_78 [in^3]
T2_76=0.477711; % volume of fixture_pivot_v5_76 [in^3]
B=0.193190; % volume of bottom_plate_v5_newscrews [in^3]
A=0.0619125; % volume of angle_arm_flag_new [in^3]

d=0.03757239; % density of ABS-P430 [lb/in^3] (specific gravity -- density 1.04 g/cm^3)

I1=0.33; % infill ("low density" configuration approximation)
I2=0.33; % infill ("low density" configuration approximation)

MT1=T1*d*I1; % mass of fixture_plate_v5
MT2=T2*d*I1; % mass of fixture_pivot_v5_78
MT2_76=T2_76*d*I1; % mass of fixture_pivot_v5_76
MB=B*d*I2; % mass of bottom_plate_v5_newscrews
MA=A*d*I1; % mass of angle_arm_flag_new

Mass = 2*(MT1+MT2+MB)+MA % total fixture mass [lb]
Mass_76 = 2*(MT1+MT2_76+MB)+MA % total fixture mass [lb]

% Mass =   0.0573 lb (not including the screws, inserts, and bearings)
% Mass_76 =   0.0572 lb (not including the screws, inserts, and bearings)
```

Figure 36: Sample MATLAB script for new fixture mass calculation

Once testing began it was determined that a much smaller than anticipated grip separation was needed to break the coupons. The nylon screws used in previous versions of the fixture stuck out too far and interfered when the grip separation was small (see Figure 37a). The screw heads touched before the coupon was bent past 45°. New inlet screws were ordered from McMaster-Carr and the base plate was adjusted to fit the inlet structure, tapering the bottom from the 9.78mm head to the 4.83mm thread diameter at the top. The necessary grip separation was so small that further modifications were necessary. The thickness of the base plate was reduced significantly and the fillet radius was tightened, though limited based on the placement of the screws. The thickness of the base plate was reduced by ½, so now 1.6mm thick, and the width was reduced from 21.6mm to 20.3mm. The surface fillet radius was also reduced from 3.2mm to 1.6mm. These adjustments allowed for a minimum grip separation as well as slightly more weight reduction. The minimum grip separation possible with the v7 fixture is 7.62mm.

Figure 37: Limitations of fixtures when small grip separations are required: a) v6 screws are interfering and b) v7 has enough clearance

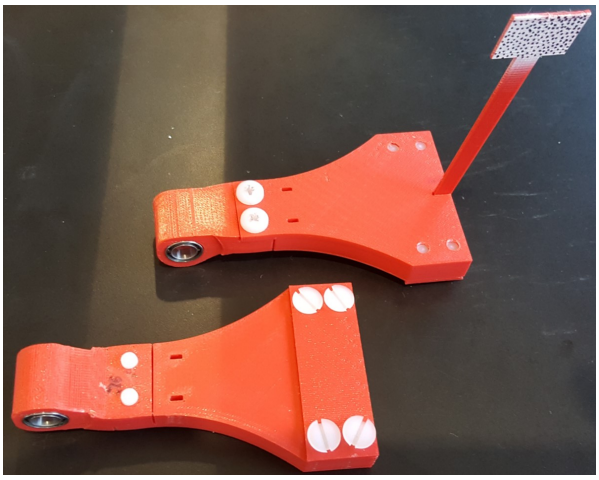

(a) Printed fixture v7

(b) Fixture v7 in use during testing

Figure 38: ABS plastic fixture v7

All testing, both campaign 1 and 2, used the aluminum fixture v2 or the ABS plastic fixture v7, with a handful of samples being tested on the plastic fixture v6.

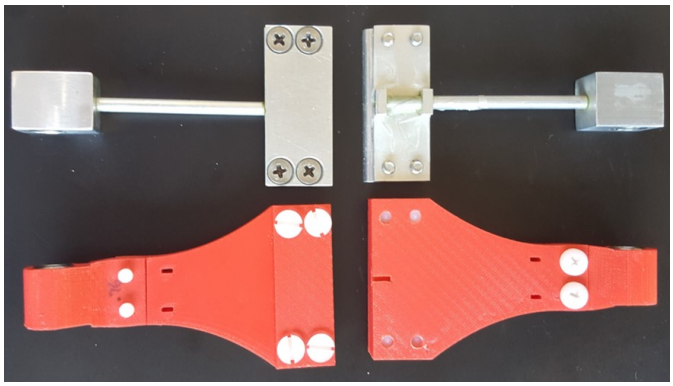

Figure 39: Aluminum fixture v2 and ABS plastic fixture v7, two fixtures utilized while validating the Column Bend Test method

5.3 Testing and Data Processing Adjustments

For testing campaign 2, there were minimal test procedure adjustments aside from the introduction of the new ABS fixture and the modifications necessary to make that work. The inclusion of the new fixture to the procedure brought new challenges. The alignment procedure was the first that needed adjustment. Alignment in the fixture is of utmost importance and the new ABS fixture has slightly different dimensions and a different feel than the metal fixture. The metal fixture arms are 25.4mm from the precision straight edge to ensure the grip profiles are flush and the U-head is parallel for the coupon to be square in the fixture. The plastic fixture with its rounded edges and sweep pattern was slighting more difficult to get square. The U-head connection clevis pin hole with bearings is the flat surface to position on the straight edge. The bearings are 17.8mm from the straight edge with the grip profiles flush to the same straight edge. The metal fixture and ABS fixture v6 base plate fillet edges extended 3.175mm beyond the fixture body/top plate so when aligning a coupon a factor of 6.35mm must be added to the grip separation to allow for that fillet and to ensure a correct grip separation. The v7 fixture was designed for extremely small grips so the base plate was reduced to allow for this. The v7 base plate does not extend beyond the top plate, in fact the edges are coincident, however there is a fillet radius of 1.5875mm on the base plate. When aligning the coupon within the v7 fixture a factor of 3.175mm must be added to the grip separation to allow for that fillet and to ensure a correct grip separation.

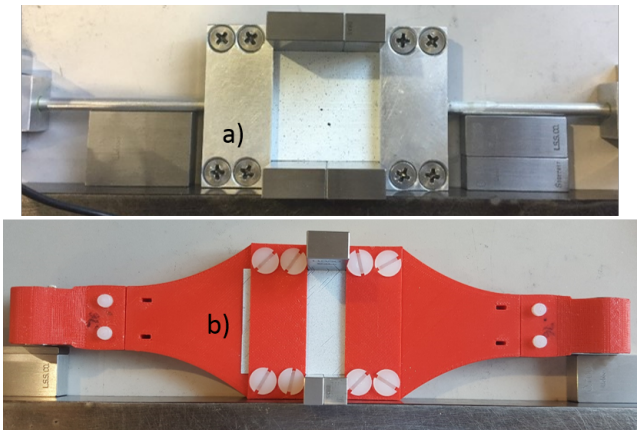

Figure 40: Alignment of a) v2 metal fixture and b) v7 plastic fixture with precision straight edge and precision blocks

Given all of the trouble with the load cells in campaign 1, a new procedure was enacted in campaign 2 to verify the load cell calibration before every run. For campaign 2, only the 25lb Futek load cell was used. It was found that every time the SignalExpress[50] software was opened and the Futek load cell connected to the system, the calibration reset. To ensure the load cell was recording correctly, the system was calibrated with the Futek calibration data sheet and verified with increments of 200g, every time. This added step provided confidence in the load cell output and eliminated the need to "clean up" or adjust the data after the fact. Another calibration verification check was with the VIC3D software. For campaign 2, the grip separations were too small to capture the compression side of the bending coupon even with the new fixture and the Aramis system was questionable and unreliable so it was decided that only the tension side would be tracked with the VIC3D DIC software. With this it became imperative to check VIC3D before every test. Once the coupon was set and the fixture placed in the load frame, the calibration of VIC3D was confirmed. A sample picture was taken and analyzed with the current calibration data. The projection error was required to be less than 0.1; VIC3D would output it as red if it was too high to proceed, and the region of interest needed to be large enough to trust the data. If either the load cell or VIC3D were out of calibration the systems were recalibrated and checked before testing would proceed.

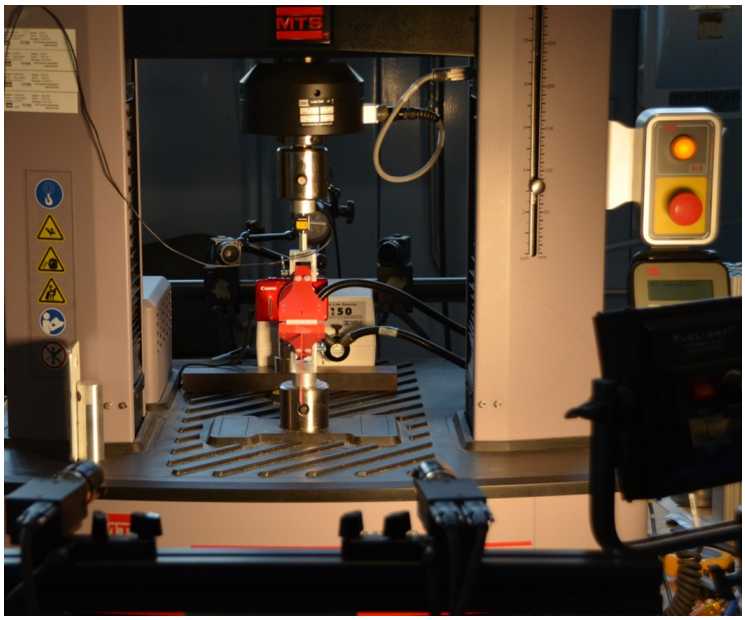

Figure 41: Column Bend Test set up for campaign 2 with new fixture

As the metal and plastic fixtures have different moment arms, for data processing the fixture in use was noted and the MATLAB script adjusted for which fixture was used. The effective distance of the rigid arm, l, for the metal fixture is 3.685" and 3.72" for the plastic fixture. This factor has minimal effect on the processed data but for accuracy is included in the processing procedure. Since the fixture modifications were all on the base plate and angle arm after version 4, the value of l remained constant through out each update. The fixture itself was measured with calipers and those values compared to the Creo CAD model length measurements to confirm an appropriate value for l.

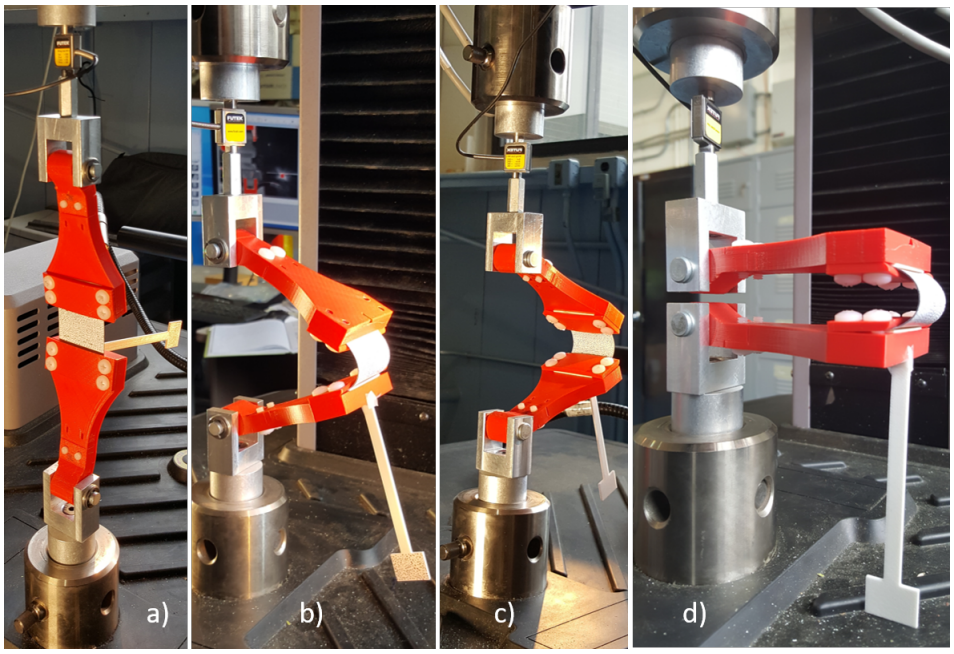

Figure 42: Progressive views of the pure moment bending test with new fixture, a) initially, b) approximately midway through tension side, c) approximately midway through compression side, d) 90° bend.

Lastly for the CPW and CUNI samples, the coupons were so thin that the loading during testing is extremely low. Often the coupons started in tension, at the order of magnitude E-1 or E-2, and ended in compression at the order of magnitude E-1 or E-2. This change in sign caused unrealistic sinusoidal moment and bending stiffness responses in the processed data. To account for this, the load data was set to start at 0 and adjusted to load in compression by subtracting the initial data point from all subsequent points prior to processing. This allowed for the correct bending stiffness response to be calculated, however it does change the moment values. As the interest is the bending stiffness and strain-to-failure values for the laminates, the incorrect moment values are not a concern. Aside from the modifications to incorporate the new fixture, the calibration verification steps for the load cell and VIC3D, and the force adjustments, the test procedure and processing is the same as explained for campaign 1.

Chapter 6: Column Bend Test Campaign 2 Data Analysis and Results

The data analysis for campaign 2 was significantly more involved than that of campaign 1.

6.1 Micrographing

Material performance in bending is highly dependent on the thickness of the laminate in question. In Classical Lamination Theory, the bending moment and curvature relationship is correlated to the cube of the laminate thickness. Therefore for analysis and modeling, the thickness of the coupons being tested is required to the best accuracy possible. A property and a reward of high stain composites is the minimum plies and therefore significant thinness. To measure the true thickness of such thin materials micrograph images are used. Five 0.5"x0.5" (12.7 x 12.7mm) samples were cut from various locations on the master panel for micrograph measurements to find the average thickness of the whole panel and subsequently all the coupons being tested. Each specimen is polished to a smooth surface and imaged with a microscope. Thickness measurements are then taken at five points along five sections across the width of the micrograph sample. Thicknesses is measured at 100x magnification.

Another vital characteristic in material performance, analysis, and modeling is the fiber volume fraction. This value can be calculated from material properties from the epoxy resin and dry fibers incorporated to create the composite laminate. As a check of this calculated value and to ensure correct numbers are used for analysis and modeling, the fiber volume fraction was also measured with micrograph images. Similar to the thickness measurements, the fiber volume fraction was calculated in five sections across the width of each of the five micrograph samples and averaged to get a value for the whole panel. Fiber volume fraction (FVF) is captured at 500x magnification and processed further with the software ImageJ[51] for measurement.

To prepare the samples for micrographing, each samples is polished with silicon carbide (SiC) metallurgical paper with increasing grit on a platen turnstile to get a smooth surface for imaging. The grit progression is, 400 to 800 to 1200 grit. The final polish is on a polishing pad with a concoction of soap, water, and Buehler Masterpolish Mastermet, a colloidal silica

polishing suspension. This solution contains silica in the range of 0.05μm to get the final finish. The platen is spun at around 70-80 rpm with a constant water stream to draw the removed particles away from the sample. The Metprep 4 from Allied High Tech Products Inc along with Buehler SiC metallurgical paper was used for the polishing.

Once polished, each sample was placed on a Reichert-Jung MeF3A microscope and imaged with a Leica DFC450 camera. Leica Application Suite Software, LAS V4.0, was used to snap a picture of the surface and measure the thickness of the composite. The calibration of the LAS V4.0 software was verified prior to imaging by imaging a metal ruler. With a valid calibration, the samples were imaged and measured. Figure 43 shows samples images from each panel at 100x magnification for thickness measurements. Panel thickness for CPW, 3 plies, was measured to be 0.19241mm, CUNI, 4 plies, 0.16559mm, and LAM1, 6 plies, 0.34171mm.

Table 9: Average laminate thickness values for all samples of each laminate in mm

Laminate	M1	M2	M3	M4	M5	Panel Average	Standard Deviation
CPW	0.195	0.188	0.188	0.199	0.191	0.1924	0.0043
CUNI	0.160	0.168	0.169	0.165	0.167	0.1656	0.0032
LAM1	0.345	0.351	0.344	0.336	0.333	0.3417	0.0065

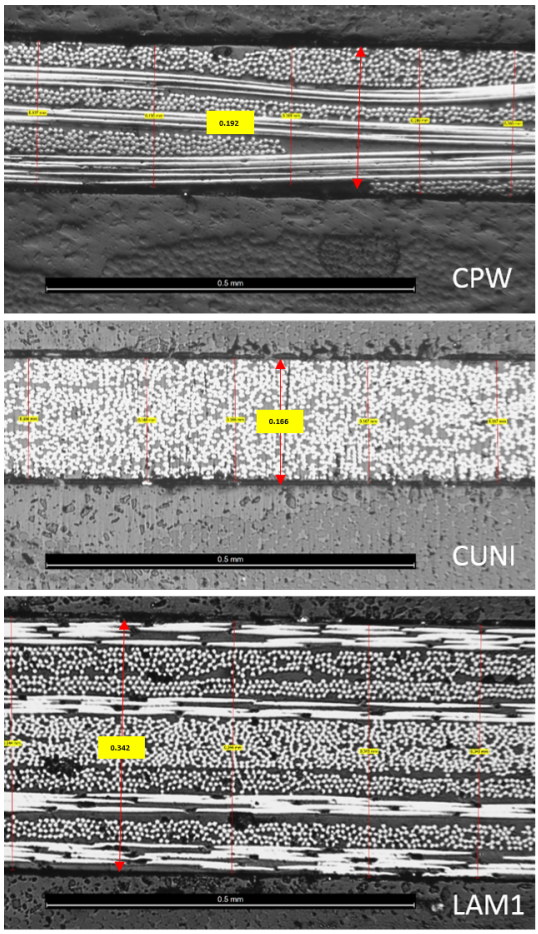

Figure 43: Sample images from micrograph thickness measurements [mm] at 100x magnification

For the measurement and calculation of the true fiber volume fraction (FVF) of each panel, images taken at 500x magnification are converted to black and white contrast images using ImageJ software. Those images were fed into a simple MATLAB script (see Appendix E) that breaks down the image into a histogram of black and white pixels. The white pixels are the fibers while the black are the matrix material. Those pixels are compared to the whole image for the fraction of white (fibers). This is the fiber volume fraction for the material. For an adequate sample size for averaging, four-to-five images were taken from the five square micrograph samples cut from the full panel. All of the images were processed and averaged together for the average fiber volume fraction for the entire panel. For the LAM1 and CPW panels, some original images were cropped to have an area where only the 0^o fibers perpendicular to the image plane are visible to get an accurate measure of fiber volume fraction.

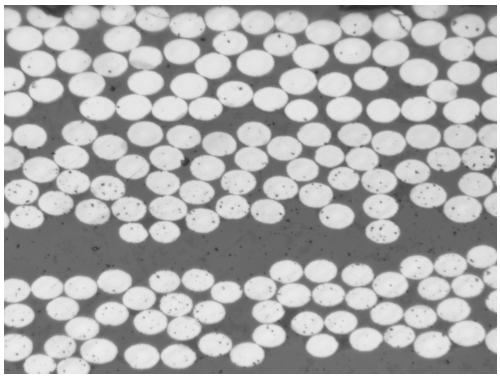

(a) Micrograph original image

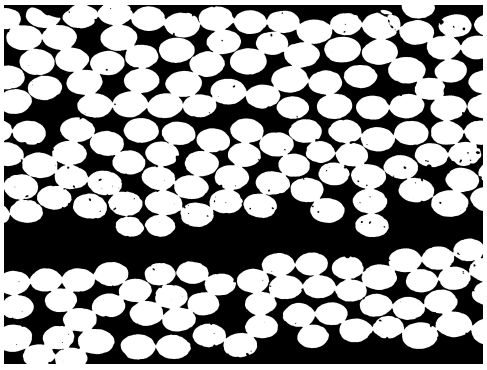

(b) Micrograph contrast processed image

Figure 44: Original vs contrast image for FVF micrograph measurements at 500x of CPW panel sample

During the contrast conversion process some of the fiber shapes inevitably get distorted. To correct this, enhanced images of individual fibers were cropped from the contrast image. These images are then reanalyzed to find the percentage of missing pixels for a complete fiber. After checking eight representative distorted fibers per panel, an average % was found to be missing from those fibers. A correction factor was established for the corrupted images with a critical number of distorted fibers. The panels each had a different factor with CUNI being the lowest at 15.2%, CPW at 16.2%, and LAM1 at 16.3%. Once the correction factor was established a new MATLAB script was run which adjusted the original image pixel count, details in Appendix E. The white (fiber) pixels were increased by the % correction before the fiber volume factor was calculated. This adjustment provided a more accurate FVF for the panel. Figure 46 shows samples of distorted fiber images and their correction factors. A large portion of the images did not need correction as the sample polishing before imaging allowed for the contrast processing to keep the fibers intact. The correction was factored into the corrupted contrast images to get a more accurate FVF value for those images that have a significant distorted fibers. The corrupted images were computed with and without the correction factor to see the effect these distorted fibers had on overall FVF. Each of the three panels needed a different amount of images corrected; CUNI only needed 8 of the 24 images, CPW 15 of 28, and LAM1 17 of 23. See Tables 10, 11, and 12 for fiber correction adjustments for the CUNI panel.

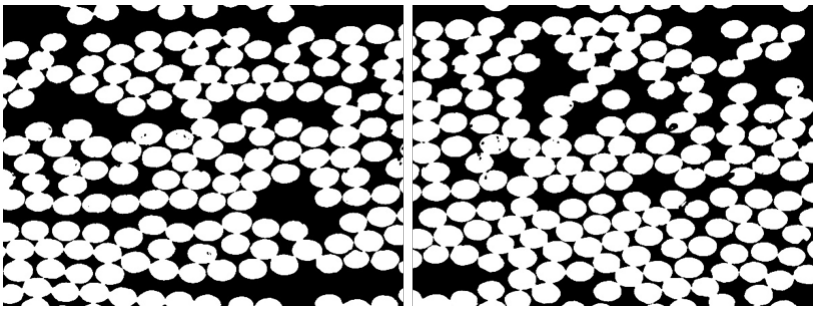

(a) Good micrograph contrast processed images (CUNI)

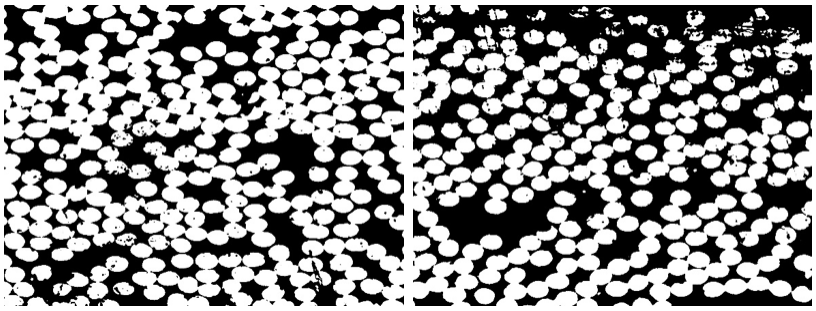

(b) Corrupted micrograph contrast processed images (CUNI)

Figure 45: Good vs bad contrast processed images

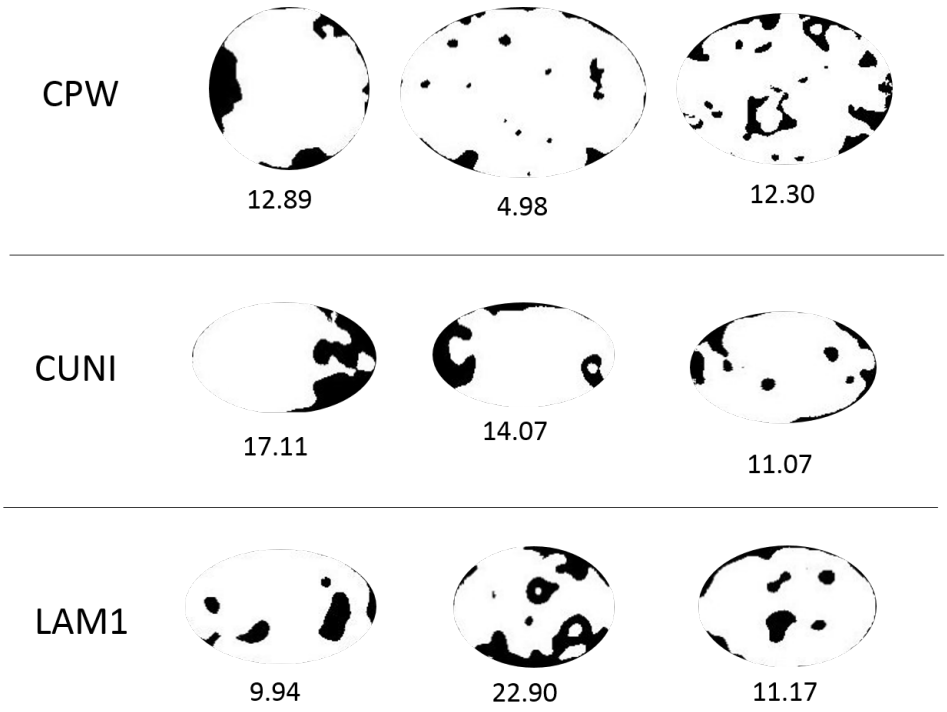

Figure 46: Sample distorted fibers with the % pixels missing for each

Note: Some fibers appear elliptical due to a 45° orientation of the micrograph sample.

Table 10: FVF calculated from original contrast images from CUNI panel

Original CUNI		
Sample	File	FVF [%]
M1	0	57.59
	1	58.51
	2	63.18
	3	69.99
	4	69.08
M2	0	55.67
	1	63.18
	2	61.14
	3	60.57
	4	63.32
M3	0	65.18
	1	63.95
	2	66.59
	3	62.42
M4	0	52.03
	1	48.21
	2	55.97
	3	57.87
	4	58.71
M5	0	51.94
	1	62.21
	2	62.71
	3	63.86
	4	66.92
	Avg	60.867
	Max	69.99
	Min	48.21
	StDev	5.33

Table 11: FVF calculated from 15.2 % corrected contrast images from CUNI panel where C indicates a corrected image

Corrected CUNI 15.2%		
Sample	File	FVF [%]
M1	0C	64.85
	1	58.51
	2C	69.98
	3	69.99
	4	69.08
M2	0C	63.05
	1	63.18
	2	61.14
	3	60.57
	4	63.32
M3	0	65.18
	1	63.95
	2	66.59
	3	62.42
M4	0C	59.57
	1C	55.84
	2C	63.33
	3	57.87
	4C	65.89
M5	0	51.94
	1	62.21
	2C	69.58
	3	63.86
	4	66.92
	Avg	63.284
	Max	69.99
	Min	51.94
	StDev	4.40

Table 12: FVF calculated values for all laminates in %

Sample	Average	Corrected Average	Average of Perfect Images Only	Max	Min
CPW	58.14	61.99	59.66	75.58	48.30
CUNI	60.87	63.28	64.40	69.99	51.94
LAM1	60.85	66.77	69.14	73.01	54.46

6.2 Analytical Model Experimental Data

Campaign 2 proved to be more complicated than anticipated but still provided a great deal of data on the properties of interest for the three laminates in question. With the new load cell calibration step in the procedure, there were no more issues with bad data due to a damaged or out of calibration load cell. The biggest challenge with campaign 2 was actually breaking the coupons. With the CPW and CUNI coupons being so extremely thin, it became quickly evident that there are limitations to the Column Bend Test, namely there is a minimum thickness that can be tested with this test set up. Working with coupons below 0.2mm thick and with the elastic moduli these composites are designed with, it was difficult not only to achieve a bend angle approaching 90^{o} but to merely break the coupons at all. The CBT was at its limit; the CPW panel with the weave in the $\pm$45^{o} direction could not be broken at all. The grip separations required were very small, which introduced issues with DIC capture and most importantly the potential for artificial stiffening. It was determined that at the grips in question and with the limitations of the software, only the tension side of the coupons would be tracked with VIC3D for DIC strain measurements. The field of view of the compression side of the coupons was too small to get reliable data or often even track the specimen at all. Even with the new fixture designed to have a better view of the compression side, the gauge lengths were still too small to properly track the compression of the coupons. As all the laminates tested in this campaign are symmetrical and with the knowledge gathered from campaign 1, the compression side strains can be assumed to be similar, presumably a little higher, than those captured on the tension side. Aside from missing out on tracking the compression side for crack propagation and strain data, the smaller grip separations also potentially introduced grip effects and artificial stiffening that could obscure the data and the true material properties.

With these concerns in mind, all data was processed, evaluated, and interpreted to determine the material properties of each laminate. Tables 13 and 14 show the average values of all evaluated properties for the data from campaign 2. The complete compilation of all of the data analysis for campaign 2 can be found in Appendix F. As the variation in grip separation was a concern for campaign 1, for campaign 2, a set grip separation was used for each laminate once an appropriate length was determined to successfully break the coupons near the 90^{o} bend point.

The 90° bend point is the goal for no particular reasons except that the difference between the maximum and minimum moments is largest at that point. Figures 47 and 48 are samples of successful failures for each laminate tested in campaign 2.

Table 13: Average observed failure for all of campaign 2 testing

Laminate	**Orientation**	**Failure**
CPW_3p	0	Crack in 90° on T side in central region; visible, smaller (not through width) 90° cracks on C side. Abrupt failure.
CPW_3p	45	Grip separations required too small; could not fail.
CUNI_4p	0	0° splitting and 90° cracking/fiber failure from one edge and the the other, propogating toward center.
CUNI_4p	90	Deformed in fixture almost immediately; 90° crack, obvious distortion of curvature during test starting early.
CUNI_4p	45	+45° crack through grip, one from lower corner up, other from upper corner down. Abrupt failure.
CUNI_4p	-45	Abrupt failure; cracking in -45° from upper corner down. Multiple large catastrophic cracks in -45 across coupon by end.
LAM1	0	±45° zigzag crack in central region of C side, failure visible on T side in shift/drop of fixture at end.
LAM1	90	±45° zigzag crack in central region of C side. Cracking heard a bit before visible failure.
LAM1	45	90° crack on C side caused total failure through T side.
LAM1	-45	90° crack on C side causing collapse on T side.

Another consideration for campaign 2 was the metal vs the plastic fixture. The plastic fixture required a much smaller grip separation than the metal fixture to achieve failure and failure strains which introduced concerns about artificial stiffening but there are already concerns about gravity loading from the metal fixture. For example for LAM1, the plastic fixture needs around 12.7mm (0.5") grip separation to reach the 2.1-2.3% strain and failure while the metal frame needs only 17.8mm (0.7") grip separation. The strains measured are similar so that is promising, but the different grip separations can cause different curvatures and moments and potentially different bending stiffnesses. The surface strains are a function of the ratio of grip separation to deflection angle so the different grips alone are not the concern. The behavior of the test as a whole, i.e. the final deflection angle achieved, the strains measured, the loading, etc., are contributing factors to assessing the fixture differences. However, new questions have arisen from this. Is this proof that the metal frame is too heavy and influencing the moment to cause failure at wrong curvatures? Or is there something going on in the plastic fixture that is obscuring the data? Given our awareness of the gravity loading influences of the metal fixture it

was decided to use the plastic fixture to eliminate the gravity loading due to the metal fixture's weight and to investigate the new fixture with awareness for potential influence from artificial stiffening due to the smaller grips required. The extreme thinness of the coupons in many cases dictated which fixture was required to break the samples. In some cases, the grip separations were so small that the plastic fixture was the only one capable of working at such small grips. As mentioned above, CPW $\pm 45^{o}$, could not be broken with these coupon dimensions. All other laminates were successfully tested to failure.

As there was some data for LAM1 from campaign 1 and the composite panel was made to the same thickness, which is slightly larger than the ultrathin CPW and CUNI panels, LAM1 was used to investigate the differences in the material response from testing with the metal fixture vs the plastic fixture. It can be seen in Table 14 that testing with the metal fixture consistently resulted in slightly higher moments, bending stiffnesses, and strains, as well as smaller curvatures at failure for the LAM1 coupons. The trends, such as the more than doubling and sometimes even a 5x increase of the bending stiffness from initial to final in the 0^{o}, are the same but the values are elevated. The data from the plastic fixture does not appear to be corrupted by the small grip separations. The weight of the metal fixture is influencing the data. It is recommended to use the lighter plastic fixture for future testing.

Table 14: Average of experimental data for all of campaign 2
(P: Plastic fixture; M: Metal fixture; Blank: All)

Laminate	Orientation	Max Moment [N-m]	Min Diameter [m]	Initial Bending Stiffness [N-m]	Final Bending Stiffness [N-m]	Change in Bending Stiffness [%]
CPW_3p	0	0.0957	0.0095	0.0041	0.0418	927.78
CPW_3p	45	–	–	–	–	–
CUNI_4p	0	0.1647	0.0067	0.0060	0.0791	1212.50
CUNI_4p	90	0.0089	0.0256	0.0025	0.0071	177.78
CUNI_4p	45	0.0256	0.0194	0.0041	0.0258	533.33
CUNI_4p	45P	0.0269	0.0181	0.0045	0.0282	525.00
CUNI_4p	45M	0.0247	0.0203	0.0038	0.0241	540.00
CUNI_4p	-45	0.0634	0.0127	0.0051	0.0328	544.44
LAM1	0	0.3393	0.0129	0.0571	0.1205	111.22
LAM1	0P	0.3214	0.0126	0.0551	0.1003	82.05
LAM1	0M	0.3751	0.0135	0.0610	0.1610	163.89
LAM1	90	0.2558	0.0126	0.0418	0.0830	98.65
LAM1	90P	0.2641	0.0123	0.0443	0.0746	68.15
LAM1	90M	0.2391	0.0134	0.0367	0.1000	172.31
LAM1	45	0.4235	0.0217	0.1305	0.1940	48.63
LAM1	45P	0.4199	0.0204	0.1251	0.1808	44.47
LAM1	45M	0.4308	0.0243	0.1412	0.2203	56.00
LAM1	-45	0.4078	0.0237	0.1390	0.2090	50.41
LAM1	-45P	0.4070	0.0237	0.1356	0.1977	45.83
LAM1	-45M	0.4087	0.0238	0.1424	0.2203	54.76

Laminate	Orientation	Max Moment [lb-in]	Min Diameter [in]	Initial Bending Stiffness [lb-in]	Final Bending Stiffness [lb-in]	Change in Bending Stiffness [%]
CPW_3p	0	0.847	0.374	0.036	0.370	927.78
CPW_3p	45	–	–	–	–	–
CUNI_4p	0	1.457	0.262	0.053	0.700	1212.50
CUNI_4p	90	0.079	1.008	0.023	0.063	177.78
CUNI_4p	45	0.227	0.764	0.036	0.228	533.33
CUNI_4p	45P	0.238	0.713	0.040	0.250	525.00
CUNI_4p	45M	0.219	0.799	0.033	0.213	540.00
CUNI_4p	-45	0.561	0.502	0.045	0.290	544.44
LAM1	0	3.003	0.507	0.505	1.067	111.22
LAM1	0P	2.844	0.496	0.488	0.888	82.05
LAM1	0M	3.320	0.530	0.540	1.425	163.89
LAM1	90	2.264	0.498	0.370	0.735	98.65
LAM1	90P	2.338	0.483	0.393	0.660	68.15
LAM1	90M	2.116	0.528	0.325	0.885	172.31
LAM1	45	3.749	0.854	1.155	1.717	48.63
LAM1	45P	3.716	0.803	1.108	1.600	44.47
LAM1	45M	3.813	0.956	1.250	1.950	56.00
LAM1	-45	3.610	0.935	1.230	1.850	50.41
LAM1	-45P	3.602	0.934	1.200	1.750	45.83
LAM1	-45M	3.617	0.935	1.260	1.950	54.76

Laminate	Orientation	Grip Separation [in]	Grip Separation [m]	Tensile Failure Strain [%]	Experimental Angle Achieved [°]	Approximate Slope of Bending Stiffness vs Curvature line [N-m^2]
CPW_3p	0	0.4800	0.0122	2.8665	72.56	0.0002
CPW_3p	45	–	–	–	–	–
CUNI_4p	0	0.4500	0.0114	1.0523	80.96	0.0002
CUNI_4p	90	0.7313	0.0186	0.5795	53.49	0.0000
CUNI_4p	45	0.7375	0.0187	0.6772	71.35	0.0002
CUNI_4p	45P	0.6750	0.0171	0.6537	65.57	0.0002
CUNI_4p	45M	0.8000	0.0203	0.7007	77.14	0.0002
CUNI_4p	-45	0.6393	0.0162	0.8115	82.31	0.0002
LAM1	0	0.5833	0.0148	2.2648	77.79	0.00045
LAM1	0P	0.5250	0.0133	2.1895	78.14	0.0003
LAM1	0M	0.7000	0.0178	2.4155	77.09	0.0006
LAM1	90	0.5500	0.0140	2.1472	74.65	0.00025
LAM1	90P	0.5000	0.0127	2.1030	74.94	0.0001
LAM1	90M	0.6500	0.0165	2.2355	74.05	0.0004
LAM1	45	0.9167	0.0233	1.4493	74.12	0.0006
LAM1	45P	0.8500	0.0216	1.4565	74.79	0.0005
LAM1	45M	1.0500	0.0267	1.4350	72.79	0.0007
LAM1	-45	0.9875	0.0251	1.3160	81.70	0.0012
LAM1	-45P	0.9250	0.0235	1.2820	77.69	0.0008
LAM1	-45M	1.0500	0.0267	1.3500	85.71	0.0015

6.2.1 Bending Stiffness

The CPW coupons were tested with the metal fixture only because the v7 plastic fixture was not available. Unlike the thicker, 8 ply coupons from campaign 1, the 0° direction, or 0-90PW, 3 ply samples show a fairly linear, in some cases a one order of magnitude increase in bending stiffness as curvature increases (slope of 0.0002 N-m^2), indicative of a highly nonlinear response in the M-κ curve. Fracture patterns were expected to be similar to campaign 1 but these coupons appeared to be failing in tension, not compression. It appears as if the thicker, 8 ply CPW from campaign 1 failed as a standard composite while the 3 ply CPW from campaign 2 had very different failure modes. The test observations are limited due to the lack of visibility of the compression side; it is possible that initial failure started on the compression side. There may have been microbuckling on the compression side that allowed the coupon to continue bending until strain-to-failure was reached on the tension side. It is probable that there was invisible microcracking on the compression side. The 0-90PW coupons had abrupt failures due to fiber fracture in the 90° direction in the central region of the specimen on the tension side. After the coupons were removed from the fixture there was visible, albeit smaller, not through the width, 90° cracks on the compression side as well (see Figure 47a). The ±45PW CPW coupons were too thin and too small to break under these testing conditions.

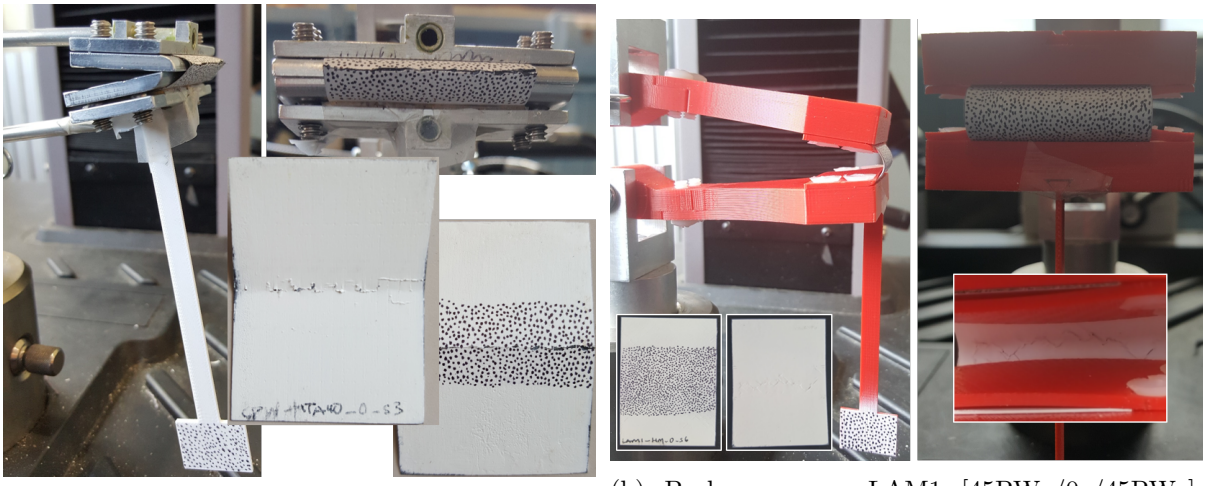

(a) Broken coupon CPW $[0PW]_3$, sample 3, orientation 0°

(b) Broken coupon LAM1 $[45PW_2/0_2/45PW_2]$, sample 6, orientation 0°

Figure 47: Test campaign 2 sample broken coupons a) CPW_0 and b) LAM1_0

Much like the thin CPW coupons, the CUNI, 0° and 45° direction samples have a nonlinear M-κ curve with a linear, 4-5x up to an order of magnitude increase in bending stiffness as curvature increases. Both fiber orientations having a slope around 0.0002 N-m^2. The CUNI, 90° samples have a near constant bending stiffness. Fracture of the CUNI coupons is the same as with the thicker coupons from campaign 1, generally abrupt and in the fiber direction. The CUNI split along the fiber direction, often causing two piece, or more, failure. The 45° and 90° coupons snap along the 45° and 90° directions respectively. The 0° coupons split in the 0° direction but as the coupon is clamped at the end of the coupon the cracks are arrested or the fibers fail at the grips (see Figure 48). The failure was the same between campaign 1 and campaign 2 but the material response was very different. Much of the CUNI from campaign 1 had a near constant bending stiffness while the CUNI from campaign 2 had a very steep linearly increasing bending stiffness. This is due to the difference in thickness of the coupons tested. The campaign 2 CUNI samples were often fragile during handling as they were so thin; the 90° coupons sometimes broke while being installed in the fixture, but were surprisingly stout during testing.

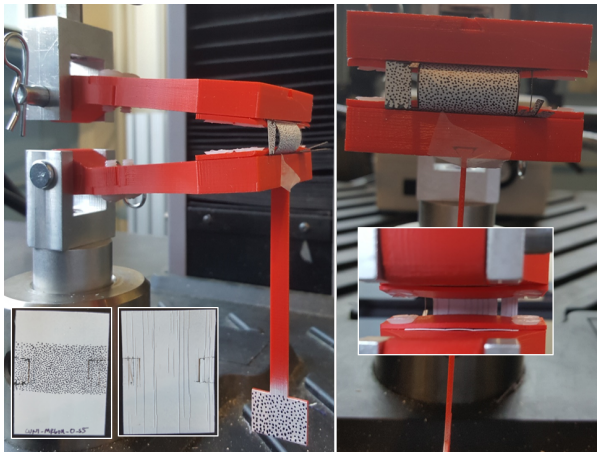

(a) Broken coupon CUNI $[0]_4$, sample 5, orientation 0°

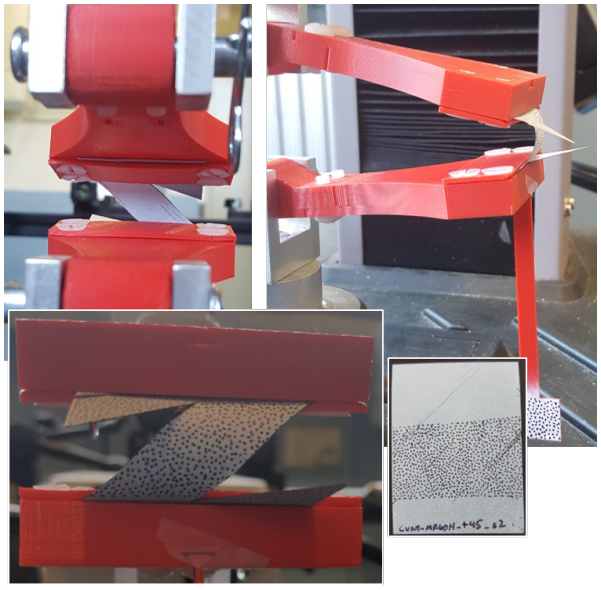

(b) Broken coupon CUNI $[0]_4$, sample 2, orientation 45°

Figure 48: Test campaign 2 sample broken coupons a) CUNI_0 and b) CUNI_45

As an example of the influence thickness has on bending, Figure 49 shows the maximum

moment, M_{max}, and bending stiffness in the coupon's axial direction (0°), D_{11}, for the two thin-ply laminates, CUNI, of the same material but different number of plies (9 vs 4). As mentioned above, the thicker, 9 ply CUNI coupon, which has a total thickness of 0.45 mm, shows a fairly linear M-κ curve that results in an almost constant bending stiffness throughout the tests. However, the thinner, 4 ply CUNI coupon of 0.166 mm thickness produced a nonlinear M-κ curve that resulted in a 4-5x increase in bending stiffness during the test. For further comparison, if the bending stiffness, D_{11}, from campaign 1 CUNI, at 9 plies, with an approximate constant value of 0.780 N-m, is scaled down to the smaller, campaign 2 thickness by the cubed thickness ratio of the two specimens, the D_{11} for the thinner CUNI is calculated to be 0.039 N-m. This value was reached during the last 20% of the test of the 4 ply CUNI during campaign 2, shown in Figure 49b. In Classical Lamination Theory, the bending stiffness matrix, D, is dependent on the cube of the ply thickness. There is obvious correlation between the bending stiffness at 9 plies and at 4 plies, but the nonlinear behavior at the smaller thicknesses is what makes high strain composites so interesting and useful. The one order magnitude increment in bending stiffness was thought to perhaps be due to the geometric stiffening effect from the small grip separations for these much thinner laminates. However, when scaling the thicker coupons down by the thickness cubed, the results are consistent. This suggests that the concerns about the artificial stiffening may be exaggerated.

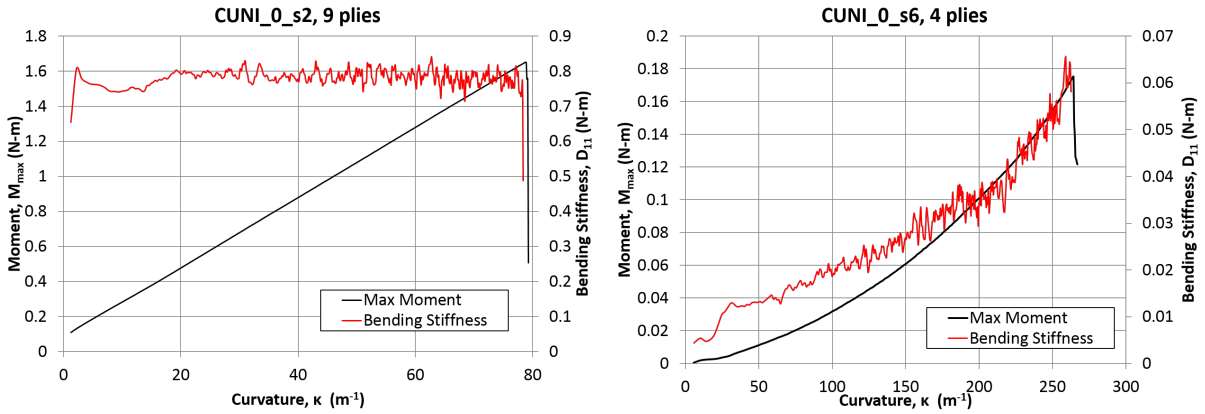

(a) M-κ and D_{11}-κ curves for CUNI, 0° orientation, sample 2 from campaign 1.

(b) M-κ and D_{11}-κ curves for CUNI, 0° orientation, sample 2 from campaign 2.

Figure 49: M-κ and D_{11}-κ curves for two CUNI, 0° orientation, $[0]_n$ laminates from a) campaign 1 with n = 9 plies and b) campaign 2 with n = 4 plies.

The LAM1 coupons tested in campaign 2 are the same layup as those in campaign 1 [$45PW_2/0_2/45PW_2$] and therefore have, more or less, the same thicknesses. LAM1 from campaign 2 was cured with caul plate so both sides are smooth and the panels are ever so slightly thinner (0.007mm). Due to the uniform smoothness of the campaign 2 LAM1 panels, the awareness of which side (rough or smooth) is in tension and which is in compression is not necessary. It is possible that the caul plates have some effect on the panels, minimizing defects or improving the FVF, but direct comparison of the material properties of LAM1 between campaign 1 and campaign 2 is difficult as the campaign 1 data is corrupted by a damaged load cell.

Unlike the CUNI and CPW test data, the LAM1 data was not adjusted prior to processing. The loads applied were left untouched so the output numbers for maximum moment are reflected properly. As expected, the failure of the campaign 2 LAM1 samples matches that of the campaign 1 samples. Again the lack of DIC capture on the compression side limits the onset of visible failure, but audible failure is often captured and upon viewing the coupons after testing, the fracture patterns are evident. LAM1, 90^o and 0^o both have $\pm$45PW as the surface plies so the fiber fracture is visible as a $\pm 45^o$ zigzag crack on the compression side. LAM1, 45^o, has 0-90PW as the surface plies, so visible fiber failure is along the 90^o direction on the compression side. All three fiber directions tested have a linear increase in bending stiffness response proving a nonlinear moment vs curvature relation (see Table 14).

6.2.2 Strains

With the small grip separations necessary to break the thinner sample on campaign 2, it was more difficult to capture the strain data. The small gauge lengths created small fields of vision for the DIC cameras which resulted in smaller regions of interest (ROI) for strain calculations. The speckle pattern for the coupons tested in campaign 2 was much better controlled and the dots much smaller and the patterns tighter to optimize the DIC tracking abilities. VIC3D is a powerful tool and did not have trouble tracking most samples even with the small ROIs. There is, however, limitation to the software, and strains below 0.8% are within the error region and needed to be noted with caution. No compression side strain data was captured for campaign 2. The tensile strains observed for each laminate can be found in Table 14. The CPW, 0^o direction

coupons reached strains approaching 2.9%, while all fiber orientations of the CUNI coupons failed before or around 1% axial strains.

The strains from campaign 1 LAM1 coupons were unaffected by the damaged load cell so comparison to campaign 2 is possible, though it should be noted that the sample size of LAM1 coupons from campaign 1 is quite small, two-to-three samples. As a whole, LAM1 campaign 2, noted at LAM1_C2, reached higher strain-to-failure than the coupons from campaign 1. This may be due to the curing process. LAM1_C2 was cured with caul plates and therefore the finished product was smooth on both sides. The rough side of LAM1_C1 effects the coupon thickness as well as introduces failure concentration points. The caul plates transmit normal pressure and temperature to the composite during cure, providing a more uniform distribution of heat which consequently lessens cure defects. LAM1_C2 coupons have better performance due to this curing process. When these laminates are used for deployable booms, however, caul plates cannot be used so the laminate would have a rough side and a smooth side. It was decided to use caul plates when fabricating LAM1_C2 to see the best case scenarios for the laminate layups rather than the closer to reality performance of LAM1_C1. Table 15 shows the average strains observed during both testing campaigns. Again it should be noted that the statistics from the strain measurements from LAM1_C1 are from only two-to-three samples for each fiber orientation.

Table 15: Tensile surface axial strain, ϵ_{11}, observed for LAM1 tested in both campaigns

	Average [%]		Max [%]		Min [%]		StDev [%]	
Orientation	**LAM1_C1**	**LAM1_C2**	**LAM1_C1**	**LAM1_C2**	**LAM1_C1**	**LAM1_C2**	**LAM1_C1**	**LAM1_C2**
0	1.890	2.265	1.91	2.471	1.87	2.143	0.020	0.115
90	1.420	2.147	1.984	2.268	0.856	2.028	0.564	0.075
45	1.247	1.449	1.48	1.555	1.07	1.315	0.172	0.082

Much like in campaign 1, the rotational kinematics of the CBT provide a nonlinear strain vs time curve but as expected the strain vs curvature curves are relatively linear. It can be seen in Figure 50b that the fixture in use (metal vs plastic) affects the slope of the strain vs curvature line but not the failure strain value. The strain vs time curves for all of the LAM1_C2, 45° orientation coupons tested, Figure 50a, show that the plastic fixture, noted at P, and metal as M, does not influence the final strains. This is another suggestion that the concerns about the artificial stiffening may be overstated.

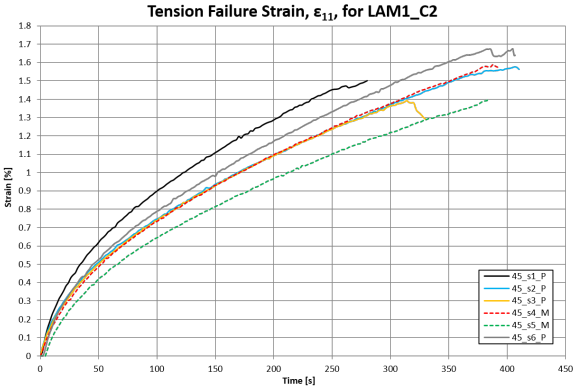

(a) Surface axial strain, ϵ_{11}, vs time for all coupons of LAM1_C2, 45°

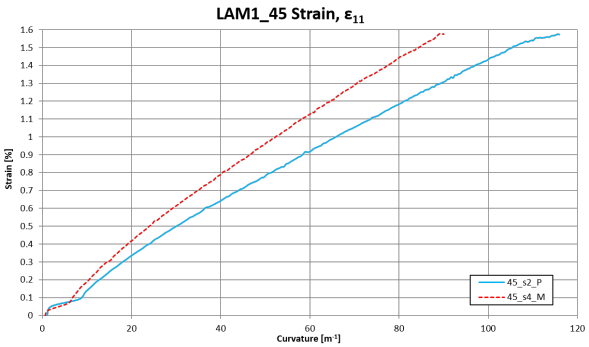

(b) Sample surface axial strain, ϵ_{11}, vs curvature for LAM1_C2, 45° coupons tested in the plastic and metal fixtures

Figure 50: Surface axial strains, ϵ_{11}, for coupons of LAM1_C2, 45° vs (a) test time and (b) curvature, κ.

6.3 Theoretical Material Properties

6.3.1 Classical Lamination Theory Predictions

Using Classical Lamination Theory, theoretical material properties were calculated using Autodesk Helius Composite 2016 software[52]. With the material properties of the fibers and resin provided by the manufacturers, shown in Table 16, Helius builds the unidirectional lamina from fiber properties and matrix properties provided with the input of fiber volume fraction using micromechanics. By combining the MR60H carbon fiber and PMT-F7 matrix resin and the micrograph and theoretical FVF calculations, four different MR60H UD laminas were created for each future laminate (CUNI and LAM1): avg corrected FVF, avg FVF, max theoretical FVF, and min theoretical FVF. For the HTA40 PW lamina, the Fabric Builder was used to create the woven fabric lamina; again fiber and resin properties are based on manufacturer-provided data. With the assigned fiber and matrix in addition to providing weave % weft and warp, assumed to be 50-50 for a 0-90PW lamina, areal weight and fiber weight %, values found in Table 17, the software calculates lamina thickness and compiles the properties. Helius calculated a thickness of 0.06382 mm; the measured per ply thickness for CPW was 0.06414 mm, that is approximately a 0.5% difference which is extremely encouraging.

Table 16: Fiber and matrix material properties

Property	Matrix (PMT-F7)	Fiber (HTA40)	Fiber (MR60H)
E11 (MPa)	3.53E+03	2.40E+05	2.90E+05
E22 (MPa)	3.53E+03	1.51E+04	1.90E+04
G12 (MPa)	1.12E+03	2.39E+04	2.70E+04
G23 (MPa)	–	6.64E+03	7.00E+03
NU12	3.77E-01	2.18E-01	2.00E-01
NU23	3.77E-01	1.36E-01	2.00E-01
CTE1 (mm/mm/C)	6.00E-05	-1.37E-06	-4.00E-07
CTE2 (mm/mm/C)	6.00E-05	1.09E-05	5.60E-06
CME1 (mm/mm/%m)	0.00E+00	0.00E+00	0.00E+00
CME2 (mm/mm/%m)	0.00E+00	0.00E+00	0.00E+00
+S1 (MPa)	7.18E+01	4.10E+03	5.68E+03
-S1 (MPa)	-1.02E+02	-2.50E+03	-3.20E+03
S12 (MPa)	9.18E+01	–	–
K1 (W/mm/K)	6.00E-04	1.00E-02	5.17E-03
K2 (W/mm/K)	–	1.00E-02	5.17E-03
Density (g/mm3)	1.25E-03	1.77E-03	1.81E-03
Tow End Area (mm2)	–	2.32E-01	2.51E-01

Table 17: Theoretical calculations of composite ply properties from manufacturer-provided data

Material	**Tensile Strength (MPa)**	**Tensile Modulus (GPa)**	**Density (g/cm^3)**
MR60H UD	5680	290	1.81
HTA40 PW	3920	238	1.76
Material	**Resin density (kg/m^3)**	**Resin RAW (g/m^2)**	
MR60H UD	1250	20.5	
HTA40 PW	1250	36.7	
Material	**Fiber density (kg/m^3)**	**Fiber FAW (g/m^2)**	**Fiber Thickness (mm)**
MR60H UD	1810	38	0.02099
HTA40 PW	1760	61	0.03466
Material	**Composite density (kg/m^3)**	**Composite AW (g/m^2)**	**Thickness (mm)**
MR60H UD	1564.4	58.5	0.03739
HTA40 PW	1526.1	97.7	0.06402
Material	**FVF**	**FC Ratio**	**After cure FVF (max/min)**
MR60H UD	0.561	0.650	0.611/0.561
HTA40 PW	0.541	0.624	0.591/0.541

With the lamina created, it is quite straightforward to build the laminates; the only inputs required are ply thickness and fiber orientation. For ply thickness, the micrograph measured thickness of the laminates was used and per ply thickness found by simply dividing by the plies per laminate for the CUNI (4 plies) and the CPW (3 plies) laminates. LAM1 was built of the average/max/min per ply thickness for the CPW to represent the plain weave plies and

the CUNI for the unidirectional plies. As a verification, the thickness calculated by Helius was checked against the measured LAM1 thickness, for the average thickness Helius found 0.339 mm while 0.341 was measured, again a less than 1% difference. For laminate creation, the FVF was held constant and ply thicknesses varied to model the laminates tested. From measured values three thicknesses were used: average, max, and min. All values used for building each laminate can be found in Table 18.

Table 18: Thickness and FVF combinations used to build laminates for CLT analysis

Laminate	Lamina	Orientation	FVF	Per Ply Thickness [mm] (avg/max/min)
CPW (3 plies)	HTA40 PW	0-90 PW	0.540	0.0641/0.0677/0.0570
		±45 PW	0.540	0.0641/0.0677/0.0570
CPW (8 plies)	HTA40 PW	0-90 PW	0.540	0.0621
		±45 PW	0.540	0.0621
CUNI (4 plies)	MR60H UD	0	0.609/0.633/0.611/0.561	0.0414/0.0430/0.0385
		90	0.633	0.0414/0.0430/0.0385
		45	0.633	0.0414/0.0430/0.0385
		-45	0.633	0.0414/0.0430/0.0385
CUNI (9 plies)	MR60H UD	0	0.611/0.561	0.05
		90	0.611/0.561	0.05
		45	0.611/0.561	0.05
		-45	0.611/0.561	0.05
LAM1 (Campaign 2)	HTA40 PW	0-90 PW	0.540	0.0641/0.0677/0.0570
		±45 PW	0.540	0.0641/0.0677/0.0570
	MR60H UD	0	0.633	0.0414/0.0430/0.0385
		90	0.633	0.0414/0.0430/0.0385
		45	0.633	0.0414/0.0430/0.0385
		-45	0.633	0.0414/0.0430/0.0385
LAM1 (Campaign 1)	HTA40 PW	0-90 PW	0.540	0.0621
		±45 PW	0.540	0.0621
	MR60H UD	0	0.611/0.561	0.05
		90	0.611/0.561	0.05
		45	0.611/0.561	0.05

For analysis of campaign 1 testing, thicknesses were measured prior to testing with micrograph techniques. Those values were used for building the CLT profile. There was no FVF data so theoretical values were calculated from manufacturer data for a range of possible values (see Table 17). Based on the thickness of the coupons, a per ply thickness was calculated for CUNI (0.050 mm) and CPW (0.0622 mm). Those values were used to build the CPW (8 plies) and CUNI (9 plies) laminates. LAM1 was built in the fashion as described above with the campaign 1 CUNI and CPW per ply thicknesses. All values used for building each laminate can be found in Table 18.

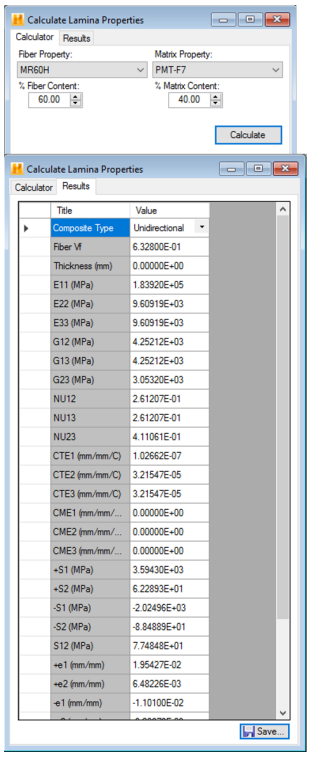

(a) Lamina construction

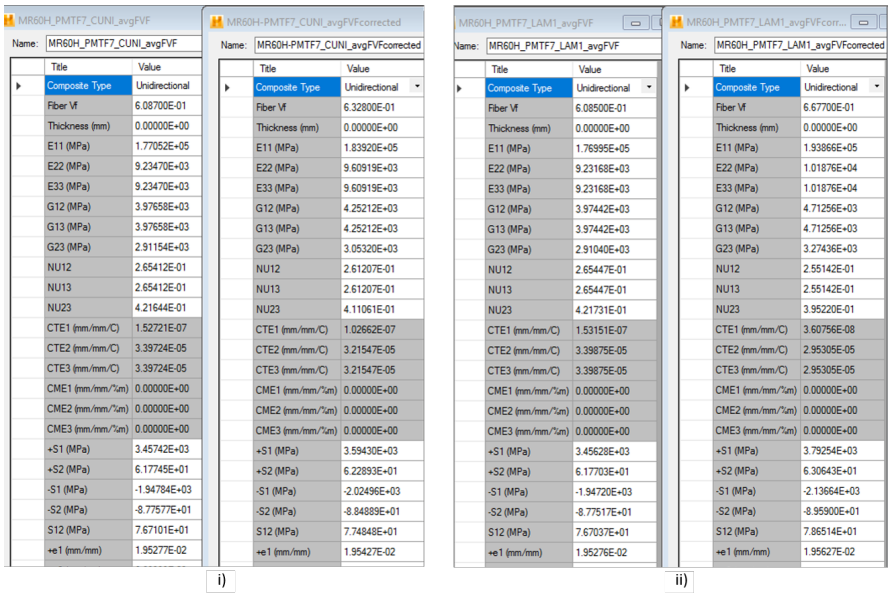

(b) Sample MR60H UD lamina for i) CUNI and ii) LAM1 laminates

Figure 51: Lamina construction with Autodesk Helius Composite 2016

Based on the ply thickness, fiber orientation, and stacking sequence, Helius calculated the ABD matrix for each laminate. For bending, the D matrix is of interest. For CLT, the bending matrix, D_{ij}, is defined as:

$$D_{ij} = \frac{1}{3}\sum_{k=1}^{n}\{\bar{Q}_{ij}\}_k({z_k}^3 - {z_{k-1}}^3) \tag{13}$$

where z represents the vertical position in the ply from the midplane. All D matrix values calculated can be found in Table 19 for campaign 1 and Table 20 for campaign 2.

Table 19: Calculated D matrix values [N-m] from Autodesk Helius Composite Software based on theoretical FVF and measured thickness for test campaign 1

Laminate	Bending Stiffness [N-m]					
CPW, 8 plies	D11	D12	D22	D16	D26	D66
0 calcFVF/measured062thick	0.71092	0.02279	0.71092	0	0	0.03361
±45 calcFVF/measured062thick	0.40046	0.33324	0.40046	0	0	0.34407
CUNI, 9 plies	D11	D12	D22	D16	D26	D66
0 maxtheoryFVF/measured050thick	1.35529	0.01873	0.0707	0	0	0.03042
0 mintheoryFVF/measured050thick	1.24701	0.01785	0.06523	0	0	0.02668
AVG	1.30115	0.01829	0.06796	0	0	0.02855
90 maxtheoryFVF/measured050thick	0.0707	0.01873	1.35529	0	0	0.03042
90 mintheoryFVF/measured050thick	0.06523	0.01785	1.24701	0	0	0.02668
AVG	0.06796	0.01829	1.30115	0	0	0.02855
+45 maxtheoryFVF/measured050thick	0.39628	0.33544	0.39628	0.32115	0.32115	0.34713
+45 mintheoryFVF/measured050thick	0.36367	0.31031	0.36367	0.29545	0.29545	0.31913
-45 maxtheoryFVF/measured050thick	0.39628	0.33544	0.39628	-0.32115	-0.32115	0.34713
-45 mintheoryFVF/measured050thick	0.36367	0.31031	0.36367	-0.29545	-0.29545	0.31913
AVG	0.37997	0.32287	0.37997	0.3083	0.3083	0.33313
LAM1, 6 plies	D11	D12	D22	D16	D26	D66
0 maxtheoryFVF/measuredUD050-PW062thick	0.14968	0.11238	0.13558	0	0	0.11615
0 mintheoryFVF/measuredUD050-PW062thick	0.14849	0.11237	0.13552	0	0	0.11611
AVG	0.14908	0.11238	0.13555	0	0	0.11613
90 maxtheoryFVF/measuredUD050-PW062thick	0.13558	0.11238	0.14968	0	0	0.11615
90 mintheoryFVF/measuredUD050-PW062thick	0.13552	0.11237	0.14849	0	0	0.11611
AVG	0.135549	0.112377	0.1490825	0	0	0.1161335
+45 maxtheoryFVF/measureUD050-PW062thick	0.24366	0.01135	0.24366	0.00352	0.00352	0.01512
+45 mintheoryFVF/measuredUD050-PW062thick	0.2433	0.01108	0.2433	0.00324	0.00324	0.01482
AVG	0.24348	0.01121	0.24348	0.00338	0.00338	0.01497

Table 20: Calculated D matrix values from Autodesk Helius Composite Software based on FVF and thickness adjustments for test campaign 2

Laminate	Bending Stiffness [N-m]					
CPW, 3 plies	D11	D12	D22	D16	D26	D66
0-90 Avg panel thickness	0.04125	0.00132	0.04125	0	0	0.00195
0-90 Max panel thickness	0.04851	0.00155	0.04851	0	0	0.00229
0-90 Min panel thickness	0.02895	0.00093	0.02895	0	0	0.00137
AVG	0.03957	0.00127	0.03957	0	0	0.00187
±45 Avg panel thickness	0.02323	0.01933	0.02323	0	0	0.01996
±45 Max panel thickness	0.02733	0.02274	0.02733	0	0	0.02348
±45 Min panel thickness	0.01631	0.01357	0.01631	0	0	0.01401
AVG	0.02229	0.01855	0.02229	0	0	0.01915
CUNI, 4 plies	D11	D12	D22	D16	D26	D66
0 avg corrected FVF/avg panel thickness	0.06983	0.00095	0.00365	0	0	0.00161
0 avg FVF/avg panel thickness	0.06723	0.00093	0.00351	0	0	0.0015
0 max theoretical FVF/avg panel thickness	0.06753	0.00093	0.00352	0	0	0.00152
0 min theoretical FVF/avg panel thickness	0.06213	0.00089	0.00325	0	0	0.00133
0 avg corrected FVF/Max panel thickness	0.08011	0.00108	0.0042	0	0	0.00189
0 avg corrected FVF/Min panel thickness	0.0575	0.00078	0.00301	0	0	0.00136
AVG	0.06739	0.00093	0.00352	0	0	0.00153
90 avg corrected FVF/avg panel thickness	0.00365	0.00095	0.06983	0	0	0.00161
90 avg corrected FVF/Max panel thickness	0.0042	0.00108	0.08011	0	0	0.00189
90 avg corrected FVF/Min panel thickness	0.00301	0.00078	0.0575	0	0	0.00136
AVG	0.00362	0.00094	0.06915	0	0	0.00162
+45 avg corrected FVF/avg panel thickness	0.02098	0.01761	0.02098	0.01694	0.01694	0.01832
+45 avg corrected FVF/Max panel thickness	0.02351	0.01973	0.02351	0.01898	0.01898	0.02054
+45 avg corrected FVF/Min panel thickness	0.01646	0.01387	0.01646	0.01331	0.01331	0.01439
-45 avg corrected FVF/avg panel thickness	0.02098	0.01761	0.02098	-0.01694	-0.01694	0.01832
AVG	0.02031	0.01707	0.02031	0.01641	0.01641	0.01775
LAM1, 6 plies	D11	D12	D22	D16	D26	D66
0 avg corrected UNI FVF/avg panel thickness	0.13433	0.10464	0.12606	0	0	0.10812
0 avg corrected UNI FVF/max panel thickness	0.1557	0.12155	0.14642	0	0	0.12559
0 avg corrected UNI FVF/min panel thickness	0.09807	0.07586	0.09142	0	0	0.07839
AVG	0.12937	0.10069	0.12130	0	0	0.10403
90 avg corrected UNI FVF/avg panel thickness	0.12606	0.10464	0.13433	0	0	0.10812
90 avg corrected UNI FVF/max panel thickness	0.14642	0.12155	0.1557	0	0	0.12559
90 avg corrected UNI FVF/min panel thickness	0.09142	0.07586	0.09807	0	0	0.07839
AVG	0.12130	0.10069	0.12937	0	0	0.10403
+45 avg corrected UNI FVF/avg panel thickness	0.22553	0.0093	0.22553	0.00207	0.00207	0.01278
+45 avg corrected UNI FVF/max panel thickness	0.2619	0.01072	0.2619	0.00232	0.00232	0.01475
+45 avg corrected UNI FVF/min panel thickness	0.1637	0.00691	0.1637	0.00166	0.00166	0.00944
-45 avg corrected UNI FVF/avg panel thickness	0.22553	0.0093	0.22553	-0.00207	-0.00207	0.01278
AVG	0.21704	0.00898	0.21704	0.00202	0.00202	0.01232

As a sanity check, the D matrices of the 0° and 90° orientations of each laminate should be identical with D_{11} and D_{22} values swapped; at 45°, the D_{11} and D_{22} values for all of these laminates are equal; and for CUNI, the +45° and -45° orientation D matrices are the same except D_{16} and D_{26} are the negative of each other. With this verified, the ABD matrices calculated can be trusted as a theoretical linear model.

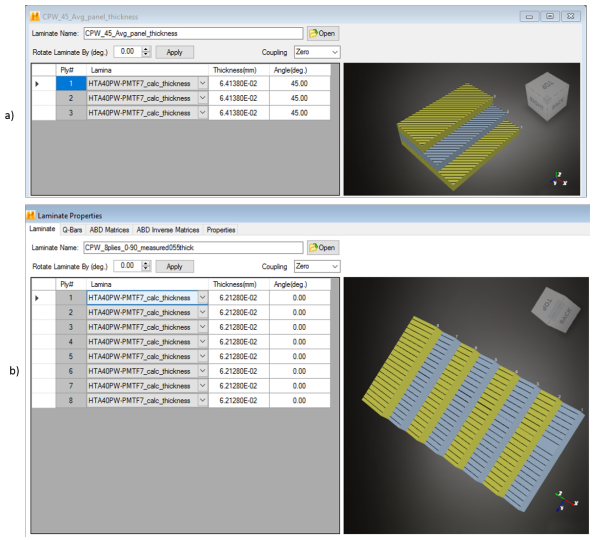

Figure 52: Sample CPW laminate "average thickness design" for a) 3 ply ($[45PW]_3$) and b) 8 ply ($[0PW]_8$) laminates

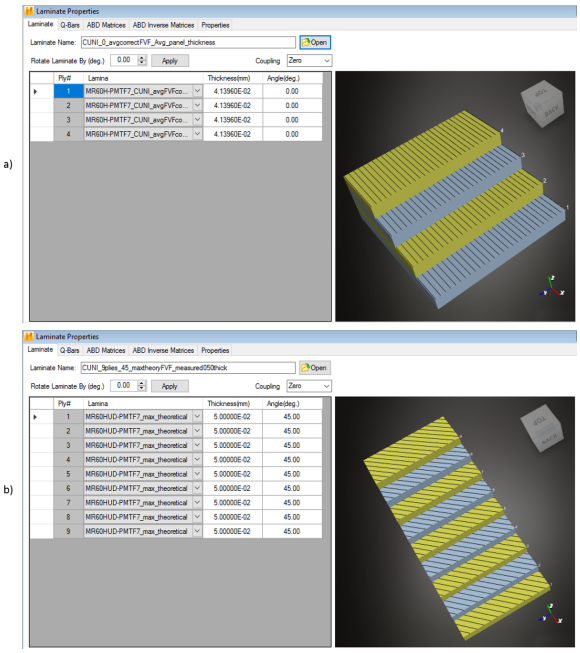

Figure 53: Sample CUNI laminate design for a) 4 ply ($[0]_4$) and b) 9 ply ($[+45]_9$) laminates

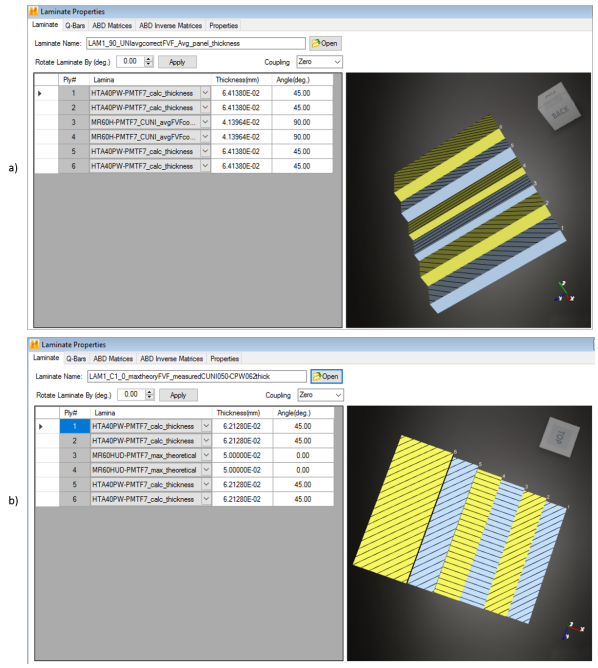

Figure 54: Sample LAM1, ($[45PW_2/90_2/45PW_2]$), laminate design for a) campaign 2 and b) campaign 1

6.3.2 CLT Predictions vs Experimentation

As observed in the data analysis when comparing the 9 ply CUNI to the 4 ply CUNI, the scaled down bending stiffness is not achieved until the last 20% of the test for the thinner laminate. This trend is also observed when comparing the D_{11} values from the CLT analysis and experimental results. Though the experimental results have a linear increase in the bending stiffness, the latter/final values reached during testing are very similar to the values calculated using Classical Lamination Theory. The data from campaign 1 is questionable as it is unclear when the load cell was damaged and the sample size of the data collected is quite small. Therefore it is difficult to compare campaign 1 to campaign 2 and the CLT analysis with much authority. Using the campaign 2 data, the theoretical values of D_{11} calculated using CLT analysis are 0.0396 N-m, 0.0692 N-m, and 0.129 N-m for the CPW, CUNI, and LAM1 coupons, respectively. These show small differences with respect to the experimentally measured values of 5.7%, 14.4%, and 6.9%, respectively. The theoretical values of D_{22} calculated using CLT analysis are 0.0396 N-m, 0.0036 N-m, and 0.121 N-m for the CPW, CUNI, and LAM1 coupons, respectively, with differences between the experimentally measured values of 7.2%, 6.34%, and 17.6%, respectively. The D_{11} values measured at 45^o have slightly higher error but within a respectable range for LAM1. Based on these comparisons, the CBT method appears to be a good candidate for large deformation bending of thin coupons up until failure. Table 21 shows the comparison between the CLT and experimental bending stiffness values as well as the percent differences.

Table 21: Average bending stiffness data comparison for CLT and experimental values for all CPW, CUNI, and LAM1 laminates

Laminate	CLT D11 [N-m]	Experimental D11 [N-m]	% Error	CLT D11 @ 45^o [N-m]	Experimental D11 @ 45^o [N-m]	% Error	CLT D22 [N-m]	Experimental D22 [N-m]	% Error
CPW 8 ply	0.71092	0.56587	20.40	0.40046	0.3141	21.57	0.71092	0.56587	20.40
CPW 3 ply	0.03957	0.04180	-5.65	0.02229	–	–	0.03957	0.03672	7.20
CUNI 9 ply	1.30115	0.77395	40.52	0.37997	0.15479	59.26	0.06796	0.23727	-249.12
CUNI 4 ply	0.06915	0.07909	-14.37	0.02031	0.02576	-26.81	0.00362	0.00339	6.34
LAM1 C1	0.14908	0.02542	82.95	0.24348	0.11863	51.28	0.13555	0.09321	31.23
LAM1 C2	0.12937	0.12052	6.84	0.21704	0.19396	10.64	0.1213	0.09999	17.57

6.4 Finite Element Analysis: Bending Strains

6.4.1 Finite Element Analysis

To perform the Finite Element Analysis (FEA), Abaqus Standard[53] was used for all computation.

Each composite coupon was built in Abaqus using the material data compiled in Helius Composite; i.e. the lamina material properties calculated with micromechanics by Helius from the fiber and matrix material data input from manufacturer data sheets. All lamina material properties came from Helius Composites Lamina or Fabric Builder functions. All ply thicknesses came from actual panel measurements averaged from the micrograph procedure. With these properties and thicknesses, Abaqus creates a composite layup for each model. All models were constructed with shell elements. For example, CPW (campaign 2) was built with HTA40PW lamina material properties and ply thickness of 0.06414mm as measured through micrographing.

∗Shell Section, elset=CPW-1, composite, layup=CPW
6.41381e-05, 3, HTA40PW, 0., Ply-1
6.41381e-05, 3, HTA40PW, 0., Ply-2
6.41381e-05, 3, HTA40PW, 0., Ply-3
(ply thickness, intergration points, ply material, fiber orientation, ply number)

The model dimensions are based on the coupon dimensions from testing. The height of the model is the grip separation and the width is the specimen width. Using the experimental grip separation is risky because most tests did not achieve the complete 90^o flex: most failed around 70^o-80^o, some significantly before. With using the test grip separation and bending it to a complete 90^o, the outputs will contain strains higher than those achieved during the test. To compare the test to the model, the moment applied is that which will achieve the failure angle from the test, in most cases around 70^o. All coupon widths are 0.0381m (1.5”); the heights vary based on the grip required for testing. The grip separations and angles used for the FEM are as follows, in Table 22.

Table 22: Dimensional and angle displacement requirements for FEA modeling from experimental data

Laminate	**Orientation**	**Grip [in]**	**Grip [mm]**	**Angle Achieved [rad]**	**Angle Achieved [°]**
CPW_8plies	0	1.7	43.18	0.91	52.4
CPW_8plies	45	1.5	38.1	1.1	63.03
CUNI_9plies	0	1.35	34.29	1.4	80.2
CUNI_9plies	45	1.95	49.53	0.95	54.4
CUNI_9plies	90	0.95	24.13	0.55	31.5
LAM1_C1	0	0.7	17.78	1.25	71.62
LAM1_C1	45	1.1	27.94	1.35	77.4
LAM1_C1	90	0.9	22.86	1.2	68.8
CPW_3plies	0	0.5	12.7	1.25	71.62
CPW_3plies	45	0.35	8.89	1.57	90.0
CUNI_4plies	0	0.4	10.16	1.4	80.2
CUNI_4plies	45	0.7	17.78	0.95	54.4
CUNI_4plies	90	0.75	19.05	1.25	71.62
LAM1_C2	0	0.6	15.24	1.35	77.4
LAM1_C2	45	0.55	13.97	1.3	74.5
LAM1_C2	90	0.9	22.86	1.3	74.5

Note: The ±45PW, 3 ply CPW was analyzed at the grip separation which was attempted during testing even though successful failure was not achieved.

The Column Bend Test was modeled by applying a moment to the top and bottom horizontal edges of the assembly mesh. Uniformity was controlled by tying each edge node to a single, corresponding MPC (multi-point constraint). This allowed for the moment loading condition to be applied to the top MPC and bottom MPC which subsequently controlled all top and bottom edge nodes. As the Column Bend Test is a pure moment design, the Abaqus FEA model is also a pure moment design. Once the composite is "made" in Abaqus, a moment is applied to each horizontal edge through the top and bottom MPC constraints. This uniformly bends the coupon about the x-axis, the width of the specimen. The moment applied, equal and opposite on each edge, was an estimate to get the coupon to flex to as close to the angle achieved during testing as possible. A boundary condition preventing translation in the horizontal (x) and sometimes the out of plane (z) directions was introduced to the MPCs to mimic the fixture grips. This condition was especially necessary for the 45° coupons as the model wanted to twist and warp from the top and bottom free edges and therefore not result in a perfectly circular bend. As in the Column Bend Test, only vertical (y) displacement is allowed at the horizontal edges, i.e. the grips.

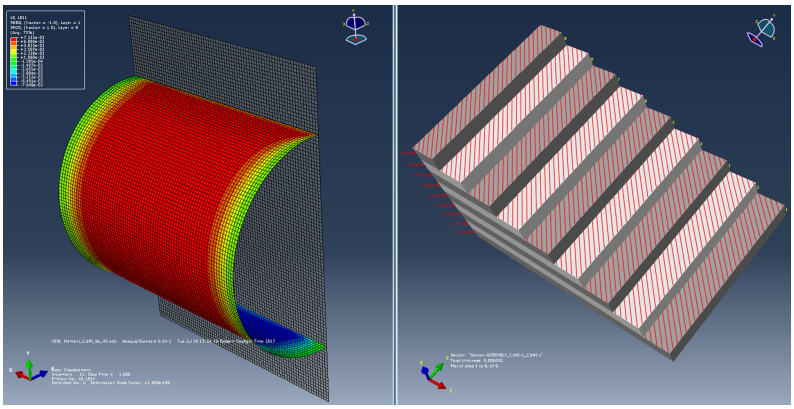

(a) FEM for CUNI $[45]_9$

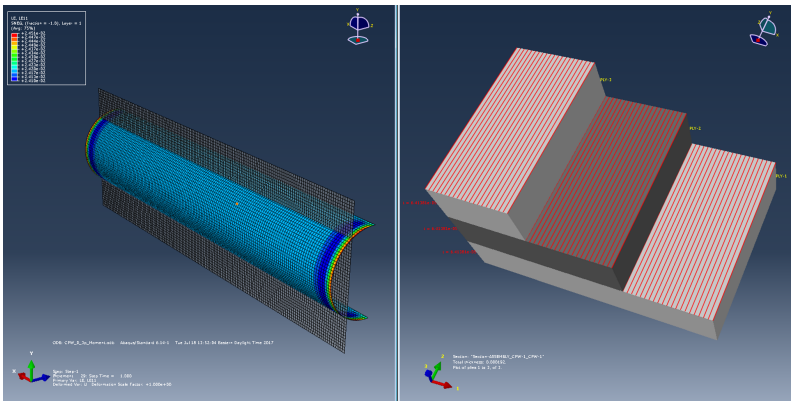

(b) FEM for CPW $[0]_3$

Figure 55: Sample finite element models using Abaqus Standard

As this material has nonlinear responses, Abaqus is run with geometric nonlinearity option, Nlgeom, turned on with automatic stabilization, dissipated energy fraction at 0.0002 (default), and adaptive stabilization with max ratio of stabilization to strain energy at 0.05 (default).

To capture data through the thickness of the composite laminate, one-to-three integration points were installed on each lamina. This allowed for calculation of through-the-thickness properties during the job run. The outer plies experience the largest magnitude of strains while the inner plies experience less strain, approaching zero at the midplane of the laminate stacking sequence. Depending on the bend direction, the topmost ply is in tension and the bottommost in compression with strains in each ply similar in magnitude and opposite in direction (tension vs compression).

This FEM is modeling an ideal pure bending case, essentially bending the coupons into a

perfect circle if the loads are high enough. This modeling of the perfect case is showcasing the imperfections and incorrect assumptions of the test. It required an applied moment two-to-three times higher than the experimental maximum moment to achieve the same deflection angle within the finite element model. It is assumed that the CBT is a pure moment test with constant curvature. In reality the test is not bending to a perfect circle nor is the curvature actually constant. A displacement model was created to apply the displacement condition of the MTS C43.504 with and without the addition of the moments to try to mimic the CBT more closely but the model resulted in strains that were impossibly high, around 5-7%, and a deformed coupon in an omega shape, not the circular deformation observed during testing. This model was clearly not modeling the CBT. The pure moment model was a better representation and so used going forward. The pure moment FEM uniformly experiences the strain through the height and width of the coupon, aside from some edge effect at the vertical edges. Given the FEM is the ideal situation, testing does not reveal uniform strain along the x and y. There is some variability of strain on the coupon surfaces during testing (see Figure 56). Sometimes even a slight strain gradient where the strain is concentrated at the midplane of the coupon and decreases moving out toward the horizontal edges. The strain gradient is mostly a result of testing with the metal fixture, further evidence that the plastic fixture is creating a more valid pure moment for the CBT. Based on the design of the composite layups through Abaqus, the strain of interest here is LE11 which corresponds to ϵ_{11} from the experimental testing. For geometrically nonlinear analysis using element formulations that support finite strains, LE (logarithmic strain) is the default strain measure for Abaqus.

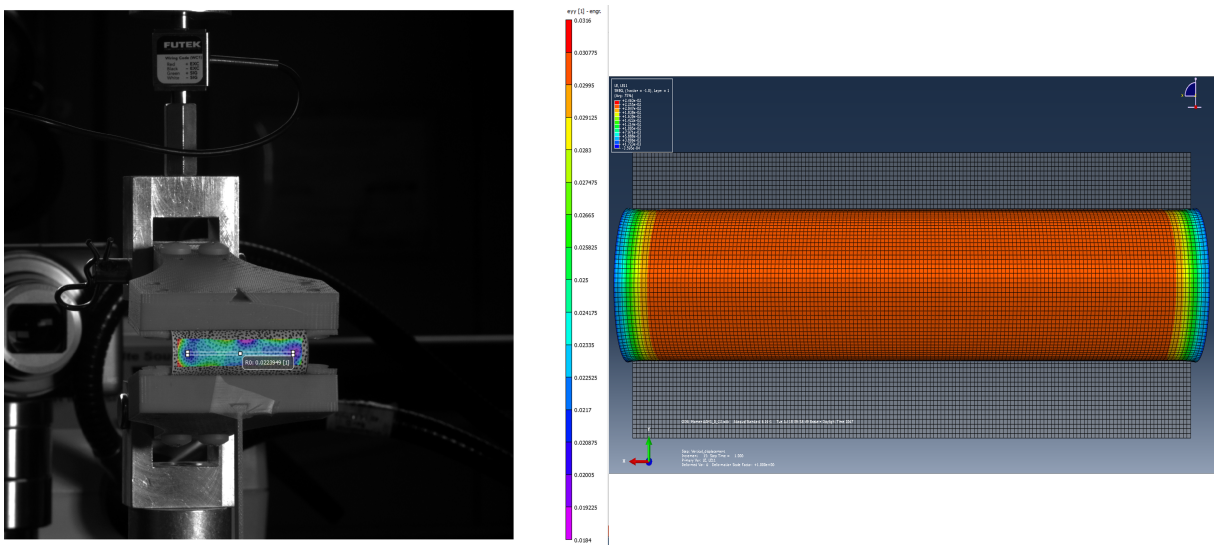

Figure 56: Strain response from VIC3D captured during experimentation vs FEM results calculated with Abaqus for LAM1_0_C2

As the CBT is a pure moment design, the pure moment FEM was used for FEA; see Appendix G for sample Abaqus input file. Table 23 shows the topmost (tension) and bottommost (compression) strains for all laminates.

Table 23: Maximum calculated axial strain, LE11, values from FEM for both tension and compression sides

Laminate	**Orientation**	**Tension [%]**	**Compression [%]**
CPW 8 ply	0	0.933	0.924
CPW 8 ply	45	1.122	1.095
CPW 3 ply	0	2.478	2.419
CPW 3 ply	45	1.698	1.642
CUNI 9 ply	0	1.933	1.896
CUNI 9 ply	45	1.617	1.642
CUNI 9 ply	90	0.722	0.706
CUNI 4 ply	0	1.885	1.85
CUNI 4 ply	45	0.778	0.772
CUNI 4 ply	90	0.684	0.67
LAM1 C1	0	1.769	1.761
LAM1 C1	45	1.423	1.415
LAM1 C1	90	2.180	2.172
LAM1 C2	0	2.139	2.127
LAM1 C2	45	2.048	2.036
LAM1 C2	90	2.294	2.286

Note: The ±45PW, 3 ply CPW was analyzed at the grip separation which was attempted during testing even though successful failure was not achieved.

The most useful aspect of the FEM is the through-the-thickness measurements. The DIC software packages while powerful can only capture the outer-most surfaces of the laminates. Using CLT and general understanding of composite structures, assumptions can be made about the inner plies but confirmation through the FEM is ideal. Based on stacking sequence and ply thicknesses it is evident how each ply handles the moment loads.

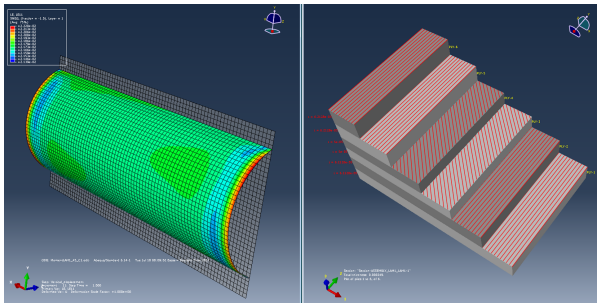

Figure 57: Curvature and stacking sequence for LAM1, campaign 1, orientation 45°

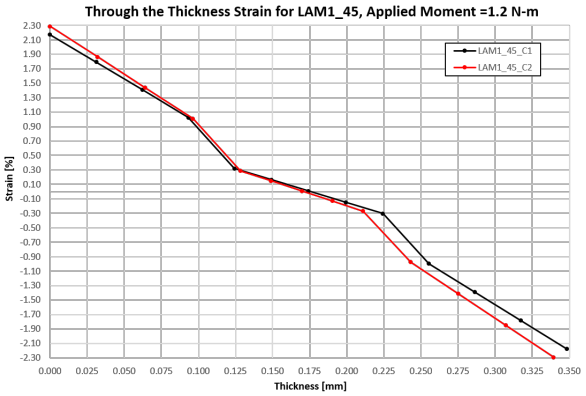

Figure 58: Through-the-thickness axial strain, LE11, for both campaigns of LAM1, orientation 45° with the same applied moment

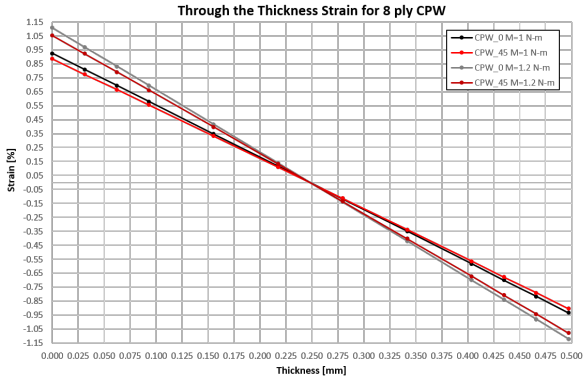

Figure 59: Through-the-thickness axial strains, LE_{11}, for all orientations of CPW, campaign 1

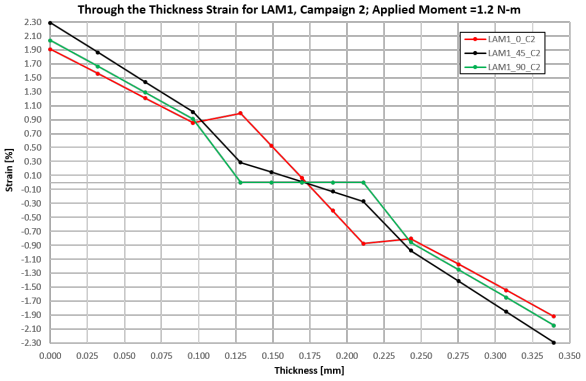

Figure 60: Through-the-thickness axial strains, LE_{11}, for all orientations of LAM1, campaign 2

Each laminate is experiencing more compression than tension though not at the difference observed during testing. The slope of the strain vs thickness curves are largely dependent on ply material. As seen in Figure 59, the strain is dispersed linearly throughout the laminate as all plies are the same material, HTA40PW, and thickness. The slope of said line varying due to fiber direction and applied moment. LAM1 is made of both lamina materials, MR60H UD and

HTA40PW. The change in ply material is obvious as the experienced strain and through-the-thickness slope changes drastically as the lamina properties change (see Figure 60). All strains are at the largest magnitude at the outer-most plies and decrease to zero at the midplane of the laminate.

6.4.2 FEA vs Experimentation

As mentioned above, the FEM was not a true representation of the CBT. The resulting strain response from the model is too uniform to mimic reality. Also the model strains, while higher in compression than tension, are not close to the noticeable strain differences between compression and tension observed during testing. The significant differences in strain values obtained at both surfaces of the coupon is thought to be related to the shift in neutral axis that the specimen experiences during the large deformation bending test, as a result of fiber material nonlinearities at higher strains. As the tensile side stiffens and the compressive side softens at high strains, the neutral axis moves towards the tension side, resulting in smaller strains when compared to the surface under compression. It is evident that the FEM is not shifting the axis when bending, therefore the experienced strains in the model are elevated on the tension side and reduced for the compression side. The model is outputting comparable strains to those seen during testing, but as it is the ideal case, it is clear that this FEM is not modeling the test or the assumptions about the test are not 100% valid. Theoretical surface strains were calculated using the relation from Equation 11. For simplicity the input values were based on the average experimental curvatures and thicknesses for each laminate. Table 24 shows the comparison between theoretical, FEM, and experimental axial strain, ϵ_{11} in both tension and compression. The FEM strains tend to be at values between the theoretical and experimental strains. As the FEM is outputting strains slightly lower for compression and slightly higher for tension, this makes sense. The FEM and theoretical strains are the maximum strain response, so should be closer to the compression strain values, but with no compressive strain data from campaign 2, it is not possible to properly compare. However, all three strain values are comparable, which is further proof that the Column Bend Test method appears to be a good candidate for large deformation bending of high strain composite coupons up until failure. The error between the

FEM strain response and the experimental values is on average approximately 22% with many less than 7%.

Table 24: Tensile and compressive axial strain data comparison for FEA and experimental values for all CPW, CUNI, and LAM1 laminates

Laminate	**Theoretical surface ϵ_{11} [%]**	**Experimental Compression ϵ_{11} [%]**	**Experimental Tension ϵ_{11} [%]**	**FEA Compression ϵ_{11} [%]**	**FEA Tension ϵ_{11} [%]**
CPW 8 ply					
0 calcFVF/measured055thick	0.961	0.857	0.898	0.933	0.924
±45 calcFVF/measured055thick	1.552	1.838	1.272	1.122	1.095
CPW 3 ply					
0-90 Avg_panel_thickness	2.027	N/A	2.867	2.478	2.419
±45 Avg_panel_thickness	N/A	N/A	N/A	1.698	1.642
CUNI 9 ply					
0 avg corrected FVF/measured050thick	1.790	2.057	1.620	1.933	1.896
90 avg corrected FVF/measured050thick	0.942	1.271	1.114	1.617	1.642
+45 avg corrected FVF/measured050thick	0.867	1.077	0.680	0.722	0.706
CUNI 4 ply					
0 avg corrected FVF/avg panel thickness	2.484	N/A	1.052	1.885	1.850
90 avg corrected FVF/avg panel thickness	0.892	N/A	0.675	0.778	0.772
+45 avg corrected FVF/avg panel thickness	0.853	N/A	0.677	0.684	0.670
LAM1_C1					
0 avg corrected FVF/measuredUD050-PW062thick	2.240	1.400	1.890	1.769	1.761
90 avg corrected FVF/measuredUD050-PW062thick	1.467	1.825	1.420	1.423	1.415
+45 avg corrected FVF/measureUD050-PW062thick	1.373	1.845	1.247	2.180	2.172
LAM1_C2					
0 avg corrected UNI FVF/avg panel thickness	2.648	N/A	2.265	2.139	2.127
90 avg corrected UNI FVF/avg panel thickness	2.696	N/A	2.147	2.048	2.036
+45 avg corrected FVF/avg panel thickness	1.501	N/A	1.449	2.294	2.286

Chapter 7: Conclusion

7.1 Conclusion

The Column Bend Test setup mechanics allow for direct calculation of the coupon flexural modulus and allowable flexural strain based on two key measurements: crosshead displacement and applied load. The design to induce a pure moment to thin laminates in large flexural strains is a bit of a reach. It is a pure moment design but this is achieved by displacing the fixture arms and applying a load to the fixture grips. While this does induce a moment, it cannot be said that the load is not also acting on the coupon, at least at the grips.

Though not a true pure moment test, the assumption of constant curvature of the specimen throughout the test, though also not reality, is a safe assumption. It was observed during experimentation that the moment varies in the coupon from minimum to maximum, with a variation of less than 15%, typically less than 6%. This difference is small enough to allow for the constant curvature assumption necessary for the simplification of the analytical model calculations.

At laminates this thin, there are significant limitations to the CBT based on the current fixture. Given that the purpose of this test is to characterize high strain composite laminates at thicknesses and layups common to deployable structures, the CBT must be able to function with coupons of the two-to-six ply order. There are limitations to the Column Bend Test, namely there is a minimum thickness that can be tested with this test set up. As this current set up of the CBT has a minimum allowable grip separation of 7.62mm, some of the thinner laminates cannot be tested to failure. The extreme thinness of the coupons in many cases dictated which fixture, metal or plastic, was required to break the samples. In some cases, the grip separations were so small that the plastic fixture was the only one capable of working at such small grips. The coupons that could not be broken can be tested to a 90^{o} deflection angle, but as failure is not achieved, the maximum moment and minimum diameter cannot be calculated. Testing could result in bending stiffness response data, but at these thicknesses the performance bending stiffnesses are not achieved until the last 20% of the test, so it would be difficult to know when those values are reached without failure. Testing thicker coupons and scaling down

by the thickness cubed or comparing against theoretical values calculated with CLT can give a range for those values. Also with this fixture design, the smaller grip separations required to break the coupons often make it difficult to image track the compression side of the samples. Aside from missing out on tracking the compression side for crack propagation and strain data, the smaller grip separations also potentially introduced grip effects and artificial stiffening that could obscure the data and the true material properties. Comparing test data for LAM1 from both test campaigns and with both the metal and plastic fixtures concluded that at the grip separations capable with this fixture, concerns over geometric stiffening from the plastic fixture are unnecessary. However, fixture or coupon adjustments for future testing to bend all laminates to failure will need to take this potential into account.

Testing with the metal fixture consistently resulted in slightly higher moments, bending stiffnesses, and strains, as well as smaller curvatures at failure for the LAM1 coupons. The trends, such as the more than doubling of the bending stiffness from initial to final, are the same, but the values are elevated. Also, the fixture in use (metal vs plastic) affects the slope of the strain vs curvature response but not the final failure strain value. The data from the plastic fixture does not appear to be corrupted by the small grip separations. The concerns about the artificial stiffening may be overstated and the weight of the metal fixture is influencing the data, therefore it is recommended to use the lighter plastic fixture for future testing.

Comparison between CLT, FEA, and experimentation show that the Column Bend Test appears to be a reasonable method for testing large deformation bending of high strain composite laminates. The thinner the laminate tested, the more confirmation of a nonlinear response of this classification of composites. The moment vs curvature curves were predominantly nonlinear resulting in a linear bending stiffness vs curvature response. At these large strains, carbon fibers are highly nonlinear resulting in the laminate flexure modulus increasing by up to 5x. The theoretical bending stiffness values calculated using CLT analysis are within a small difference with respect to the experimentally measured values: errors of approximately 5-10% for both D_{11} and D_{22}. For the strain response, the FEA modeled strains were within a reasonable margin. The error between the FEM strain response and the experimental values was on average around 22%, with 35% of the laminates and orientation having errors less than 7%. The biggest issue

with the FEM is the lack of shift in the neutral axis during bending. The shift in neutral axis that the specimen experiences during the large deformation bending test as a result of fiber material nonlinearities at higher strains is what causes the significant differences in surface strain values in compression vs tension. As the tensile side stiffens and the compressive side softens at high strains, the neutral axis moves towards the tension side; accordingly the distance to the surface under tension diminishes, resulting in smaller strains when compared to the surface under compression. Due to this phenomenon, being able to distinguish these strains is critical in accurate performance predictions of the material. The vertical test nature of the CBT when compared to other test methods proves to be helpful for visually capturing with DIC the distinct behavior of the flexure on both sides. The FEM is not shifting the axis, so the output compression strains are reduced and the tension elevated, i.e. not modeling the actual coupon behavior. However, comparison between CLT, FEA, and experimentation shows that, though using linear models to represent nonlinear responses is limited, the values of interest are within a reasonable percent error. Based on these comparisons, the Column Bend Test appears to be a promising candidate for characterization of large deformation bending behavior of thin-ply high strain composite laminates.

7.2 Future Work

Immediate future work involves testing more laminate thicknesses and layups, specifically LAM2, $[45PW_3/0_3]$, and LAM3, $[45PW_3/0PW_3]$. These laminates are often the design for deployable boom structures. Further testing on thinner versions of all laminates, LAM1 (3 plies), LAM2 (2 plies), and LAM3 (2 plies), is of interest but as the current test set-up and fixture are limited in grip separation, laminates of those thicknesses would be hard, if not impossible to break. Adjusted coupon dimensions as well as a modified fixture are necessary to be able to test those laminates.

The composite manufacturing community is active in fabricating thinner and thinner carbon fiber unidirectional as well as plain weave fabrics. Several thin-ply materials from vendors across the globe have been sourced in the search of materials with consistently good quality. These carbon fiber materials are some of the lightest intermediate modulus (IM) and high modulus

(HM) products available worldwide to date with resin systems that have space heritage. Future testing will involve these materials to determine the best strength-to-weight relationship as well as stiffness and curvature for future boom design.

Reasons for the high nonlinearity measured in the thinner coupons or why it seems like the true material stiffness is not achieved until high curvatures are reached is currently unknown. Further exploration into the last 20% region of the bending stiffness vs curvature of the thinner laminates is needed to see why it takes so long to reach the bending stiffnesses that are constant on thicker composites or to see at what curvature those bending stiffnesses are achieved.

Due to time limitations, the manufacturer data was used for fiber and matrix properties. An extensive testing campaign will begin shortly to capture the "real" material properties through tension, compression, shear, and platen testing. With these tests in addition to the CBT, a thorough material characterization can be completed. The FEM of the CBT needs further development to more accurately model the test reality. The immediate next steps are to update the material properties to better reflect the true laminate and to add more detailed integration points to track the laminate properties more precisely through the thickness and also in the intralaminar spaces.

The most expansive future work is adding the test steps to explore the viscoelastic relaxation effect. Due to the length of storage before deployment and mission length of deployable space structures, creep is a large concern. There is a growing need for further research into the viscoelastic effect of deployable structures and tape springs. As discussed, part of the design of the new test fixture was to incorporate test steps to analyze the viscoelastic relaxation and response to the Column Bend Test in future work. Though not utilized in this thesis, the new fixture was designed to enable the sample to be removed from the load frame in the bent position, placed in a thermal chamber for creep testing using the Time-Temperature Superposition Principle (TTSP)[24], and then placed back in the load frame and unloaded to "flat." This addition will be incorporated into the test design. Another option is to install a thermal chamber on the MTS C43.504 test frame to use the TTSP in line with the CBT. Incorporating these new steps to the test procedure will be crucial for future designing of deployable space structures.

References

[1] Peterson, M.E. and Murphey, T.W., "Large Deformation Bending of Thin Composite Tape Spring Laminates," *54th AIAA/ASME/ASCE/AHS/ASC Structures, Structural Dynamics, and Materials Conference*, Boston, Massachusetts, 2013.

[2] Kwok, K. and Pellegrino, S., "Shape Recovery of Viscoelastic Deployable Structures," *California Institute of Technology*, Pasadena, CA, 2010.

[3] Murphey T. W., Sanford G. E., and Grigoriev M. M., "Nonlinear Elastic Constitutive Modeling of Large Strains in Carbon Fiber Composite Flexures," *16th International Conference on Composite Structures*, Porto, Portugal, 2011.

[4] Sanford G. E., Ardelean E. V., Murphey T. W., and Grigoriev M. M., "High Strain Test Method for Thin Composite Laminates," *16th International Conference on Composite Structures*, Porto, Portugal, 2011.

[5] Autodesk, Inc. Autodesk Helius PFA Customer Success Story. "Opterus finds all the right elements with Autodesk Helius PFA," *Opertus Research and Development, Inc.*, Syracuse, NY, 2015.

[6] "AIAA Spacecraft Structures Technical Committee: High Strain Composites Technical Subcommittee (HSC-TSC)," `https://info.aiaa.org/tac/adsg/SCSTC/default.aspx`, 2014.

[7] Murphy, T.W., Francis, W.H., Davis, B.L., Mejia-Ariza, J., Santer, M., Footdale, J.N., Schmid, K., Soykasap, O., Guidanean, K., and Warren, P.A., "High Strain Composites", *2nd AIAA Spacecraft Structures Conference*, Kissimmee, FL, January 2015.

[8] Sanford G. E., Biskner A., and Murphey T. W., "Large Strain Behavior of Thin Unidirectional Composite Flexures," *51st AIAA/ASME/ASCE/AHS/ASC Structures, Structural Dynamics, and Materials Conference*, Orlando, FL, 2010.

[9] Murphey, T.W., Peterson, M.E. and Grigoriev, M.M., "Four Point Bending of Thin Unidirectional Composite Laminas," *54th AIAA/ASME/ASCE/AHS/ASC Structures, Structural Dynamics, and Materials Conference*, Boston, Massachusetts, April 2013.

[10] Murphey T. W., Peterson M. E., and Grigoriev M. M., "Large Strain Four-Point Bending of Thin Unidirectional Composites", *Journal of Spacecraft and Rockets*, Vol. 52, No. 3, 2015, pp. 882-895.

[11] Peterson, M.E., and Murphy, T.W., "High Strain Flexural Characterization of Thin CFRP Unidirectional Composite Lamina," *31st Annual American Society for Composites (ASC) Technical Conference*, Williamsburg, VA, September 2016.

[12] "ASTM D638 Standard Test Method for Tensile Properties of Plastics," *Book of Standards*, Volume 08.01.

[13] "ASTM D3039 Standard Test Method for Tensile Properties of Polymer Matrix Composite Materials 1," *Transition*, vol. i, pp. 1-13, 2008.

[14] Marks, G. W., Reilly, M. T., and Huff, R. L., "The Lightweight Deployable Antenna for the MARSIS Experiment on the Mars Express Spacecraft," *Proceedings of the 36th Aerospace Mechanisms Symposium*, NASA CP-2002-211506, April 2002, pp. 183–196.

[15] Kwok, K., and Pellegrino, S., "Viscoelastic Effects in Tape-Springs," *52nd AIAA/ASME/ASCE/AHS/ASC Structures, Structural Dynamics and Materials Conference*, Denver, CO, April 2011.

[16] Mobrem, M. and Adams, D. S., "Deployment Analysis of Lenticular Jointed Antennas Onboard the Mars Express Spacecraft," *AIAA Journal of Spacecraft and Rockets*, Vol. 46, No. 2, March–April 2009, DOI: 10.2514/1.36890. (pp. 394-402).

[17] Yee, J.C.H., Soykasap, Ö., and Pellegrino, S., "Carbon Fibre Reinforced Plastic Tape Springs," *45th AIAA/ASME/ASCE/AHS/ASC Structures*, Structural Dynamics, and Materials Conference, Palm Springs, California, April 2004.

[18] Leipold, M., Runge, H., and Sickinger, C. "Large SAR Membrane Antennas with Lightweight Deployable Booms," *28th ESA Antenna Workshop on Space Antenna Systems and Technologies*, ESA/ESTEC, May 31 - June 03, 2005.

[19] Fernandez, J.M., Lourens, V., Schenk, M., Stohlman, O.R, Aglietto, G.S., Lappas, V.J., and Erb, S., "Design and Development of a Gossamer Sail System for Deorbiting in Low Earth Orbit." *Acta Astronautica*, Vol. 103, October-November 2014, pp. 204-225.

[20] Mallikarachchi, H.M.Y.C. and Pellegrino, S., "Design of Ultrathin Composite Self-Deployable Booms," *Journal of Spacecraft and Rockets*, Vol. 51, No. 6, November-December 2014. (DOI: 10.2514/1.A32815)

[21] Fernandez, J.M., "Advanced Deployable Shell-Based Composite Booms For Small Satellite Structural Applications Including Solar Sails," *4th International Symposium on Solar Sailing*, Kyoto, Japan, 2017.

[22] Fernandez, J.M., Rose, G.K., Younger, C.J., Dean, G.D., Warren, J.E., Stohlman, O.R, Wilkie, W.K., "NASA's Advanced Solar Sail Propulsion System for Low-cost Deep Space Exploration and Science Missions that uses High Performance Rollable Composite Booms," *4th International Symposium on Solar Sailing*, Kyoto, Japan, 2017.

[23] Fernandez, J.M. and Murphey T.W., "A simple vertical test method for large deformation bending of thin high strain composite flexures," *AIAA SciTech Forum and Exposition*, 2018 (not yet published).

[24] Williams, M.L., Landel, R.F, and Ferry, J.D., "The Temperature Dependence of Relaxation Mechanisms in Amorphous Polymers and Other Glass-forming Liquids." *Journal of the American Chemical Society*, Vol. 77, Issue 14, July 1955, pp. 3701-3707. DOI: 10.1021/ja01619a008

[25] Yee, J.C.H. and Pellegrino, S., "Biaxial Bending Failure Locus for Woven-Thin-Ply Carbon Fibre Reinforced Plastic Structures," *46th AIAA/ASME/ASCE/AHS/ASC Structures, Structural Dynamics, and Materials Conference*, Austin, Texas, April 2005.

[26] Aguirre-Martinez, M. Bowen, D.H, Davidson, R., Lee, R.J., and Thorpe, T., "The Development of a Continuous Manufacturing Method for a Deployable Satellite Mast in CFRP," *British Plastics Congress*, September 1986.

[27] "ASTM D 6272 Standard Test Method for Flexural Properties of Unreinforced and Reinforced Plastics and Electrical Insulating Materials by Four-Point Bending 1," vol. 8, no. June, pp. 1-11, 2002.

[28] Brinkmeyer, A. Pellegrino, S., and Weaver, P.M., "Effects of Long-Term Stowage on the Deployment of Bistable Tape Springs," *Journal of Applied Mechancis*, Vol. 83, Issue 1, 2016.

[29] Violette, M.G., Schapery, R.A., "Time-Dependent Compressive Strength of Unidirectional Viscoelastic Composite Materials," *Mechanics of Time-Dependent Materials*, Vol. 6, 2002, pp. 133-145.

[30] Scott, D. W., Lai, J. S., Zureick, A.-H. "Creep Behavior of Fiber-Reinforced Polymeric Composites: A Review of the Technical Literature." *Journal of Reinforced Plastics and Composites*, Vol. 14, 1995, pp. 588 - 617.

[31] Lilholt, H., "Creep of Fibrous Composite Materials." *Composites Science and Technology*, Vol. 22, Issue 4, 1985, pp. 277-294.

[32] Mallikarachchi, H. M. Y. C., and Pellegrino, S., "Quasi-Static Folding and Deployment of Ultrathin Composite Tape-Spring Hinges," *Journal of Spacecraft and Rockets*, Vol. 48, No. 1, 2011, pp. 187–198. doi:10.2514/1.47321

[33] Mallikarachchi, H. M. Y. C., and Pellegrino, S., "Failure Criterion for Two-Ply Plain Weave CFRP Laminates," *Journal of Composite Materials*, Vol. 47, No. 11, 2013, pp. 1357–1375. doi:10.1177/0021998312447208

[34] Meyer, S., Zander, M., and Hühne, C., "Preliminary Creep Test for Estimating the Long Term Stowage Behavior of DLR'S CFRP Booms," *14th European Conference on Spacecraft Structures, Materials and Environmental Testing (ECSSMET)*, Toulouse, France, September 2016.

[35] Peterson, M.E. and Murphey, T.W., "Large Deformation Bending of Thin Composite Tape Spring Laminates," *54th AIAA/ASME/ASCE/AHS/ASC Structures, Structural Dynamics, and Materials Conference*, Boston, Massachusetts, 2013.

[36] Nettles, A.T., "Basic Mechanics of Laminated Composite Plates." NASA Reference Publication 1351, Marshall Space Flight Center, Huntsville, AL, October 1994.

[37] Makuch, A.J. and Reynolds, W.D., "In-situ Measurement of Viscoelastic Effects in Composite Tape Springs," *Proc. of SPIE Vol 8348, Health Monitoring of Structural and Biological Systems*, San Diego, CA, 2012.

[38] Jeon, S.K., and Murphy, T.W., "Design and analysis of a meter-class CubeSat boom with a motor-less deployment by bi-stable tape springs," *52nd AIAA/ASME/ASCE/AHS/ASC Structures, Structural Dynamics, and Materials Conference*, Denver, CO, April 2011.

[39] "Storable Tubular Extendable Member," Astro Aerospace, Northrop Grumman Corporation, Carpinteria, CA, 2013.

[40] C.P. Rubin. Deployable boom. US Patent 3434254. March 1969.

[41] G. Marks. Flattenable foldable boom hinge. US Patent 6343442. February 2002.

[42] T.W. Murphey and J. Banik. Triangular Rollable and Collapsible Boom. US Patent 7895795. March 2011.

[43] *MTS TestSuite TW Essential, Ver. 4.1.0.481*, MTS Systems Corporation, Eden Prairie, MN, 2015.

[44] *MATLAB R2016b*, Mathworks, Inc., Natick, MA, 2016.

[45] *VIC3D, Ver. 7.2.2*, Correlated Solutions, Inc., Irmo, SC, 2013.

[46] *Aramis, Ver. 6.3*, GOM mbH, Braunschweig, Germany, 2015.

[47] *VIC2D, Ver. 2009.1.0*, Correlated Solutions, Inc., Irmo, SC, 2009.

[48] *GIMP 2.8.20*, GNU Image Manipulation Program, Charlotte, NC, 2017.

[49] *Creo Parametric 2.0*, PTC, Needham, MA, 2014.

[50] *SignalExpress, Ver. 15.0.0*, National Instruments Corporation, Austin, TX, 2015.

[51] *ImageJ 1.51n*, National Institutes of Health, Bethesda, MD, 2017.

[52] *Helius Composite 2016*, Autodesk Inc., San Rafael, CA, 2016.

[53] *ABAQUS/Standard, Ver. 6.14-1*, Simulia, Providence, RI, 2007.

Appendix A: Futek Load Cell Calibration Data Sheet Sample

FUTEK
ADVANCED SENSOR TECHNOLOGY, INC.

Calibration Data

Sensor Info

Model LRM200
Item # FSH01671
S/N 668788
Capacity ..... 25 lb

Calibration Data

Test Temp ..... 76.4 °F (24.67 °C)
Relative Humidity ..... 40.2 %
Excitation ..... 5.00 (Vdc)
Input Resistance ..... 351 (Ohms)
Output Resistance ..... 352 (Ohms)

direction: Tension

Rated Output ..... 2.387 (mV/V)
Linearity ..... -0.036 % of R.O.

Data Points

Load	Output	Non-Lin Error (%)	Hysteresis (%)
channel: 1			
(lb)	(mV/V)		
direction: Tension			
0.000	0.0000	0.000	
5.000	0.4773	-0.002	
10.000	0.9542	-0.020	
15.000	1.4314	-0.026	
20.000	1.9085	-0.036	
25.000	2.3867	0.000	
0.000	0.0002		

Shunt Calibration

Shunt Value (K ohm)	Output ( )	Load (lb)
channel: 1		
direction: Tension		
60.4	1.453825	15.229

Shunt Cal is placed across (-E)(-S)

FUTEK Advanced Sensor Technology Inc. 10 Thomas Irvine CA. 92618 Tel: 1(800)23-FUTEK Fax: (949)465-0905

Appendix B: Column Bending Analysis MATLAB Script and Accompanying Functions


```
clear;
clc;

prompt = {'Enter a value for the length of the specimen (s) [in]: ',
    'Enter a value for theta in [radians]: ',
    };

dlg_title = ['Inputs for Column Bending Analysis'];
num_lines = 1;
defaultans = { '1.7', '0.1628392'};
answer = inputdlg(prompt,dlg_title,num_lines, defaultans);

filename = ['Test_Data.xlsx'];

l = 3.685;
s = str2num(cell2mat(answer(1,1)));
theta = str2num(cell2mat(answer(2,1)));


p_prime = xlsread(filename,1, 'E5:E1048576');

for i = 1001:2000:length(p_prime)
    if (i+1000)> length(p_prime)
    else
    p(i) = abs(mean(p_prime((i-1000):(i+1000))));
    end
end
p = nonzeros(p);

delta = xlsread(filename,1, 'A5:A1500');
time = xlsread(filename,1,'C5:C1500');

if length(p) > length(delta)
    p = p(1:length(delta));
elseif length(p) < length(delta)
    delta = delta(1:length(p));
end

for i=1:length(p)
    %Finds the phi value
    myfun = @f_phi;

    if i == 1
        fun = @(phi) myfun(phi,l,s,theta,delta(i));
        phi(i)=(fzero(fun, 0.000001));
    else
        fun = @(phi) myfun(phi,l,s,theta,delta(i));
        phi(i)=(fzero(fun, phi(i-1)));
    end

    %Finds the radius
```

```
    myfun = @f_r;

    if i == 1
        fun = @(r) myfun(phi(i),l,s,theta,r);
        r(i)=fzero(fun,(0.001));
    else
        fun = @(r) myfun(phi(i),l,s,theta,r);
        r(i)=fzero(fun,r(i-1));

    end

end

k = phi./s;
m_max = p'.*r;
m_min = p'.*l.*sin(theta'+phi./2);
for i = 2:(length(m_max))
    bs(i) = (m_max(i)-m_max(i-1))/(k(i)-k(i-1));
end
for i = 3:(length(m_max))

    if i == length(m_max)-1| i == length(m_max)
        bs_5pt_avg(i) = 0;
    else
        bs_5pt_avg(i) = mean(bs((i-2):(i+2)));
    end
end
% for i = 3:(length(m_max))
%
%
%     if i == length(m_max)-1| i == length(m_max)
%         bs_5pt_reg(i) = 0;
%     else
%         [a,b,c] = regression(k((i-2):(i+2)), m_max((i-2):(i+2)));
%         bs_5pt_reg(i) = b;
%     end
% end

excel = actxserver('excel.application');
excelWorkbooks = excel.Workbooks;
excelWorkbook = excelWorkbooks.Open([char(pwd)'/' filename]);
excelSheet = excelWorkbook.Sheets.Item(1);
excel.Visible = 1;

excelChart01 = excelSheet.ChartObjects.Add(800, 50, 600, 400);
excelChart01.Chart.ChartType = 73;

excelChart1 = excelChart01.Chart;

ver_val_array = ['J5:J' num2str(length(p)+4)];
horz_val_array = ['I5:I' num2str(length(p)+4)];
```

```
excelChart1.SeriesCollection.NewSeries;
excelChart1.SeriesCollection(1).Value = excelSheet.Range(ver_val_array);
excelChart1.SeriesCollection(1).XValue = excelSheet.Range(horz_val_array);
excelChart1.SeriesCollection(1).Name ='Max_Moment';

% ver_val_array = ['M7:M' num2str(length(p)+2)];
% horz_val_array = ['I7:I' num2str(length(p)+2)];
%
% excelChart1.SeriesCollection.NewSeries;
% excelChart1.SeriesCollection(2).Value = excelSheet.Range(ver_val_array);
% excelChart1.SeriesCollection(2).XValue = excelSheet.Range(horz_val_array);
% excelChart1.SeriesCollection(2).Name = 'Bending Stiffness 5pt Reg';
% excelChart1.SeriesCollection(2).AxisGroup = 2;


ver_val_array = ['M7:M' num2str(length(p)+2)];
horz_val_array = ['I7:I' num2str(length(p)+2)];

excelChart1.SeriesCollection.NewSeries;
excelChart1.SeriesCollection(2).Value = excelSheet.Range(ver_val_array);
excelChart1.SeriesCollection(2).XValue = excelSheet.Range(horz_val_array);
excelChart1.SeriesCollection(2).Name ='Bending Stiffness 5pt Avg';
excelChart1.SeriesCollection(2).AxisGroup = 2;

excelChart1.HasTitle = true;
excelChart1.ChartTitle.Text = ['Moment vs. Curvature'];
excelChart1.HasLegend = true;
excelChart1.Axes(1).HasMajorGridlines = 1;

excelChart1.Axes(1).HasTitle = 1;
excelChart1.Axes(1).AxisTitle.Text ='Curvature (in^-1)';
excelChart1.Axes(2).HasTitle = 1;
excelChart1.Axes(2).AxisTitle.Text ='Moment (lb-in)';
excelChart1.Axes(2,2).HasTitle = 1;
excelChart1.Axes(2,2).AxisTitle.Text ='Bending Stiffness (lb)';

excelSheet.Range('A3:C3').Merge;

excelSheet.Range('A:AA').Columns.AutoFit;

excelWorkbook.Save;
excelWorkbook.Close;
excel.Quit;
delete(excel);

xlswrite(filename, {'Specimen Length [in]', 'Initial Theta [rads]'}, 1, 'A1');
xlswrite(filename, [s,theta], 1,'A2');


xlswrite(filename, {'Load Cell Data'}, 1, 'E3');
```

```
xlswrite(filename, {'Load [lb]'}, 1, 'E4');
xlswrite(filename, [p], 1, 'E5');

xlswrite(filename, {'Phi [rads]' , 'R [in]', 'Curvature [in^-1]', 'Max Moment [lb-in]',↙
'Min Moment [lb-in]', 'Bending Stiffness [lb-in]', 'Bending Stiffness 5pt Avg. [lb-in]'},↙
1, 'G4');
xlswrite(filename, [phi', r',k',m_max', m_min', bs', bs_5pt_avg'], 1,'G5');

xlswrite(filename, {'Calculated'}, 2, 'A1');
xlswrite(filename, {'Time [s]', 'Phi/2 [rads]', 'Phi/2 [deg]'}, 2, 'A2');
xlswrite(filename, [time(1:length(p)), (phi./2)',((phi./2)*180/pi)'], 2,'A3');

excel = actxserver('excel.application');
excelWorkbooks = excel.Workbooks;
excelWorkbook = excelWorkbooks.Open([char(pwd)'\' char(filename)]);
excelSheet = excelWorkbook.Sheets.Item(2);
excel.Visible = 1;

excelChart01 = excelSheet.ChartObjects.Add(600, 50, 600, 400);
excelChart01.Chart.ChartType = 73;

excelChart1 = excelChart01.Chart;
ver_val_array = ['B3:B' num2str(length(p)+2)];
horz_val_array = ['A3:A' num2str(length(p)+2)];
excelChart1.SeriesCollection.NewSeries;
excelChart1.SeriesCollection(1).Value = excelSheet.Range(ver_val_array);
excelChart1.SeriesCollection(1).XValue = excelSheet.Range(horz_val_array);
excelChart1.SeriesCollection(1).Name ='Analytical';

excelChart1.HasTitle = true;
excelChart1.ChartTitle.Text = ['Phi/2 [Rad]'];
excelChart1.HasLegend = true;
excelChart1.Axes(1).HasMajorGridlines = 1;

excelChart1.Axes(1).HasTitle = 1;
excelChart1.Axes(1).AxisTitle.Text ='Time [s]';
excelChart1.Axes(2).HasTitle = 1;
excelChart1.Axes(2).AxisTitle.Text ='Phi/2 [rad]';

excelChart02 = excelSheet.ChartObjects.Add(600, 550, 600, 400);
excelChart02.Chart.ChartType = 73;

excelChart2 = excelChart02.Chart;
ver_val_array = ['C3:C' num2str(length(p)+2)];
horz_val_array = ['A3:A' num2str(length(p)+2)];
excelChart2.SeriesCollection.NewSeries;
excelChart2.SeriesCollection(1).Value = excelSheet.Range(ver_val_array);
excelChart2.SeriesCollection(1).XValue = excelSheet.Range(horz_val_array);
excelChart2.SeriesCollection(1).Name ='Analytical';

excelChart2.HasTitle = true;
```

```
excelChart2.ChartTitle.Text = ['Phi/2 [deg]'];
excelChart2.HasLegend = true;
excelChart2.Axes(1).HasMajorGridlines = 1;

excelChart2.Axes(1).HasTitle = 1;
excelChart2.Axes(1).AxisTitle.Text ='Time [s]';
excelChart2.Axes(2).HasTitle = 1;
excelChart2.Axes(2).AxisTitle.Text ='Phi/2 [deg]';

excelSheet.Range('C3').Formula = ['=B3*180/pi()'];
excelSheet.Range(['C3:C' num2str(length(p)+2)]).FillDown;

excelWorkbook.Save;
excelWorkbook.Close;
excel.Quit;
delete(excel);

display('Complete!')
```

```
%This is a MATLAB function that calculates the value of a specific function
%at a user defined x variable. This is a local function that is stored in
%the secant method folder so it can only be called by that master script
%or when the user has that current folder set to its path
%Calls our function and asks for the input variable
function y = f_phi(phi,l, s, theta, delta)

%Calculates our output variable and closes the function
y = (1-(2/phi)*sin(phi/2)+2*(l/s)*(cos(theta)-cos(theta+(phi/2))))-(delta/s);
end
```

```
%This is a MATLAB function that calculates the value of a specific function
%at a user defined x variable. This is a local function that is stored in
%the secant method folder so it can only be called by that master script
%or when the user has that current folder set to its path
%Calls our function and asks for the input variable
function y = f_r(phi,l,s,theta,r)

%Calculates our output variable and closes the function
y = ((1/phi)*(1-cos(phi/2))+l/s*sin(theta+phi/2))-r/s;
end
```

Appendix C: Fabric and Resin Material Data Sheets from Manufacturer

TohoTenax

TEIJIN

Delivery programme and characteristics for Tenax® HTA filament yarn

Brand name		**Tenax®**	**Tenax®**	**Tenax®**
Production site		**J**	**J / E**	**J / E**
Fiber family & tensile properties		**HTA40**	**HTA40**	**HTA40**
Sizing properties		F15 / H15	E13	E13
Number of filaments		1K	3K	6K
Nominal linear density [1)]	[tex]	67	200	400
Twist	[t/m]	15S	0/15Z	0/10Z
Running length per kg	[m/kg]	15000	5000	2500
Package weight, net	[kg]	0,2 • 0,5	1,0 • 2,0	2,0 • 4,0

1) ohne Präparationsauftrag

Characteristics (typical values)		
Filament diameter	[µm]	7
Density	[g/cm^3]	1,76
Tensile strength	[MPa]	3950
Tensile modulus	[GPa]	238
Elongation at break	[%]	1,7
Specific heat capacity	[J/kgK]	710
Thermal conductivity	[W/mK]	10
Coefficient of thermal expansion [	[10^{-6}/K]	-0,1
Specific electrical resistance	[Ω cm]	1,6 x 10^{-3}

Sizing properties for fiber family **HTA**

HTA is a classic Tenax® high performance carbon fiber. The high tenacity (HT) fibers provide excellent mechanical laminate properties.

F15 = Type with ca. 2,5 % sizing based on polyurethane
H15 = Type with ca. 2,5 % sizing based on epoxy resin

E13 = Type with ca. 1,3 % sizing based on epoxy resin

Please contact our sales team any time for choosing the right type. The stated numbers are typical values. For design purposes please request fiber specification.

Please note the application (aerospace or industry & sports) on your order.

The export or transfer of carbon fibers can be subject to authorization, depending on end-use and final destination.

Toho Tenax Europe GmbH Kasinostraße 19-21 42103 Wuppertal, Deutschland Tel.: +49 202 32 - 2339 Fax: +49 202 32 - 2360 www.tohotenax-eu.com sales@tohotenax-eu.com (04/2011)

GRAFIL INC.

PYROFIL™ MR60H 24K

Typical Fiber Properties

Tow Tensile	Strength	825 5,680	ksi MPa	JISR 7601
	Modulus	42 290	msi GPa	
Typical Density		0.065 1.81	$lb.in^3$ g/cm^3	JISR 7601
Typical Yield	24K	517 960	yds/lb mg/m	JISR 7601

5900 88th Street
Sacramento, CA
95828, USA
Tel: 916.386.1733
Fax: 916.383.7668
Web: www.grafil.com

ISO 9001:2008
FM 56416

6, Orchard Court
Binley Business Park
Harry Weston Road
Binley, Coventry CV3 2TQ UK
Tel: +44 (0) 2476 447272
Fax: +44 (0) 2476 449565

03/2010

PATZ MATERIALS & TECHNOLOGIES
4968 INDUSTRIAL WAY, BENICIA, CA 94510 • PH: 707-748-7577 • FAX: 888-203-8791

PMT-F7

Description:

PMT-F7 is a latent 350°F curing epoxy resin matrix. PMT-F7 is formulated to provide the highest glass transition temperature of any epoxy matrix. It also features a very high resin modulus. PMT-F7 has excellent handelability and room temperature tack and is a drop in replacememnt for standard 350°F curing systems.

Features:

- Maximum Tg greater than 440°F
- Work life at RT of 3 months
- OOA Processable
- Less than 0.2% Volitales
- Excellent toughness and strength
- Space qualified

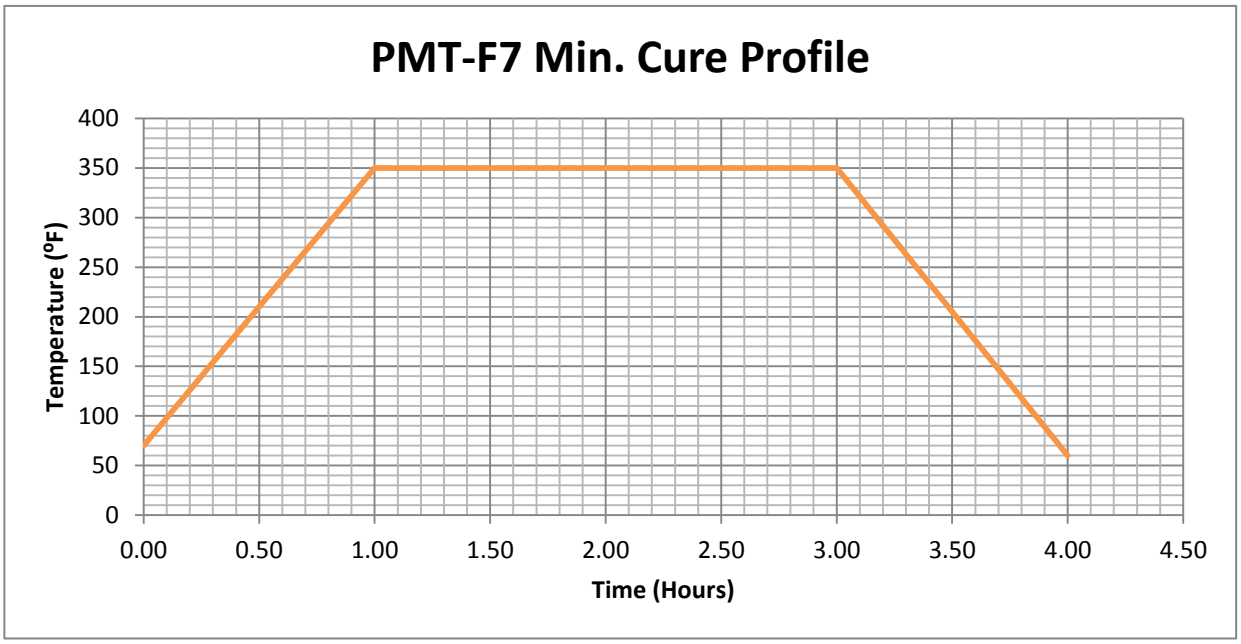

Cure Procedure:

PMT-F7 is offered as unidirectional or fabric prepreg. It is compatible with standard 350°F release materials and bagging procedures. PMT-F7 can be vacuum bag cured with standard release liners at a minimum of 26 inches Hg. For autoclave cured panels use the same ramp rate and transition to maximum autoclave pressure before 245°F. PMT-F7 should be cured with a ramp rate of 3°F/min to a dwell point of 350°F for a minimum of 2 hours.

Post Cure:

PMT-F7 laminates can be removed from the bag after initial cure and ramped at 5°F/min to a dwell point of 450°F for 2 hours to maximize Tg.

Mechanical Properties for PMT-F7 Resin:

	Kic	GIC(J/m²)	Tensile Strength (psi)	Tensile Modulus (ksi)	Maximum Strain at Break(%)
PMT-F7	**0.87**	**9**	10,418	433.7	4.14

Mechanical Properties for Glass Fabric:
Laminate: PMT-F7 / 7781 Eglass Fabric

	Strength (ksi)	Modulus (Msi)	Test Method
Compression	**61.3**	**3.7**	**ASTM D6641**
Tension	**62.8**	**3.9**	**ASTM D3039**
Flex	**71.2**	**3.6**	**ASTM D790**

Mechanical Properties for IM fiber:
Laminate: PMT-F7 / IM7 12K Unidirectional Fiber

	Strength (ksi)	Modulus (Msi)	Test Method
0° Compression	**285.5**	**22.0**	**ASTM D6641**
0° Tension	**398.6**	**23.1**	**ASTM D3039**
0° ILS	**16.8**	**--**	**ASTM D2344**

Storage:
PMT-F7 has a storage life of 2 years when stored at 10°F and a handling life of 3 months when stored at 75°F.
For more information contact Patz Materials and Technology at Development@PatzMandT.com

Appendix D: Test Campaign 1 Data Analysis

Laminate	Orientation	Sample	Smooth Side	Rough Side	Load Cell	Grip Separation [in]	Grip Separation [m]	Max Moment [lb-in]	Max Moment [N-m]	Min Diameter [in]	Min Diameter [m]	Initial Bending Stiffness [lb-in]	Final Bending Stiffness [lb-in]	Initial Bending Stiffness, D11 [N-m]	Final Bending Stiffness, D11 [N-m]	Compressive Failure Strain [%]	Tensile Failure Strain [%]	Last Strain Frame	Test End Frame	Initial Angle (rad)	Analytical Angle Achieved (rad)	Experimental Angle Achieved (rad)	Data G/B?	Aramis?	VIC3D	Failure
CPW	0	1	N/A	N/A	50	1.45	0.03683	5.75	0.649663	1.912	0.048565	5.35	4.7	0.604	0.531	1.17	0.988	78	79	0.0764	0.78	0.78	G?	Y	Compression	Snapped, Center, 90 direction
CPW	0	2	N/A	N/A	50	1.7	0.04318	3.011	0.340197	2.744	0.069698	4	3.85	0.452	0.435	0.455	0.452	213	242	0.0791	1.08	1.2	G?	Y	Compression	At bottom grip, C side? Distorted
CPW	0	3	N/A	N/A	25	1.7	0.04318	6.06	0.684688	1.682	0.042723	5.2	4.8	0.588	0.542	N/A	1.078	127	128	0.0465	1.04	N/A	G	N	Tension	Center region, 90 direction, C side
CPW	0	4	N/A	N/A	50	1.55	0.03937	5.411	0.611361	1.926	0.04892	5.2	5.1	0.588	0.576	0.95	0.893	59	60	0.0658	0.94	0.79	G?	Y	Compression	At top grip, C side? Distorted.
CPW	0	5_T1	N/A	N/A	25	1.7	0.04318	4.916	0.555433	2.096	0.053238	5.4	5.2	0.610	0.588	0.85	N/A			0.03	0.89	0.72	G	?	Compression	TEST 1: At grip, delamination near top grip
CPW	0	5_T2	N/A	N/A	25	1.2	0.03048	4.06	0.458718	2.543	0.064592	6.5	1.3	0.734	0.147	0.8	N/A	94	94	0.0456	0.87	0.75	G	N	Tension	TEST 2: At grip, C side, delam from first test progogated, 90 direction
CPW	0	6	N/A	N/A	50	1.85	0.04699	5.55	0.627066	1.851	0.047015	4.9	5.2	0.554	0.588	0.86	1.08	131	133	0.0557	1.08	1.07	G?	Y	Compression	At bottom grip, visible C side? No displacement data, used crosshead data from CPW_0_s2, same day, similar grip
CPW	**0**	**AVERAGE**	--	--	--	**1.6583**	**0.0421217**	**5.1163**	**0.578068**	**2.0352**	**0.051693**	**5.0083**	**4.8083**	**0.566**	**0.543**	**0.8570**	**0.8982**			**0.0589**	**0.9683**	**0.9120**			--	
CPW	**0**	**STDEV**	--	--	--	--	--	**1.0033**	**0.113356**	**0.3396**	**0.008625**	**0.4782**	**0.0454**	**0.054**	**0.053**	**0.2316**	**0.2335**	--	--	--	--	--	--	--	--	
CPW	45	1	N/A	N/A	50	1.75	0.04445	2.286	0.258283	1.627	0.041326	1.55	2.2	0.175	0.249	1.55	0.85	146	160	0.1082	1.46	1.54	G?	Y	Compression	±45 zig zag crack, C side, central region
CPW	45	2	N/A	N/A	50	1.45	0.03683	4.144	0.468209	1.225	0.031115	2.2	3.1	0.249	0.350	1.85	1.37	122	123	0.1197	1.29	0.129	G?	Y	Compression	±45 zig zag crack, C side, central region
CPW	45	3	N/A	N/A	50	1.55	0.03937	3.802	0.429568	1.118	0.028397	1.6	2.9	0.181	0.328	1.93	1.3	140	151	0.1038	1.43	N/A	G?	Y	Compression	±45 crack, C side, central region, spread to one grip
CPW	45	4	N/A	N/A	50	1.45	0.03683	3.595	0.40618	1.211	0.030759	1.8	2.7	0.203	0.305	1.79	1.3	114	117	0.1086	1.22	1.23	G?	Y	Compression	±45 crack, C side, central region
CPW	45	5	N/A	N/A	50	1.45	0.03683	4.363	0.492953	1.122	0.028499	2.0	3.0	0.226	0.339	2.07	1.54	0	133	0.1187	1.30	1.34	G?	Y	Compression	±45 zig zag crack, C side, central region
CPW	45	6	N/A	N/A	10	1.55	0.03937	--	--	--	--	--	--	--	--	--	--	288	298	--	--	--	terrupt	N	Tension	No Failure; MTS stopped halfway through, all other data continued; MTS data put together
CPW	**45**	**AVERAGE**	--	--	--	**1.5300**	**0.038862**	**3.6380**	--	**1.2606**	--	**1.8300**	**2.7800**	**0.207**	**0.314**	**1.8380**	**1.2720**	--	--	--	--	--	--	--	--	
CPW	**45**	**STDEV**	--	--	--	--	--	**0.7264**	--	**0.1884**	--	**0.2441**	**0.3187**	**0.028**	**0.036**	**0.1719**	**0.2285**	--	--	--	--	--	--	--	--	
CUNI	0	1_1	N/A	N/A	50	1.95	0.04953	--	--	--	--	--	--	--	--	--	--	--	--	--	--	--	--	--	--	No Failure; Data missing
CUNI	0	1_2	N/A	N/A	50	1.95	0.04953	--	--	--	--	--	--	--	--	--	--	--	--	--	--	--	--	--	--	No Failure; Data missing
CUNI	0	1_3	N/A	N/A	50	1.95	0.04953	--	--	--	--	--	--	--	--	--	--	--	--	--	--	--	--	--	--	No Failure; Data missing
CUNI	0	1_4	N/A	N/A	50	1.3	0.03302	13.866	1.566648	1.034	0.026264	6.2	6.9	0.701	0.780	2.05	1.25	125	?	0.1143	1.26	1.27	G?	Y	Compression	Broke close to the center, 0.25" from the grip; shattered in 0 direction
CUNI	0	2_1	N/A	N/A	50	1.6	0.04064	14.226	1.607322	1.087	0.02761	7.0	7.5	0.791	0.847					0.1347	1.47	1.53	G?	Y	Compression	No Failure
CUNI	0	2_2	N/A	N/A	50	1.35	0.03429	14.623	1.652177	0.999	0.025375	6.7	7.0	0.757	0.791	1.98	1.75	137	138	0.1065	1.37	N/A	G?	Y	Compression	Piece broke off, crack in 0 direction, piece about 1/3 width
CUNI	0	3	N/A	N/A	50	1.4	0.03556	14.333	1.619412	0.956	0.024282	6.3	6.9	0.712	0.780	2.14	1.43	222	234	0.0915	1.49	1.58	G?	Y	Compression	Broke at center, left 1/3 of specimen unbroken, shattered in 0 direction, broke in 90?
CUNI	0	4	N/A	N/A	50	1.3	0.03302	14.420	1.629241	0.970	0.024638	6.3	6.6	0.712	0.746	N/A	2.05	69	175	0.1480	1.35	1.37	G?	Y	Compression	Broke close to the center, sheared off at one grip
CUNI	**0**	**AVERAGE**	--	--	--	**1.3375**	**0.0339725**	**14.3105**	**1.616869**	**0.98975**	**0.02514**	**6.375**	**6.85**	**0.720**	**0.774**	**2.056666667**	**1.62**	--	--	--	--	--	--	--	--	
CUNI	**0**	**STDEV**	--	--	--	--	--	**0.277368**	**0.031338**	**0.029886**	**0.000759**	**0.192028644**	**0.15**	**0.022**	**0.017**	**0.065489609**	**0.306104557**	--	--	--	--	--	--	--	--	
CUNI	45	1	--	--	--	--	--	--	--	--	--	--	--	--	--	--	--	--	--	--	--	--	--	--	--	???
CUNI	45	2	N/A	N/A	10	1.95	0.04953	0.489	0.05525	2.33	0.059182	0.54	1.08	0.061	0.122	1.08	0.6	387	388	0.1501	0.84	N/A	G	Y	Compression	2 piece failure in ±45 direction (45deg GM)
CUNI	45	3	N/A	N/A	10	1.95	0.04953	0.711	0.080332	1.88	0.047752	0.47	1.51	0.053	0.171	1.1	0.8	127	128	0.1004	1.04	N/A	G	Y	Compression	2 piece failure in ±45 direction (45deg GM)
CUNI	45	4	N/A	N/A	10	1.95	0.04953	0.647	0.073101	1.92	0.048768	0.47	1.52	0.053	0.172	1.05	0.64	124	125	0.1707	1.02	N/A	G	Y	Compression	2 piece failure in ±45 direction (45deg GM)
CUNI	**45**	**AVERAGE**	--	--	--	**1.95**	**0.04953**	**0.615667**	**0.069561**	**2.043333**	**0.051901**	**0.493333333**	**1.37**	**0.056**	**0.155**	**1.076666667**	**0.68**	--	--	--	--	--	--	--	--	
CUNI	**45**	**STDEV**	--	--	--	--	--	**0.0933**	**0.010541**	**0.203361**	**0.005165**	**0.032998316**	**0.205101601**	**0.004**	**0.023**	**0.020548047**	**0.086409876**	--	--	--	--	--	--	--	--	
CUNI	90	1	--	--	--	--	--	--	--	--	--	--	--	--	--	--	--	--	--	--	--	--	--	--	--	???
CUNI	90	2	N/A	N/A	25	0.95	0.02413	--	--	--	--	--	--	--	--	--	--	--	--	--	--	--	--	--	--	Broke before being placed on load frame; snapped into 2 pieces; 90 crack near top grip
CUNI	90	3	N/A	N/A	25	0.95	0.02413	2.515	0.284157	1.771	0.044983	2.3	2.2	0.260	0.249	1.398	1.034	42	43	0.0908	0.56	0.64	G	Y	Compression	Snapped into 3 pieces; 90 crack near top and bottom grips; broke into thirds
CUNI	90	4	N/A	N/A	25	0.95	0.02413	2.413	0.272632	1.99	0.050546	1.9	2.2	0.215	0.249	1.143	1.194	36	37	0.0919	0.49	0.49	G	Y	Compression	Snapped into 2 pieces; 90 crack near top grip
CUNI	**90**	**AVERAGE**	--	--	--	**0.95**	**0.02413**	**2.464**	**0.278395**	**1.8805**	**0.047765**	**2.1**	**2.2**	**0.237**	**0.249**	**1.2705**	**1.114**	--	--	--	--	--	--	--	--	
CUNI	**90**	**STDEV**	--	--	--	--	--	**0.051**	**0.005762**	**0.1095**	**0.002781**	**0.2**	**0**	**0.023**	**0.000**	**0.1275**	**0.08**	--	--	--	--	--	--	--	--	
LAM1	0	1	T	C	50	0.7	0.01778	7.097	0.801853	0.788	0.020015	2.3	3.3	0.260	0.373	N/A	1.91	160	160	0.1656	1.10	1.16	B	N	Tension	Failed near top grip on C side
LAM1	0	2	T	C	50	1.2	0.03048	0.181	0.02045	1.081	0.027457	0.09	0.05	0.010	0.006	N/A	1.5	239	239	0.1410	1.11	1.55	B	N	Tension	No Failure
LAM1	0	3	C	T	50	0.95	0.02413	0.191	0.02158	0.69	0.017526	0.09	0.01	0.010	0.001	2.68	N/A	216	222	0.1000	1.43	N/A	B	N	Tension	No Failure; no initial angle: guessed 0.1 rad
LAM1	0	4	T	C	25	0.7	0.01778	0.55	0.062142	0.624	0.01585	0.15	0.058	0.017	0.007	N/A	1.87	171	171	0.1258	1.20	1.17	G	N	Tension	Failed near grip on C side, ±45 zig zag crack
LAM1	0	5	C	T	50	0.8	0.02032	0.161	0.018191	0.846	0.021488	0.07	0.02	0.008	0.002	3.48	N/A	210	223	0.0904	0.95	1.54	B	N	Compression	No Failure
LAM1	0	6	C	T	25	0.7	0.01778	0.731	0.082592	0.601	0.015265	0.3	0.08	0.034	0.009	1.4	N/A	204	214	0.0408	1.49	1.51	G	N	Compression	Failed near bottom grip on C side, ±45 zig zag crack
LAM1	**0**	**AVERAGE**	--	--	--	**0.7**	**0.01778**	**0.6405**	**0.072367**	**0.6125**	**0.015558**	**0.225**	**0.069**	**0.025**	**0.008**	**1.4**	**1.89**	--	--	--	--	--	--	--	--	
LAM1	**0**	**STDEV**	--	--	--	--	--	**0.0905**	**0.010225**	**0.0115**	**0.000292**	**0.075**	**0.011**	**0.008**	**0.001**	**0**	**0.02**	--	--	--	--	--	--	--	--	
LAM1	45	1	T	C	25	1.2	0.03048	1.709	0.193091	0.876	0.02225	0.5	1.2	0.056	0.136	1.99	N/A	217	217	0.0511	1.37	N/A	G	N	Compression	Crack in 90 direction 3/5 down
LAM1	45	2	C	T	25	1.2	0.03048	1.729	0.195351	0.912	0.023165	0.5	1.25	0.056	0.141	1.7	N/A	206	206	0.0625	1.32	N/A	G	N	Compression	Crack in 90 direction at bottom grip, C side
LAM1	45	3	C	T	25	1.2	0.03048	1.783	0.201452	0.805	0.020447	0.4	1.2	0.045	0.136	1.58	N/A	209	209	0.065	1.51	1.59	G	N	Compression	No Failure
LAM1	45	4	C	T	25	1.0	0.0254	1.626	0.183713	0.939	0.023851	0.5	1.1	0.056	0.124	N/A	1.48	197	228	0.0666	1.48	1.45	G	N	Compression	Crack in 90 direction, central region, C side, starting at one edge progressively moves through
LAM1	45	5	C	T	25	1.0	0.0254	1.32	0.14914	1.13	0.028702	0.6	0.8	0.068	0.090	N/A	1.19	176	176	0.008	1.33	1.4	G	N	Tension	Crack in 90, C side, 3/5 down, transferred to T side
LAM1	45	6	T	C	25	1.2	0.03048	1.049	0.118521	1.14	0.028956	0.4	0.9	0.045	0.102	N/A	1.07	189	189	0.0649	1.3	1.28	G	N	Tension	Crack in 90, C side, 2/5 down, through width
LAM1	**45**	**AVERAGE**	--	--	--	**1.12**	**0.028448**	**1.4866**	**0.167963**	**0.9994**	**0.025385**	**0.5**	**1.05**	**0.056**	**0.119**	**1.845**	**1.246666667**	--	--	--	--	--	--	--	--	
LAM1	**45**	**STDEV**	--	--	--	--	--	**0.263401**	**0.02976**	**0.112551**	**0.002859**	**0.063245553**	**0.173205081**	**0.007**	**0.020**	**0.145**	**0.172111075**	--	--	--	--	--	--	--	--	
LAM1	90	1	T	C	50	0.8	0.02032	4.897	0.553287	1.158	0.029413	2.3	3.2	0.260	0.362	1.67	N/A	117	117	0.0936	0.99	0.99	B	N	Compression	Progressive failure, final crack ±45 zig zag, C side, near bottom grip
LAM1	90	2	C	T	50	1.0	0.0254	0.196	0.022145	0.759	0.019279	0.09	0.04	0.010	0.005	1.98	N/A	216	234	0.106	1.46	1.53	B	N	Compression	Delamination on one edge
LAM1	90	3	T	C	50	0.9	0.02286	0.157	0.017739	1.01	0.025654	0.07	0.02	0.008	0.002	N/A	0.856	128	128	0.0803	1.03	1.05	B	N	Tension	Progressive failure, final crack ±45 zig zag, C side, central region
LAM1	90	4	C	T	50	0.9	0.02286	0.181	0.02045	0.815	0.020701	0.09	0.04	0.010	0.005	N/A	1.984	180	181	0.1279	1.23	1.24	B	N	Tension	Progressive failure, final crack ±45 zig zag, C side, central region, edge delamination too
LAM1	**90**	**AVERAGE**	--	--	--	**0.9**	**0.02286**	**1.35775**	**0.153405**	**0.9355**	**0.023762**	**0.6375**	**0.825**	**0.072**	**0.093**	**1.825**	**1.42**	--	--	--	--	--	--	--	--	
LAM1	**90**	**STDEV**	--	--	--	--	--	**2.043434**	**0.230877**	**0.158689**	**0.004031**	**0.95987955**	**1.371231199**	**0.108**	**0.155**	**0.155**	**0.564**	--	--	--	--	--	--	--	--	
LAM2	0	1	±45PW C	0UNI T	50	1.05	0.02667	0.125	0.014123	1.019	0.025883	-0.2	0.3	-0.023	0.034	1.319	1.276	44	156	0.69	1.5	1.56	B	Y	Compression	No Failure
LAM2	0	2	±45PW T	0UNI C	50	0.65	0.01651	9.394	1.061379	0.462	0.011735	1.7	3.0	0.192	0.339	N/A	2.837	201	219	0.0865	1.42	1.53	G?	N	Tension	No Failure
LAM2	0	3	±45PW C	0UNI T	50	0.8	0.02032	0.549	0.062029	0.552	0.014021	0.04	0.35	0.005	0.040	3.7	N/A	293	314	0.06	1.5	1.5	B	N	Compression	No Failure; sample misaligned?
LAM2	0	4	±45PW T	0UNI C	50	0.55	0.01397	11.264	1.272661	0.486	0.012344	2.4	3.0	0.271	0.339	N/A	3.484	228	228	0.1402	1.37	1.54	G?	N	Tension	No Failure
LAM2	0	5	±45PW C	0UNI T	50	0.65	0.01651	6.167	0.696777	0.48	0.012192	1.6	1.1	0.181	0.124	3.8	N/A	108	150	0.646	1.45	N/A	G?	N	Compression	Crack ±45 zig zag, C side, central region; VIC3D not recording to failure
LAM2	0	6	±45PW T	0UNI C	50	0.45	0.01143	9.994	1.12917	0.535	0.013589	2.4	2.7	0.271	0.305	N/A	2.95	216	216	0.1524	1.36	1.54	G?	N	Tension	Delamination on one edge, central region; ±45 crack
LAM2	**0**	**AVERAGE**	--	--	--	**0.55**	**0.01397**	**8.0805**	**0.912974**	**0.5075**	**0.012891**	**2**	**1.9**	**0.226**	**0.215**	**3.8**	**2.95**	--	--	--	--	--	--	--	--	
LAM2	**0**	**STDEV**	--	--	--	--	--	**1.9135**	**0.216196**	**0.0275**	**0.000699**	**0.4**	**0.8**	**0.045**	**0.090**	**0**	**0**	--	--	--	--	--	--	--	--	
LAM2	45	1	±45PW T	0UNI C	50	0.65	0.01651	0.182	0.020563	0.048	0.001219	0.05	0	0.006	0.000	N/A	1.46	222	222	0.1	1.43	N/A	B	N	Tension	No Failure; no initial angle: guessed 0.1 rad
LAM2	45	2	±45PW C	0UNI T	10	0.55	0.01397	0.758	0.085643	0.615	0.015621	0.32	0.15	0.036	0.017	N/A	2.02	79	98	0.078	1.0	N/A	G	N	Tension	Crack in ±45, shearing off
LAM2	45	3	±45PW T	0UNI C	25	0.55	0.01397	1.522	0.171963	0.425	0.010795	0.27	0.54	0.031	0.061	N/A	1.13	142	276	0.0912	1.42	1.5	G	N	Tension	Crack in ±45, C side, transferred to T side; VIC3D loses tracking early
LAM2	45	4	±45PW C	0UNI T	25	0.65	0.01651	0.368	0.041578	0.5	0.0127	0.25	0.08	0.028	0.009	N/A	1.56	227	227	0.0392	1.52	1.53	G	N	Tension	Cracking in ±45, early; shearing off at the edges; weird data
LAM2	45	5	±45PW T	0UNI C	25	0.5	0.0127	1.367	0.15445	0.382	0.009703	0.23	0.45	0.026	0.051	N/A	1.67	126	191	0.0793	1.34	1.37	G	N	Tension	Crack (almost 2 piece), progressive ±45 crack on C side, transferred to 90 crack in T, central region
LAM2	45	6	±45PW T	0UNI C	25	0.55	0.01397	1.024	0.115696	0.389	0.009881	0.2	0.43	0.023	0.049	N/A	1.69	203	204	0.0623	1.42	1.51	G	N	Tension	Progressive cracking ±45, C side; 90 crack, central region, T side
LAM2	**45**	**AVERAGE**	--	--	--	**0.56**	**0.014224**	**1.0078**	**0.113866**	**0.4622**	**0.011174**	**0.254**	**0.33**	**0.029**	**0.037**	**N/A**	**1.614**	--	--	--	--	--	--	--	--	
LAM2	**45**	**STDEV**	--	--	--	--	--	**0.416037**	**0.047006**	**0.087122**	**0.002213**	**0.040298883**	**0.180776105**	**0.005**	**0.020**	**N/A**	**0.286677519**	--	--	--	--	--	--	--	--	
LAM3	0	1	0-90PW C	±45PW T	25	0.65	0.01651	2.047	0.23128	1.104	0.028042	0.86	0.95	0.097	0.107	1.25	N/A	64	67	0.131	0.83	0.92	G	N	Compression	Crack in 90, central region, C side
LAM3	0	2	0-90PW C	±45PW T	25	1.5	0.0381	1.241	0.140214	1.055	0.026797	0.35	1.5	0.040	0.169	1.093	N/A	214	232	0.1545	1.46	1.53	G	N	Compression	No Failure: cracking heard but no visible damage

LAM3	0	3	0-90PW T	±45PW C	25	1.3	0.03302	1.146	0.129481	1.226	0.03114	0.25	1	0.028	0.113	1.67	N/A	193	215	0.1106	1.46	1.56	G	N	Compression	Crack in ±45 zig zag, central region, C side (Compressive stain at peak moment (1.207/1.72567) = 1.89 @308)
LAM3	0	4	0-90PW T	±45PW C	25	1.3	0.03302	1.282	0.144847	1.209	0.030709	0.54	1.1	0.061	0.124	1.664	N/A	205	225	0.0841	1.46	1.5	G	N	Compression	Crack in ±45 zig zag, central region 3/5 down, C side; Experimental angle data is odd. (Compressive stain at peak moment (1.669/2.0934) = 2.73 @407)
LAM3	0	5	0-90PW C	±45PW T	25	1.3	0.03302	1.711	0.193317	1.011	0.025679	0.52	1.35	0.059	0.153	1.492	1.490	301	311	0.0788	1.5	1.56	G	Y	Compression	No Failure: cracking heard but no visible damage; some residual curvature suggesting plastic deformation (Compressive stain at peak moment (2.014/2.2574) = 1.821 (A1.554) @456)
LAM3	0	6	0-90PW T	±45PW C	25	1.3	0.03302	1.96	0.22145	0.987	0.02507	0.55	1.4	0.062	0.158	1.952	0.869	225	241	0.1478	1.44	1.57	G	Y	Compression	No Failure: cracking heard but no visible damage; some residual curvature suggesting plastic deformation
LAM3	**0**	**AVERAGE**	--	--	--	--	--	**1.491667**	**0.168536**	**1.179667**	**0.029964**	**0.55**	**1.016666667**	**0.062**	**0.115**	**1.528**	**#DIV/0!**	--	--	--	--	--	--	--	--	--
LAM3	**0**	**STDEV**	--	--	--	--	--	**0.396586**	**0.044808**	**0.053953**	**0.00137**	**0.249131826**	**0.062360956**	**0.028**	**0.007**	**0.196590946**	**#DIV/0!**	--	--	--	--	--	--	--	--	--
LAM3	45	1	±45PW C	0-90PW T	25	1.3	0.03302	0.796	0.089936	1.223	0.031064	0.4	0.8	0.045	0.090	1.707	N/A	206	207	0.1368	1.41	1.39	G	N	Compression	±45 zig zag crack, C side, central region
LAM3	45	2	±45PW C	0-90PW T	25	1.3	0.03302	1.206	0.13626	1.01	0.025654	0.45	1.0	0.051	0.113	1.568	N/A	218	225	0.1126	1.4	1.43	G	N	Compression	±45 zig zag crack, C side, 2/5 down
LAM3	45	3	±45PW T	0-90PW C	25	1.3	0.03302	1.116	0.126091	1.004	0.025502	0.4	1.0	0.045	0.113	1.538	N/A	222	241	0.1144	1.47	1.6	G	N	Compression	Slight crack down middle, C side, 90 direction
LAM3	45	4	±45PW T	0-90PW C	25	1.2	0.03048	0.8705	0.098353	1.159	0.029439	0.48	0.75	0.054	0.085	1.211	N/A	203	212	0.0408	1.44	1.31	G	N	Compression	Crack in 90, 2/5 down, C side
LAM3	45	5_1	±45PW C	0-90PW T	25	1.3	0.03302	1.034	0.116826	0.918	0.023317	0.4	1.5	0.045	0.169	2.339	N/A			0.1486	1.44	1.54	G	N	Compression	No Failure: ±45 striations but no crakcing seen or heard
LAM3	45	5_2	±45PW C	0-90PW T	25	1.3	0.03302	1.408	0.159083	1.16	0.029464	0.3	1.48	0.034	0.167	2.261	0.86			0.0901	1.49	1.61	G	Y	Compression	No Failure: no visible or audible cracking
LAM3	45	5_3	±45PW C	0-90PW T	25	1.1	0.02794	0.735	0.083044	1.17	0.029718	0.25	0.7	0.028	0.079	2.103	0.696	106	112	0.1373	1.38	1.56	G	Y	Compression	Crack in ±45 zig zag, C side, near bottom grip, transferred to T side
LAM3	45	6	±45PW T	0-90PW C	25	1.2	0.03048	1.281	0.144734	1.185	0.030099	0.5	1.1	0.056	0.124	1.146	1.227	213	236	0.1700	1.41	1.56	G	Y	Compression	Crack in 90, C side, near bottom grip, plastic deformation
LAM3	**45**	**AVERAGE**	--	--	--	**1.2333333**	**0.0313267**	**1.00075**	**0.11307**	**1.125167**	**0.028579**	**0.413333333**	**0.891666667**	**0.047**	**0.101**	**1.5455**	**0.9615**	--	--	--	--	--	--	--	--	--
LAM3	**45**	**STDEV**	--	--	--	--	--	**0.209547**	**0.023676**	**0.085879**	**0.002181**	**0.081989159**	**0.148370782**	**0.009**	**0.017**	**0.318575344**	**0.2655**	--	--	--	--	--	--	--	--	--
LAM4	0	1_1	0-90PWc C	±45PWaq T	25	1.1	0.02794	--	--	--	--	--	--	--	--	--	--	--	--	--	--	--	G	Y	Compression	No Failure: no visible or audible cracking, slight curvature
LAM4	0	1_2	0-90PWc C	±45PWaq T	25	0.8	0.02032	1.565	0.176821	0.64	0.016256	0.35	0.68	0.040	0.077	2.162	1.566	215	222	0.096	1.44	1.53	G	Y	Compression	Crack in 90, C side, 3/5 down, transferred to T side; failed immediately after MTS stopped, DIC captured failure
LAM4	0	2	0-90PWc C	±45PWaq T	25	0.7	0.01778	N/A	N/A	N/A	N/A	N/A	N/A	N/A	N/A	1.458	1.686	197	198	0.0375	1.42	1.55	B	Y	Compression	Crack in 90, C side, central region; Load cell went crazy at end of test, data extremely noisy and useless
LAM4	0	3	0-90PWc T	±45PWaq C	25	0.7	0.01778	1.285	0.145186	0.792	0.020117	0.45	0.54	0.051	0.061	1.859	0.641	178	179	0.1088	1.25	1.46	G	Y	Compression	Sudden failure, no cracking heard prior, 90 crack on T side, falking on AQ, near (at?) bottom grips
LAM4	0	4	0-90PWc T	±45PWaq C	25	0.7	0.01778	1.133	0.128012	0.992	0.025197	0.55	0.4	0.062	0.045	1.359	0.668	151	151	0.0076	1.14	1.27	G?	N	Compression	Crack on C side, started at bottom grip and moved up to central region, distorted shape on T side; BAD ARAMIS DATA
LAM4	0	5	0-90PWc C	±45PWaq T	25	0.7	0.01778	0.955	0.107901	0.897	0.022784	0.3	0.45	0.034	0.051	1.126	N/A	202	222	0.1149	1.42	1.59	G	N	Compression	Failed immediately after test; crack in 90, C side, central region; significant delamination on one edge around middle
LAM4	0	6	0-90PWc T	±45PWaq C	25	0.7	0.01778	0.897	0.101347	1.06	0.026924	0.55	0.42	0.062	0.047	1.729	0.499	170	189	0.094	1.32	1.33	G	Y	Compression	Cracking in ±45, central region, C side; 90 crack in T side
LAM4	**0**	**AVERAGE**	--	--	--	**0.7166667**	**0.0182033**	**1.167**	**0.131853**	**0.8762**	**0.022255**	**0.44**	**0.498**	**0.050**	**0.056**	**1.6155**	**1.012**	--	--	--	--	--	--	--	--	--
LAM4	**0**	**STDEV**	--	--	--	--	--	**0.241383**	**0.027273**	**0.148664**	**0.003776**	**0.10198039**	**0.102839681**	**0.012**	**0.012**	**0.341820006**	**0.506031224**	--	--	--	--	--	--	--	--	--
LAM4	45	1_1	±45PWc C	0-90PWaq T	25	0.7	0.01778	0.944	0.106658	0.574	0.014587	0.32	0.15	0.036	0.017	3.683	1.85	--	--	0.063	1.47	1.67	G	Y	Compression	No Failure: no visible or audible cracking; some residual curvature suggesting plastic deformation. **Mid Bending Stiffness: 0.05**
LAM4	45	1_2	±45PWc C	0-90PWaq T	25	0.5	0.0127	0.848	0.095811	0.401	0.010192	0.10	0.10	0.011	0.011	4.07	1.665	194	218	0.1649	1.4	1.6	G	Y	Compression	±45 zig zag crack , C side, central region. **Mid Bending Stiffness: 0.35**
LAM4	45	2	±45PWc C	0-90PWaq T	25	0.5	0.0127	2.156	0.243595	0.576	0.014632	0.45	0.58	0.051	0.066	1.549	1.06	41	132	0.1675	0.99	1.14	G	Y	Compression	Abrupt failure in 90 on T side, ±45 zig zag crack on C side propogated to T? cracking hear immediately prior to failure; VIC3D data stops VERY early. **Mid Bending Stiffness: 0.50**
LAM4	45	3	±45PWc C	0-90PWaq T	25	0.6	0.01524	1.832	0.206988	0.555	0.014088	0.35	0.35	0.040	0.040	3.446	0.911	173	173	0.1824	1.17	1.49	G	Y	Compression	Abrupt failure, ±45 zig zag crack on C side, transferred to T, cracking hear immediately before failure. **Mid Bending Stiffness: 0.60**
LAM4	45	4	±45PWc T	0-90PWaq C	25	0.6	0.01524	1.162	0.131288	1.044	0.026518	0.54	0.55	0.061	0.062	1.5	1.185	150	217	0.1318	1.39	1.52	G	Y	Compression	Crack in 90, C side, near (at?) top grip; delamination between carbon and AQ on one edge; minor cracking T side at delam site; VIC3D data is all over the place. **Mid Bending Stiffness: 0.30**
LAM4	45	5	±45PWc T	0-90PWaq C	25	0.6	0.01524	1.077	0.121685	0.856	0.021742	0.45	0.55	0.051	0.062	1.48	1.206	193	219	0.0633	1.46	1.53	G	Y	Compression	Crack in 90, C side at top grip; minor delamination at one edge, small minor crack in center of C side; VIC3D data is all over the place. **Mid Bending Stiffness: 0.35**
LAM4	45	6	±45PWc T	0-90PWaq C	25	0.5	0.0127	1.052	0.11886	0.972	0.024689	0.48	0.43	0.054	0.049	1.185	1.494	145	219	0.1142	1.42	1.57	G	Y	Compression	Crack in 90, C side by bottom grip; transferred to minor cracking on edge of T side ±45; VIC3D data is all over the place. **Mid Bending Stiffness: 0.25**
LAM4	**45**	**AVERAGE**	--	--	--	**0.55**	**0.01397**	**1.3545**	**0.153038**	**0.733999**	**0.018644**	**0.395**	**0.426666667**	**0.04463**	**0.04821**	**2.3362**	**1.2535**	--	--	--	--	--	--	--	--	--
LAM4	**45**	**STDEV**	--	--	--	--		**0.471261**	**0.053245**	**0.236449**	**0.006006**	**0.143381775**	**0.166599987**	**0.01620**	**0.01882**	**1.182817721**	**0.254581192**	--	--	--	--	--	--	--	--	--

Appendix E: FVF MATLAB Scripts for Histogram Calculation from Contrast Image


```
function fiberVf = fvf(image)
A = imread(image);
N = histcounts(A,2, 'Normalization', 'probability');
fiberVf = N(2);
N
end
```

```
function fiberVf = fvf(image)
A = imread(image);
B = histcounts(A,2);
N = histcounts(A,2, 'Normalization', 'probability');
C = [B(1)*.837 B(2)*(1.163)];
FVf = [C(1)/(C(1)+C(2)) C(2)/(C(1)+C(2))];
fiberVf = N(2)
FVF=FVf(2)
end
```

Appendix F: Test Campaign 2 Data Analysis

Laminate	Orientation	Sample	Fixture	Grip Separation [in]	Grip Separation [m]	Max Moment [lb-in]	Max Moment [N-m]	Min Diameter [in]	Min Diameter [m]	Initial Bending Stiffness [lb-in]	Final Bending Stiffness [lb-in]	Initial Bending Stiffness, D11 [N-m]	Final Bending Stiffness, D11 [N-m]	Compressive Failure Strain [%]	Tensile Failure Strain [%]	Last Strain Frame	Test End Frame	Initial Angle (rad)	Analytical Angle Achieved (rad)	Experimental Angle Achieved (rad)	Data G/B?	Aramis?	VIC3D Failure
CFW_3p	0	1	M	0.5	0.0127	0.915	0.103181	0.376	0.010	0.03	0.43	0.003	0.049	N/A	2.400	201	200	0.118	1.341	1.208	G	NO	Tension Crack in 90 on T side (2/5 down), visible, smaller (not through width) 90 cracks on C side, paint still attached in places with no/no cracking, cracking heard around 6:25, complete failure 15 sec after failed at 200.
CFW_3p	0	2	M	0.5	0.0127	0.870	0.098297	0.406	0.010	0.03	0.41	0.003	0.046	N/A	3.36	189	190	0.179	1.244	1.349	G	NO	Tension Crack in 90 on center of side, visible, smaller 90 cracks on C side., Cracking heard just before failure at 4:18 (at 150).
CFW_3p	0	3	M	0.5	0.0127	0.930	0.105076	0.380	0.010	0.03	0.42	0.003	0.047	N/A	2.925	198	199	0.098	1.348	1.356	G	NO	Tension C side, visible, smaller (not through width) 90 cracks on C side, cracking heard cracking a few seconds before complete failure around 6:35. Failed at 199.
CFW_3p	0	5	M	0.45	0.01143	0.802	0.090614	0.353	0.009	0.04	0.31	0.005	0.035	N/A	2.781	178	176	0.035	1.313	1.035	G	NO	Tension C side, Abrupt failure. Failed at 176. (questionable angle data)
CFW_3p	0	6_1	P	1.3	0.03302	--	--	--	--	--	--	--	--	--	--	--	--	--	--	--	B	Y	Compression No Failure
CFW_3p	0	6_2	P	1.15	0.02921	--	--	--	--	--	--	--	--	--	--	--	--	--	--	--	B	Y	Compression No Failure
CFW_3p	0	6_3	P	0.8	0.02032	--	--	--	--	--	--	--	--	--	--	--	--	--	--	--	B	Y	Compression No Failure: new quick-release cleats pin, new nylon screws
CFW_3p	0	6_4	P	0.8	0.02032	--	--	--	--	--	--	--	--	--	--	--	--	--	--	--	B	Y	Compression No Failure: old cleats pin to verify new one wasn't interfering
CFW_3p	0	6_5	P	0.6	0.01524	--	--	--	--	--	--	--	--	--	--	--	--	--	--	--	B	Y	Compression No Failure
CFW_3p	0	6_6	M	0.6	0.01524	--	--	--	--	--	--	--	--	--	--	--	--	--	--	--	B	Y	Compression No Failure
CFW_3p	0	6_7	P	0.45	0.01143	--	--	--	--	--	--	--	--	--	--	--	--	--	--	--	B	Y	Compression No Failure: had to stop around 45° not enough clearance with screws
CFW_3p	0	6_8	M	0.45	0.01143	0.720	0.081349	0.354	0.009	0.05	0.28	0.006	0.032	Bad	Bad	58	185	0.093	1.307	1.384	B	Y	Compression Crack in the 90 at center of T side. Visible microcracking in 90 at center of C side. Aramis failed between 185 & 186 (VIC3D dropped at 51, both strain data sets don't make any sense. (used 4.745 correction factor)
CFW_3p	0	7	M	0.5	0.0127	0.558	0.063046	0.376	0.010	0.03	0.28	0.003	0.032	3.353	Bad	208	215	--	1.410	--	B	Y	Compression No Failure; Aramis data doesn't make sense, VICID noisy; less paint to make sure paint thickness wasn't the issue with breaking the specimen. Angle data missing.
CFW_3p	90	3_1	M	0.5	0.0127	0.896	0.101214	0.350	0.009	0.01	0.63	0.001	0.071	N/A	2.115	213	213	0.080	1.427	--	G	NO	Tension Crack in 90 in center of T side, slight 90 cracks on C side, Abrupt failure. Failed at 197, may have some grip effect.
CFW_3p	90	3_2	M	0.45	0.01143	1.041	0.117617	0.320	0.008	0.05	0.40	0.006	0.045	N/A	2.243	198	197	0.032	1.407	1.475	G	NO	Tension Crack in 90 in center of T side, slight 90 cracks on C side, Abrupt failure. Failed at 199, paint obscured some cracks?
CFW_3p	90	4	M	0.45	0.01143	0.804	0.09084	0.329	0.008	0.02	0.35	0.002	0.040	N/A	2.452	200	199	0.073	1.380	1.352	G	NO	Tension Crack in 90 in center of T side, slight 90 cracks on C side, cracked a few times before complete failure. First visible crack at 186, total failure at 187.
CFW_3p	90	5	M	0.45	0.01143	0.721	0.081462	0.335	0.009	0.03	0.26	0.003	0.029	N/A	2.018	188	186	0.045	1.348	1.324	G	NO	Tension Crack in 90 in center of T side, slight 90 cracks on C side, Abrupt failure. Failed at 182.
CFW_3p	90	6	M	0.45	0.01143	0.657	0.074231	0.352	0.009	0.03	0.29	0.003	0.033	N/A	1.574	183	182	0.052	1.321	1.202	G	NO	Tension Crack in 90 in center of T side (not straight, slopes down), slight 90 cracks on C side, Abrupt failure. Failed at 182.
CFW_3p	90	AVERAGE	--	0.4500	0.01143	0.8058	0.091038	0.3342	0.008	0.0325	0.3250	0.004	0.037	N/A	2.0718	--	--	--	1.3640	1.3383	--	--	--
CFW_3p	90	STDEV	--	--	--	0.1455	0.016437	0.0117	0.000	0.0109	0.0541	0.001	0.006	N/A	0.3258	--	--	--	--	--	--	--	--
CFW_3p	45	1_1	M	0.45	--	0.968	0.10939	0.304	0.008	0.05	0.60	0.006	0.068	N/A	2.314	211	211	0.019	--	--	G	NO	Tension No Failure; had to stop before 45 bend due to fixture plates touching
CFW_3p	45	1_2	M	0.35	--	--	--	--	--	--	--	--	--	--	--	--	--	--	--	--	G	NO	Tension
CFW_3p	45	AVERAGE	--	0.45	--	--	--	--	--	--	--	--	--	--	--	--	--	--	--	--	--	--	--
CFW_3p	45	STDEV	--	--	--	--	--	--	--	--	--	--	--	--	--	--	--	--	--	--	--	--	--
CUN_4p	0	1	M	0.4	0.01016	1.357	0.15332	0.307	0.008	0.03	0.50	0.003	0.056	N/A	1.072	190	178	0.044	1.380	1.391	G	NO	Tension Already splitting in 0 on edges prior to testing; 90 crack and fiber failure started at one edge. 0 splitting at crack tip; crack propagated slowly toward middle in 90 with 0 splitting; cracks at both ends meeting in center. Initial crack at 178, total abrupt failure at 192
CUN_4p	0	2_1	M	0.7	0.01778	1.058	0.11953	0.479	0.012	0.05	0.83	0.006	0.094	N/A	0.902	220	220	0.064	1.460	--	G	NO	Tension No Failure
CUN_4p	0	2_2	M	0.6	0.01524	1.198	0.13536	0.425	0.011	0.04	0.85	0.005	0.096	N/A	0.961	218	218	0.107	1.413	1.385	G	NO	Tension No Failure
CUN_4p	0	2_3	M	0.5	0.0127	1.359	0.15354	0.342	0.009	0.04	0.78	0.005	0.088	N/A	1.064	213	213	0.044	1.460	1.458	G	NO	Tension No Failure
CUN_4p	0	2_4	M	0.4	0.01016	1.530	0.17287	0.299	0.008	0.1	0.60	0.006	0.088	N/A	1.124	192	199	0.085	1.372	1.456	G	NO	Tension 90 crack/fiber failure causing splitting in 0 about 1/5 from edge. Caused progressive failure with 90 cracking then 0 splitting propogating from one edge to other. Initial at 190, across width by 199.
CUN_4p	0	3_1	M	0.45	0.01143	1.581	0.17867	0.322	0.008	0.06	0.78	0.007	0.088	N/A	1.023	210	210	0.110	1.396	1.431	G	NO	Tension No Failure
CUN_4p	0	3_2	M	0.4	0.01016	1.432	0.16179	0.123	0.003	0.06	0.54	0.007	0.061	N/A	1.070	195	185	0.1460	1.303	1.350	G	NO	Tension 90 crack and fiber failure at edges, crack propogating toward center with 0 splitting propogating periodically. Middle 1/2 of coupon remained unbroken.
CUN_4p	0	5	P	0.475	0.012065	0.313	0.035364	0.552	0.014	0.02	0.2	0.002	0.025	N/A	0.823	197	112	0.200	1.242	1.381	G	NO	Tension Cracking/splitting in 0 direction starting early on; 0 side splitting about 1/6 in. Test continued, splitting continued until central 2/3 of specimen left intact. Initial failure 112, split 118.
CUN_4p	0	6	M	0.4	0.01016	1.552	0.17535	0.298	0.008	0.7	0.6	0.079	0.062	N/A	1.052333333	1.083	187	0.063	1.407	1.455	G	NO	Tension 0 splitting and 90 cracking fiber failure from one edge and the the other, propogating toward center. Failed one side 187, other 191.
CUN_4p	0	AVERAGE	--	0.4500	0.01143	1.5573	0.176457	0.2624777	0.007	0.053333333	0.7	0.006	0.079	N/A	1.052333333	--	--	--	1.3863333	1.413	--	--	--
CUN_4p	0	STDEV	--	--	--	0.092284	0.010438	0.099131	0.003	0.009342809	0.113137085	0.001	0.013	N/A	0.020885934	--	--	--	0.0230139	--	--	--	--
CUN_4p	90	1	M	0.7	0.01778	0.03	0.00339	1.535	0.039	0.02	0.04	0.002	0.005	N/A	0.303	54	43	0.215	0.701	--	G	NO	Tension Striation on C side cause deformation almost immediately; Failed almost immediately; 90 crack in center of specimen. Tiny visible crack on T side on edge at 43, complete failure 54.
CUN_4p	90	3	M	0.8	0.02032	0.131	0.014801	0.731	0.019	0.03	0.08	0.003	0.009	N/A	0.675	184	182	0.194	1.189	--	G	NO	Tension Deformed in fixture almost immediately, cracking heard periodically. Broke at bottom (AG) grip. 90 crack, obvious distortion of curvature during test starting early.
CUN_4p	90	5	P	0.725	0.018415	0.046	0.005197	1.028	0.026	0.01	0.05	0.001	0.006	N/A	0.498	96	93	0.265	0.726	0.837	G	NO	Tension Failed very quickly at bottom grip. Failed at 93.
CUN_4p	90	6	M	0.7	0.01778	0.109	0.012315	0.738	0.019	0.03	0.08	0.003	0.009	N/A	0.842	131	131	0.219	0.957	1.030	G	NO	Tension Failed at bottom (AG) grip. 90 crack, eventual 2 piece failure. Coupon slightly distorted in grip prior to failure.
CUN_4p	90	AVERAGE	--	0.73125	0.018577375	0.079	0.008926	1.00825	0.02561	0.0225	0.0625	0.002542159	0.00706152	N/A	0.5795	--	--	--	0.89325	0.9335	--	--	--
CUN_4p	90	STDEV	--	--	--	0.042113	0.004758	0.327153	0.00831	0.008291562	0.017853571	0.000936821	0.002017183	N/A	0.206599402	--	--	--	0.963	1.051	--	--	--
CUN_4p	45	1	M	0.8	0.02032	0.173	0.019546	0.845	0.021	0.04	0.2	0.005	0.023	N/A	0.665	130	131	0.199	0.963	1.051	G	NO	Tension Corner of specimen (UL) already broken from cutting, proceeded with test to see if it would interfere; doesn't seem to though perhaps obsuring strain data. FAILURE: +45 crack through central diagonal, failed separately from preexisting crack, started in UR corner.

CUNI_4p	45	2	P	0.825	0.020955	0.267	0.030167	0.736	0.019	0.04	0.30	0.005	0.034	N/A	0.657	183	180	0.254	1.134	1.244	G	NO	Tension	Cracking heard around 6th minute; +45 crack through grip, one from lower L up, other from upper R down. Abrupt failure.
CUNI_4p	45	4	P	0.525	0.013335	--	#VALUE!	--	#VALUE!	--	--	#VALUE!	#VALUE!	N/A	0.722	132	132	0.201	--	1.055	B	NO	Tension	Bad force data 200 lbs and constant the whole test; Cracking heard around 3:30; +45 crack from L edge up to top grip.
CUNI_4p	45	5	M	0.8	0.02032	0.353	0.039884	0.679	0.017	0.03	0.30	0.003	0.034	N/A	0.808	199	197	0.301	1.193	1.469	G	NO	Tension	Crack, +45, from edge of bottom grip up. Abrupt failure.
CUNI_4p	45	7_1	M	0.8	0.02032	0.131	0.014801	0.871	0.022	0.03	0.14	0.003	0.016	N/A	0.629	221	117	0.167	1.375	1.519	G	NO	Tension	Cracking heard around minute 4, small crack on edge near top grip visible, +45 crack, no further failure.
CUNI_4p	45	7_2	M	0.65	0.01651	0.570	0.064401	0.434	0.011	0.03	0.45	0.003	0.051	N/A	0.869	221	221	0.020	1.498	1.425	G	NO	Tension	Immediately failed after test; +45 crack from bottom grip left egde through mid specimen
CUNI_4p	45	12	P	0.675	0.017145	0.209	0.023614	0.689	0.018	0.04	0.2	0.005	0.023	N/A	0.582	152	144	0.237	1.012	1.134	G	NO	Tension	Slight crack in lower R corner at 2:55; crack in +45 direction from bottom L grip up to top. Failed initially at 82, second/larger crack at 144
CUNI_4p	**45**	**AVERAGE**	**--**	**0.73750**	**0.01873**	**0.22660**	**0.025602**	**0.76422**	**0.019**	**0.03600**	**0.22800**	**0.004**	**0.026**	**N/A**	**0.67717**	**--**	**--**	**--**	**1.13540**	**1.24533**	**--**	**--**	**--**	
CUNI_4p	**45**	**STDEV**	**--**	**--**	**--**	**0.07737**	**0.008742**	**0.07963**	**0.002**	**0.00490**	**0.06274**	**0.001**	**0.007**	**N/A**	**0.07195**	**--**	**--**	**--**	**--**	**--**	**--**	**--**	**--**	
CUNI_4p	**45P**	**AVERAGE**	**--**	**0.67500**	**0.01715**	**0.23800**	**0.02689**	**0.71260**	**0.018**	**0.04000**	**0.25000**	**0.005**	**0.028**	**N/A**	**0.65367**	**--**	**--**	**--**	**1.07300**	**1.14433**	**--**	**--**	**--**	
CUNI_4p	**45P**	**STDEV**	**--**	**--**	**--**	**0.02900**	**0.003277**	**0.02339**	**0.001**	**0.00000**	**0.05000**	**0.000**	**0.006**	**N/A**	**0.05720**	**--**	**--**	**--**	**--**	**--**	**--**	**--**	**--**	
CUNI_4p	**45M**	**AVERAGE**	**--**	**0.80000**	**0.02032**	**0.21900**	**0.024744**	**0.79863**	**0.020**	**0.03333**	**0.21333**	**0.004**	**0.024**	**N/A**	**0.70067**	**--**	**--**	**--**	**1.17700**	**1.34633**	**--**	**--**	**--**	
CUNI_4p	**45M**	**STDEV**	**--**	**--**	**--**	**0.09629**	**0.010879**	**0.08510**	**0.002**	**0.00471**	**0.06600**	**0.001**	**0.007**	**N/A**	**0.07731**	**--**	**--**	**--**	**--**	**--**	**--**	**--**	**--**	
CUNI_4p	-45	4_1	P	0.725	0.018415	0.408	0.046098	0.548	0.014	0.04	0.30	0.005	0.034	N/A	0.767	215	215	0.191	1.328	1.474	G	NO	Tension	No Failure
CUNI_4p	-45	4_2	P	0.625	0.015875	0.442	0.049939	0.482	0.012	0.03	0.30	0.003	0.034	N/A	0.830	210	210	0.187	1.302	1.447	G	NO	Tension	No Failure
CUNI_4p	-45	4_3	P	0.525	0.013335	0.550	0.062142	0.412	0.010	0.05	0.28	0.006	0.032	N/A	0.849	211	208	0.226	1.278	1.425	G	NO	Tension	Small crack in -45 from L edge immediately after test, captured by VIC3D.
CUNI_4p	-45	6_1	M	0.8	0.02032	0.508	0.057396	0.565	0.014	0.06	0.28	0.007	0.032	N/A	0.800	224	224	0.088	1.446	1.400	G	NO	Tension	No Failure
CUNI_4p	-45	6_2	M	0.7	0.01778	0.633	0.071519	0.492	0.012	0.06	0.33	0.007	0.037	N/A	0.940	222	222	0.096	1.438	--	G	NO	Tension	No Failure
CUNI_4p	-45	6_3	M	0.6	0.01524	0.669	0.075587	0.445	0.011	0.07	0.33	0.008	0.037	N/A	0.945	215	215	0.161	1.363	1.327	G	NO	Tension	No Failure
CUNI_4p	-45	6_4	M	0.5	0.0127	0.718	0.081123	0.372	0.009	0.05	0.27	0.006	0.031	N/A	1.031	212	190	0.064	1.442	1.381	G	NO	Tension	Small -45 crack on upper R corner about 30 sec before end of test. Failed immediately after test crack in -45 on R edge
CUNI_4p	-45	7	M	0.45	0.01143	0.150	0.016948	0.819	0.021	0.05	0.16	0.006	0.018	N/A	0.467	49	40	0.064	0.598	--	G	NO	Tension	Failed almost immediately; -45 crack from central edge on R; failed at bottom grip. Failed at 40, visibly cracked by 20.
CUNI_4p	-45	10	P	0.625	0.015875	0.436	0.049261	0.542	0.014	0.06	0.28	0.007	0.032	N/A	0.864	182	181	0.226	1.160	1.425	G	NO	Tension	Abrupt failure; small crack in -45 in upper R corner at 155. Multiple large catastrophic cracks in -45 across coupon by 181
CUNI_4p	-45	13	M	0.7	0.01778	0.227	0.025648	0.972	0.025	0.07	0.2	0.008	0.023	N/A	0.531	84	78	0.147	0.752	--	G	NO	Tension	Failed very early; -45 crack from left side, bottom grip up; seems to line up with striations on C side.
CUNI_4p	**-45**	**AVERAGE**	**--**	**0.63928571**	**0.01623786**	**0.561143**	**0.063401**	**0.501659**	**0.013**	**0.045**	**0.29**	**0.005**	**0.033**	**N/A**	**0.8115**	**--**	**--**	**--**	**1.3385**	**1.4365**	**--**	**--**	**--**	
CUNI_4p	**-45**	**STDEV**	**--**	**--**	**--**	**0.055399**	**0.006259**	**0.060253**	**0.002**	**0.01118034**	**0.01**	**0.001**	**0.001**	**N/A**	**0.031068473**	**--**	**--**	**--**	**--**	**--**	**--**	**--**	**--**	
LAM1	0	1_1	P	0.725	0.018415	2.838	0.320651	0.548	0.014	0.45	1.30	0.051	0.147	N/A	2.029	216	216	0.188	1.33	1.459	G	NO	Tension	No Failure
LAM1	0	1_2	P	0.625	0.015875	3.180	0.359292	0.487	0.012	0.46	1.20	0.052	0.136	N/A	2.299	214	214	0.2240	1.289	1.411	G	NO	Tension	No Failure
LAM1	0	1_3	P	0.525	0.013335	2.558	0.289015	0.505	0.013	0.45	0.81	0.051	0.092	N/A	2.143	190	190	0.1820	1.226	1.389	G	NO	Tension	±45 zig-zag crack in central region of C side, no visible damage to T side; Cracking heard around minute 6.
LAM1	0	2	M	0.7	0.01778	3.331	0.376352	0.562	0.014	0.63	1.40	0.071	0.158	N/A	2.360	218	218	0.220	1.322	1.338	G	NO	Tension	±45 zig-zag crack in central region (2/5 down) of C side, failure visible on T side in shift/drop of fixture at 214
LAM1	0	3	P	0.525	0.013335	2.907	0.328447	0.498	0.013	0.50	0.93	0.056	0.105	N/A	2.175	205	205	0.196	1.299	1.290	G	NO	Tension	Large ±45 zig-zag crack in central region of C side. No visible failure on T side.
LAM1	0	4_1	P	0.675	0.017145	2.993	0.338164	0.513	0.013	0.45	1.30	0.051	0.147	N/A	2.219	216	216	0.197	1.321	1.455	G	NO	Tension	No Failure
LAM1	0	4_2	M	0.7	0.01778	3.309	0.373867	0.498	0.013	0.45	1.45	0.051	0.164	N/A	2.471	219	219	0.075	1.453	1.353	G	NO	Tension	±45 zig-zag crack in central region of C side
LAM1	0	5	P	0.525	0.013335	3.192	0.360648	0.450	0.011	0.50	0.95	0.056	0.107	N/A	2.233	202	205	0.202	1.270	1.403	G	NO	Tension	Failed near bottom grip; ±45 zig-zag crack in central region of C side. Cracking heard around 6:18 and then again at 6:30. Visible failure as slow deformation at grips 199-202.
LAM1	0	6	P	0.525	0.013335	2.720	0.307319	0.529	0.013	0.50	0.86	0.056	0.097	N/A	2.207	196	197	0.193	1.239	1.373	G	NO	Tension	Cracking heard around 6th minute; ±45 zig-zag crack in central region of C side; started at one end and progressively propogated to the other. No visible failure on T side.
LAM1	**0**	**AVERAGE**	**--**	**0.58333333**	**0.01481667**	**3.002833**	**0.339275**	**0.506977**	**0.013**	**0.505**	**1.066666667**	**0.057**	**0.121**	**N/A**	**2.264833333**	**--**	**--**	**--**	**1.3015**	**1.357666667**	**--**	**--**	**--**	
LAM1	**0**	**STDEV**	**--**	**--**	**--**	**0.295598**	**0.033398**	**0.034041**	**0.001**	**0.060207973**	**0.257854395**	**0.007**	**0.029**	**N/A**	**0.114624629**	**--**	**--**	**--**	**--**	**--**	**--**	**--**	**--**	
LAM1	**0P**	**AVERAGE**	**--**	**0.525**	**0.013**	**2.844**	**0.321357**	**0.496**	**0.013**	**0.488**	**0.888**	**0.055**	**0.100**	**N/A**	**2.190**	**--**	**--**	**--**	**1.259**	**1.364**	**--**	**--**	**--**	
LAM1	**0P**	**STDEV**	**--**	**--**	**--**	**0.235714**	**0.026632**	**0.028683**	**0.001**	**0.021650635**	**0.05584577**	**0.002**	**0.006**	**N/A**	**0.033804585**	**--**	**--**	**--**	**--**	**--**	**--**	**--**	**--**	
LAM1	**0M**	**AVERAGE**	**--**	**0.7**	**0.01778**	**3.32**	**0.37511**	**0.529889**	**0.013**	**0.54**	**1.425**	**0.061**	**0.161**	**N/A**	**2.4155**	**--**	**--**	**--**	**1.3875**	**1.3455**	**--**	**--**	**--**	
LAM1	**0M**	**STDEV**	**--**	**--**	**--**	**0.011**	**0.001243**	**0.032303**	**0.001**	**0.09**	**0.025**	**0.010**	**0.003**	**N/A**	**0.0555**	**--**	**--**	**--**	**--**	**--**	**--**	**--**	**--**	
LAM1	90	1	M	0.65	0.01651	2.053	0.231958	0.527	0.013	0.35	0.82	0.040	0.093	N/A	2.203	185	186	0.132	1.267	1.267	G	NO	Tension	Abrupt failure; no cracking heard; ±45 zig zag crack in center of C side. Visible failure at 186.
LAM1	90	2_1	P	0.775	0.019685	1.762	0.199079	0.610	0.015	0.30	1.05	0.034	0.119	N/A	1.825	212	212	0.245	1.271	1.395	G	NO	Tension	No Failure
LAM1	90	2_2	P	0.675	0.017145	2.166	0.244725	0.518	0.013	0.30	1.10	0.034	0.124	N/A	1.962	211	211	0.206	1.308	1.434	G	NO	Tension	No Failure
LAM1	90	2_3	P	0.575	0.014605	2.409	0.27218	0.450	0.011	0.30	1.05	0.034	0.119	N/A	2.170	208	208	0.211	1.281	1.409	G	NO	Tension	No Failure
LAM1	90	2_4	P	0.475	0.012065	2.362	0.26687	0.418	0.011	0.35	0.68	0.040	0.077	N/A	2.147	173	174	0.212	1.146	1.257	G	NO	Tension	Tight ±45 zig-zag crack in 90 direction in central region of C side. Visible failure at 174
LAM1	90	3_1	M	0.75	0.01905	2.110	0.238398	0.521	0.013	0.25	1.30	0.028	0.147	N/A	2.247	222	222	0.091	1.443	1.463	G	NO	Tension	No Failure
LAM1	90	3_2	M	0.65	0.01651	2.179	0.246194	0.528	0.013	0.30	0.95	0.034	0.107	N/A	2.268	193	194	0.201	1.242	1.318	G	NO	Tension	±45 zig-zag crack in central region of C side. Cracking heard a bit before failure; visible failure at 194
LAM1	90	4	P	0.475	0.012065	2.352	0.26574	0.549	0.014	0.40	0.65	0.045	0.073	N/A	2.117	168	165	0.192	1.125	1.237	G	NO	Tension	Failed at top grip; ±45 zig-zag crack in 90 direction. Visible failure at 166
LAM1	90	5	P	0.525	0.013335	2.325	0.26269	0.486	0.012	0.40	0.65	0.045	0.073	N/A	2.120	174	189	0.210	1.216	1.334	G	NO	Tension	Failed near bottom grip; ±45 zig-zag crack on C side. Cracking heard around minute 6; visible failure at 190
LAM1	90	6	P	0.525	0.013335	2.312	0.261221	0.479	0.012	0.42	0.66	0.047	0.075	N/A	2.028	196	197	0.182	1.237	1.404	G	NO	Tension	Failed near bottom grip; tight ±45 zig-zag crack on C side. Visible failure at 197
LAM1	**90**	**AVERAGE**	**--**	**0.55000**	**0.01397**	**2.26383**	**0.255779**	**0.498**	**0.013**	**0.37**	**0.74**	**0.042**	**0.083**	**N/A**	**2.14717**	**--**	**--**	**--**	**1.20550**	**1.30283**	**--**	**--**	**--**	
LAM1	**90**	**STDEV**	**--**	**--**	**--**	**0.11189**	**0.012642**	**0.04319**	**0.001**	**0.04082**	**0.11295**	**0.005**	**0.013**	**N/A**	**0.07480**	**--**	**--**	**--**	**--**	**--**	**--**	**--**	**--**	
LAM1	**90P**	**AVERAGE**	**--**	**0.500**	**0.013**	**2.338**	**0.26413**	**0.483**	**0.012**	**0.393**	**0.660**	**0.044**	**0.075**	**N/A**	**2.103**	**--**	**--**	**--**	**1.181**	**1.308**	**--**	**--**	**--**	
LAM1	**90P**	**STDEV**	**--**	**--**	**--**	**0.02010**	**0.002271**	**0.04619**	**0.001**	**0.02586**	**0.01225**	**0.003**	**0.001**	**N/A**	**0.04485**	**--**	**--**	**--**	**--**	**--**	**--**	**--**	**--**	
LAM1	**90M**	**AVERAGE**	**--**	**0.65**	**0.01651**	**2.116**	**0.239076**	**0.52770**	**0.013**	**0.325**	**0.885**	**0.037**	**0.100**	**N/A**	**2.2355**	**--**	**--**	**--**	**1.2545**	**1.2925**	**--**	**--**	**--**	
LAM1	**90M**	**STDEV**	**--**	**--**	**--**	**0.063**	**0.007118**	**0.00042**	**0.000**	**0.025**	**0.065**	**0.003**	**0.007**	**N/A**	**0.0325**	**--**	**--**	**--**	**--**	**--**	**--**	**--**	**--**	
LAM1	45	1	P	0.775	0.019685	3.685	0.416349	0.819	0.021	1.15	1.50	0.130	0.169	N/A	1.451	140	141	0.171	1.045	1.181	G	NO	Tension	Failed at bottom grip; 90° crack on C side caused total failure through T side. Cracking heard at 1:50, then loud crack heard at 4:30. Visible failure at 141

LAM1	45	2	P	0.875	0.022225	3.569	0.403243	0.793	0.020	1.05	1.65	0.119	0.186	N/A	1.444	205	206	0.199	1.289	1.417	G	NO	Tension	Failed near bottom grip; 90° crack started at C side bottom grip, moved up to more central region. Cracking heard at 4:15, again at 4:50, continually from 5:30 on. Visible failure at 206
LAM1	45	3	P	0.875	0.022225	3.921	0.443014	0.811	0.021	1.17	1.60	0.132	0.181	N/A	1.393	165	166	0.197	1.121	1.220	G	NO	Tension	Failed at top grip; 90° crack started on C side. Continuous cracking (progressive failure?) from 5:10 on. Visible failure at 166.
LAM1	45	4	M	1.05	0.02667	4.335	0.489789	0.908	0.023	1.40	2.05	0.158	0.232	N/A	1.555	196	197	0.256	1.204	1.305	G	NO	Tension	Failed at top grip; 90° crack on C side, crack slopes away from grip towards center slightly. Cracking heard around 6:15. Visible failure at 197.
LAM1	45	5	M	1.05	0.02667	3.291	0.371833	1.003	0.025	1.10	1.85	0.124	0.209	N/A	1.315	192	193	0.326	1.133	1.236	G	NO	Tension	90° crack on C side causing collapse on T side. Cracking heard around 4:32. Visible failure at 193.
LAM1	45	6	P	0.875	0.022225	3.690	0.416914	0.788	0.020	1.06	1.65	0.120	0.186	N/A	1.538	211	212	0.170	1.325	1.403	G	NO	Tension	Failed near bottom grip; 90° crack at C side, collapsed T side. Cracking heard at 4:50, continually from 6:25 on. Visible failure at 212.
LAM1	**45**	**AVERAGE**	--	**0.91666667**	**0.02328333**	**3.7485**	**0.423524**	**0.853826**	**0.022**	**1.155**	**1.716666667**	**0.130**	**0.194**	**N/A**	**1.449333333**	--	--	--	**1.1861667**	**1.293666667**	--	--	--	
LAM1	**45**	**STDEV**	--	--	--	**0.322159**	**0.036399**	**0.07754**	**0.002**	**0.117862915**	**0.181811869**	**0.013**	**0.021**	**N/A**	**0.081932221**	--	--	--	--	--	--	--	--	
LAM1	**45P**	**AVERAGE**	--	**0.850**	**0.022**	**3.716**	**0.41988**	**0.803**	**0.020**	**1.108**	**1.600**	**0.125**	**0.181**	**N/A**	**1.457**	--	--	--	**1.195**	**1.305**	--	--	--	
LAM1	**45P**	**STDEV**	--	--	--	**0.127741**	**0.014433**	**0.012492**	**0.000**	**0.053091901**	**0.061237244**	**0.006**	**0.007**	**N/A**	**0.052108061**	--	--	--	--	--	--	--	--	
LAM1	**45M**	**AVERAGE**	--	**1.05**	**0.02667**	**3.813**	**0.430811**	**0.955514**	**0.024**	**1.25**	**1.95**	**0.141**	**0.220**	**N/A**	**1.435**	--	--	--	**1.1685**	**1.2705**	--	--	--	
LAM1	**45M**	**STDEV**	--	--	--	**0.522**	**0.058978**	**0.04706**	**0.001**	**0.15**	**0.1**	**0.017**	**0.011**	**N/A**	**0.12**	--	--	--	--	--	--	--	--	
LAM1	-45	1	P	0.925	0.023495	3.602	0.406971	0.934	0.024	1.20	1.75	0.136	0.198	N/A	1.282	225	225	0.192	1.348	1.356	G	NO	Tension	Collapsed immediately after test. Cracking heard at 4:49, continually from 6:30. Failed near bottom grip. Grip deforms slightly (failure) at 193.
LAM1	-45	2	M	1.05	0.02667	3.617	0.408666	0.935	0.024	1.26	1.95	0.142	0.220	N/A	1.350	242	243	0.112	1.455	1.496	G	NO	Tension	Failed immediately after test, VIC3D still running though. 90° crack in center of C side, collapsed T side at 243. Cracking heard at 6:30, continually from 7 to failure. Failed near bottom grip. Fixture shifts slightly between 238 and 239.
LAM1	**-45**	**AVERAGE**	--	**0.9875**	**0.0250825**	**3.6095**	**0.407819**	**0.934528**	**0.023737**	**1.23**	**1.85**	**0.13897134**	**0.209021934**	**N/A**	**1.316**	--	--	--	**1.4015**	**1.426**	--	--	--	
LAM1	**-45**	**STDEV**	--	--	--	**0.0075**	**0.000847**	**0.000912**	**2.32E-05**	**0.03**	**0.1**	**0.003389545**	**0.011298483**	**N/A**	**0.034**	--	--	--	--	--	--	--	--	
LAM1	**-45P**	**AVERAGE**	--	**0.925**	**0.023**	**3.602**	**0.407**	**0.934**	**0.024**	**1.200**	**1.750**	**0.136**	**0.198**	**N/A**	**1.282**	--	--	--	**1.348**	**1.356**	--	--	--	
LAM1	**-45P**	**STDEV**	--	--	--	**0**	**0**	**0**	**0**	**0**	**0**	**0**	**0**	**N/A**	**0**	--	--	--	--	--	--	--	--	
LAM1	**-45M**	**AVERAGE**	--	**1.05**	**0.02667**	**3.617**	**0.408666**	**0.93544**	**0.02376**	**1.26**	**1.95**	**0.142360885**	**0.220320417**	**N/A**	**1.35**	--	--	--	**1.455**	**1.496**	--	--	--	
LAM1	**-45M**	**STDEV**	--	--	--	**0**	**0**	**0**	**0**	**0**	**0**	**0**	**0**	**N/A**	**0**	--	--	--	--	--	--	--	--	

NO WAY OF KNOWING BEFORE TEST +45 OR -45 BECAUSE THEY ARE THE INTERNAL FIBERS

Appendix G: Abaqus Sample Input File for LAM1_0_C2 FEM

```
*Heading
** Job name: LAM1_0_C2-PureMoment Model name: Model-1
** Generated by: Abaqus/CAE 6.14-1
*Preprint, echo=NO, model=NO, history=NO, contact=NO
**
** PARTS
**
*Part, name=LAM1
*Node
      1 - 9486
*Element, type=S4R
       1 - 9272
*Nset, nset=BottomNodes, generate
   1,  153,    1
*Nset, nset=TopNodes, generate
 9334,  9486,     1
** Region: (LAM1-1: Generated From Layup)
*Elset, elset=LAM1-1, generate
    1,  9272,     1
** Section: LAM1-1
*Shell Section, elset=LAM1-1, composite, offset=SPOS, layup=LAM1
6.4138e-05, 3, HTA40PW, 45., Ply-1
6.4138e-05, 1, HTA40PW, 45., Ply-2
4.1396e-05, 3, MR60H_CUNI, 90., Ply-3
4.1396e-05, 3, MR60H_CUNI, 90., Ply-4
6.4138e-05, 1, HTA40PW, 45., Ply-5
6.4138e-05, 3, HTA40PW, 45., Ply-6
*End Part
**
**
** ASSEMBLY
**
*Assembly, name=Assembly
**
*Instance, name=LAM1, part=LAM1
*End Instance
**
*Node
      1, -0.0110499999, 0.00400000019,           0.
*Node
      2, -0.0110499999, -0.0112399999,           0.
*Nset, nset=LAM1Bottom
 2,
*Nset, nset=LAM1Top
 1,
*Nset, nset=Set-3
 1,
*Nset, nset=Set-4
 2,
*Nset, nset=Set-5
 2,
*Surface, type=NODE, name=LAM1_BottomNodes_CNS_, internal
```

```
LAM1.BottomNodes, 1.
*Surface, type=NODE, name=LAM1_TopNodes_CNS_, internal
LAM1.TopNodes, 1.
** Constraint: Equation
** Constraint: LAM1_BottomMPC
*MPC
TIE, LAM1.BottomNodes, LAM1Bottom
** Constraint: LAM1_TopMPC
*MPC
TIE, LAM1.TopNodes, LAM1Top
*End Assembly
**
** MATERIALS
**
*Material, name=HTA40PW
*Density
 1530.81,
*Elastic, type=ENGINEERING CONSTANTS
 6.94104e+10, 6.94104e+10, 9.01612e+09,   0.0320506,    0.406363,
0.406363, 3.28489e+09, 2.89689e+09
 2.89689e+09,
*Material, name=MR60H_CUNI
*Density
 1604.37,
*Elastic, type=ENGINEERING CONSTANTS
 1.8392e+11, 9.60919e+09, 9.60919e+09,    0.261207,    0.261207,
0.411061, 4.25212e+09, 4.25212e+09
  3.0532e+09,
** ----------------------------------------------------------------
**
** STEP: NotUsed
**
*Step, name=NotUsed, nlgeom=YES, inc=10000
*Static, stabilize=0.0002, allsdtol=0.05, continue=NO
0.05, 1., 1e-06, 1.
**
** OUTPUT REQUESTS
**
*Restart, write, frequency=0
**
** FIELD OUTPUT: F-Output-1
**
*Output, field
*Node Output
CF, RF, U
*Element Output, directions=YES
1, 2, 3, 4, 5, 6, 7, 8, 9, 10, 11, 12, 13, 14
E, EE, LE, PE, PEEQ, PEMAG, S, SE
*Contact Output
CDISP, CSTRESS
**
** HISTORY OUTPUT: H-Output-1
```

```
**
*Output, history, variable=PRESELECT
*End Step
** ----------------------------------------------------------------
**
** STEP: Pure_Moment
**
*Step, name=Pure_Moment, nlgeom=YES, inc=10000
*Static
0.05, 1., 1e-06, 1.
**
** BOUNDARY CONDITIONS
**
** Name: Bottom_Disp_Constraint Type: Displacement/Rotation
*Boundary
LAM1Bottom, 1, 1
LAM1Bottom, 3, 3
** Name: Top_Disp_Constraint Type: Displacement/Rotation
*Boundary
LAM1Top, 1, 1
LAM1Top, 3, 3
**
** LOADS
**
** Name: Bottom_Moment   Type: Moment
*Cload, follower
LAM1Bottom, 4, -1.35
** Name: Top_Moment   Type: Moment
*Cload, follower
LAM1Top, 4, 1.35
**
** OUTPUT REQUESTS
**
*Restart, write, frequency=0
**
** FIELD OUTPUT: F-Output-1
**
*Output, field
*Node Output
CF, RF, U, V
*Element Output, directions=YES
1, 2, 3, 4, 5, 6, 7, 8, 9, 10, 11, 12, 13, 14
E, EE, LE, MISES, PE, PEEQ, PEMAG, S, SE
**
** HISTORY OUTPUT: H-Output-1
**
*Output, history, variable=PRESELECT
*End Step
```